5-4-2020

Heme Uptake in Group A Streptococcus: A Role in Physiology and Disease

Nilanjana Chatterjee

HEME UPTAKE IN GROUP A STREPTOCOCCUS: A ROLE IN PHYSIOLOGY AND DISEASE

by

NILANJANA CHATTERJEE

Under the Direction of Zehava Eichenbaum, PhD

ABSTRACT

The Group A streptococcus (GAS) produces millions of infections worldwide, leading to acute diseases, post-infection sequelae, and severe complications. This leading human pathogen requires iron for growth and relies on the heme-iron it obtains from host hemoproteins to fulfill its need for the metal during infection. Since heme is a critical nutrient for GAS within the host environment, the proteins involved in heme capture and metabolism could be targeted for the development of new modalities to treat and prevent GAS infections and their devastating complications. The 10-gene *sia* operon, which consists of two surface receptors (Shr and Shp), and an ABC transporter (SiaABC), is the best-described heme capture and import system in GAS. The function of the remaining *siaDEFGH* genes is not yet characterized. Mutants in the characterized

heme uptake proteins (*shr*, *shp*, or *siaABC*) exhibit reduced ability to grow on heme iron, but the partial phenotype indicates other GAS genes contribute to heme metabolism. This dissertation addresses the knowledge gaps in the current understanding of heme uptake in GAS and investigates the potential of targeting the surface receptor, Shr, for the development of new therapy. The first chapter describes a new surface receptor, HupY, and demonstrates that HupY binds heme *in vitro*, contributes to iron acquisition from hemoglobin or serum, and GAS colonization of the mucosal surfaces in mice. The second chapter shows that the *siaFGH* genes encode a new type of heme importer that is vital for GAS growth on hemoglobin iron, colonization of the vaginal surface, and systemic infections in murine models. The third chapter describes high-affinity human monoclonal antibody against the surface receptor Shr, their efficacy in protecting from GAS infection in murine models, and investigate their defense mechanism. Altogether this dissertation significantly expands the current understanding of heme metabolism in GAS and lays the groundwork for the development of new therapeutic measures.

INDEX WORDS: *Streptococcus pyogenes*, Heme uptake, HupY, SiaFGH, Shr, Protection, Monoclonal antibody

HEME UPTAKE IN GROUP A STREPTOCOCCUS: A ROLE IN PHYSIOLOGY AND DISEASE

by

NILANJANA CHATTERJEE

A Dissertation Submitted in Partial Fulfillment of the Requirements for the Degree of

Doctor of Philosophy

in the College of Arts and Sciences

Georgia State University

2020

HEME UPTAKE IN GROUP A STREPTOCOCCUS: A ROLE IN PHYSIOLOGY AND DISEASE

by

NILANJANA CHATTERJEE

Committee Chair: Zehava Eichenbaum

Committee: Kuk-Jeong Chin

Roberta Attanasio

Electronic Version Approved:

Office of Graduate Services

College of Arts and Sciences

Georgia State University

May 2020

DEDICATION

This work is dedicated to my beautiful parents,

Gayatry Chatterjee and Kartik Chatterjee,

who have always encouraged me and supported me in all my scholarly pursuits.

"... because all things have contributed to your advancement,

you should include all things in your gratitude."

— Wallace D. Wattles

ACKNOWLEDGEMENTS

This dissertation would not have been possible without the continued support and love of several people in my life. First and foremost, I would like to express my deepest appreciation and sincere gratitude to my dearest supervisor Dr. Zehava Eichenbaum. I could not have completed this journey without her support, guidance, and inspiration. She has been my mentor, philosopher, and guide throughout this journey. Thank you, Dr. Eichenbaum, for being the kind and caring person that you are. Thank you for everything you have done for me.

I would like to extend my sincere gratitude to my committee members, Dr. Kuk-Jeong Chin and Dr. Roberta Attanasio, for their guidance, continued support, motivation, and encouragement. I would also like to thank Dr. Parjit Kaur for her support and encouragement. I am very thankful to Dr. Laura C. C. Cook and her lab for being such an excellent collaborator. Many thanks to the wonderful staff and core facility of the Biology department. I am especially indebted to Late Ms. LaTesha Warren for her warmth and continuous assistance. This work would not have been possible without the financial support from the Department of Biology.

Eichenbaum lab was a friendly and joyful place to work. I want to express my profound appreciation to all my previous and current lab members who have made my journey comfortable and memorable. A special thanks to my excellent lab colleagues Edroyal Womack, Fahmina Akhter, and Kristin Lyles. Thank you for all the moments that we have shared. I would also like to thank my two undergraduate friends Kieffer Hellmeister and Kolbi Gray. Thank you for all the fun, laughter, and smiles that we had together. Also, special thanks to Sadia Rahman and Elizabeth Peterson for being the best lab neighbors.

I would like to express my heartiest thanks to my Atlanta friends and family, who have always showered me with love and encouragement through this journey. I am especially grateful to Jami Husain, Sohani Fatehin, Mudabbir Husain, and my Lenox family for their unconditional love and support. I am deeply indebted to Raiyan Tasnim Hridita and Fahima Aqtar for their help; otherwise, it would be challenging to continue the journey. I would like to extend my special thanks and gratitude to Tania Afsana for being the most loving, caring, and supportive big sister.

No words can ever be strong enough to express how grateful I am to my wonderful parents Gayatry Chatterjee and Kartik Chatterjee. Today what I have achieved, it is only because of your tireless support, unconditional love, and countless sacrifices. You are the pillar of my strength; you are the heroes of my success. My baby sister, Suranjana Chatterjee, thank you for being my powerhouse; thank you for always there for me, listening to me, encouraging me, and supporting me. The journey became more comfortable with the love, support, and encouragement I have received from my parents-in-law, Nilima Datta and Biswajit Kumar Datta. A special thanks to Pallab Kumar Datta, for being the most supportive brother.

My baby, Aradhya, you were my calm in those stressful days. You always welcomed me with your heavenly smile even when I came home late. Without your support, my angel, working those long tiring hours in the lab would not be that easy. My sunshine, you made me stronger than I ever thought I could be. Thank you very much for being the best baby in the world.

Finally, I want to acknowledge the dreamer behind this journey, my amazing husband Biplab Kumar Datta. It was you who always supported and believed in me even when I did not believe in myself. Thank you for being the biggest cheerleader for my every success; thank you for being my steady rock. Without your encouragement, constant reassurance, and love, I would not be able to finish this journey.

TABLE OF CONTENTS

LIST OF TABLES

LIST OF FIGURES

1 GENERAL INTRODUCTION

This dissertation focuses on iron and heme metabolism in pathogenic streptococci, primarily Group A Streptococcus (GAS). The introduction is intended to provide background information about the pathogen and the area of iron homeostasis.

1.1 Group A Streptococcus (GAS)

Group A streptococcus (GAS), also known as *Streptococcus pyogenes,* is an obligate human pathogen and a leading cause of human morbidity and mortality globally. This beta-hemolytic pathogen presents diverse clinical manifestations. Most frequently, GAS causes mild infections such as pharyngitis and impetigo, which can resolve upon medical intervention at the early stage of the disease. On rare occasions, or as a result of delayed treatment, GAS produces life-threatening invasive infections, such as necrotizing fasciitis and Streptococcal Toxic Shock Syndrome. Conventional GAS episodes may also lead to severe immune-based sequelae, including post-streptococcal glomerulonephritis, acute rheumatic fever (ARF), and rheumatic heart disease (RHD) [1].

1.2 Global GAS burden

GAS produces several million infections worldwide. Based on this heavy burden, the World Health Organization ranked this pathogen as the ninth leading infectious agent of human morbidity and mortality. Every year GAS claims approximately 500,000 lives [2]. About 700 million people suffer from non-invasive GAS diseases annually, of which more than 600,000 cases progress to severe invasive infections with more than160,000 deaths [2]. RHD, which is the most common cause of non-congenital heart disease in children, alone, is contributing to a substantial

death toll and chronic disability worldwide, especially in the developing parts of the world. 33.4 million cases of rheumatic heart disease were recorded in 2015, of which 1.2 million cases led to heart failure [3]. GAS infections are prevalent in low-income countries with low socioeconomic conditions and overpopulation as major contributing factors [4]. Wealthy nations in the western hemisphere (e.g., USA, UK, Canada) have been experiencing in the past few years an unprecedented resurgence in GAS infections. These resurging infections include serious diseases such as scarlet fever, invasive infections, and puerperal sepsis. England, for example, has suffered in 2014 from a dramatic escalation in scarlet fever incidences with a case rate increase of more than 3-fold over one year (8.2 and 27.2 cases per 100,000 in 2013 and 2014 respectively) [5]. The frequency of invasive GAS infections has recently reached 7-10 cases per 100,000 in the US and Canada [6, 7]. Notably, the rate of invasive diseases in pregnant and post-partum women is higher compared to the rest of the population. For example, 109 cases per 100,000 of GAS puerperal sepsis had occurred in England between 2010-2016 [8]. Penicillin is the recommended antibiotic to treat uncomplicated GAS infections. However, resistance to drugs (macrolides [9] and clindamycin [10]) that are used in penicillin-sensitive patients is increasing. Intensive surgical procedures are required to handle severe invasive infections. Currently, no licensed vaccine is available against streptococcal diseases. The lack of vaccine along with the rising rate of antibiotic resistance demands a better understanding of GAS pathogenesis, that may facilitate the design of novel therapeutics for combating this dangerous human pathogen.

1.3 Leading GAS vaccine candidates

The majority of the vaccine development studies in GAS target the leading virulence factor, M protein. It is an immunogenic and protective antigen, which elicits long-lasting immunity and present in a high amount on the GAS surface [11]. However, some serious concerns impede the M

protein-based vaccine development. Some M proteins (M1 type) induce a dangerous inflammatory response by triggering the Th1-type cytokine release [12]. Moreover, some of the M epitopes cross-react with the host antigens and lead to ARF development [13]. Besides, the most exposed and immunogenic part (amino terminus) of the M protein is hypervariable; there are more than 200 circulating M-based serotypes. Hence, vaccination that targets that hypervariable region often protects against a limited number of GAS strains [14]. Because of the urgent need, the search for an M-based vaccine that is safe and broad continues. Two vaccine candidates are currently in human trials (Phase I). The MJ8VAX vaccine encompasses epitopes for the conserved carboxyl terminus region of the M-protein [15], and StreptAnova is a 30-valent vaccine that consists of a mixture of peptides from the hypervariable amino terminus of M protein that represent the most prevalent serotypes in North America and Europe [16]. Additional vaccine targets consist of several surface virulence factors. These including the C5a peptidase, Fibronectin-binding protein, Serum opacity factor, Streptococcal pyrogenic exotoxin, Pili (T antigen), Serine protease (SpyCEP), and the Metal transporter of streptococcus (MtsA). A recent study from our lab suggested that the Streptococcal hemoprotein receptor (Shr) is a promising candidate. [17].

1.4 The role of iron in bacterial infections

With only a few exceptions (e.g., *Borrelia burgdorferi* and some *Lactococcal specie)*, pathogenic bacteria require iron [18, 19]. Nutritional immunity, which limits the bioavailability of essential metals such as iron, is a primary defense mechanism used by mammals to protects themselves against bacterial infection. The vast majority of the iron within the human body is located intracellularly. Almost 75% of the metal is complexed with the protoporphyrin IX molecule to form heme, which serves as the prosthetic group of hemoglobin, myoglobin, and other proteins. Most of the remaining intracellular iron is in ferrihydrite mineral and sequestered within

the shell of the iron storage protein, ferritin. Hemoglobin and heme that are released into circulation are rapidly captured and removed by the host carrier proteins, haptoglobin, and hemopexin. The glycoproteins transferrin (plasma) or lactoferrin (secretion) eliminates free iron from the extracellular fluids. Altogether, the host withholding of iron results in 10^{-18} M of the free metal in the interstitial fluids, an extremely low concentration that is several orders of magnitude below the 10^{-6}-10^{-7} M of iron, which most bacteria require to grow [20]. Hence bacteria that invade the human body deploy high-affinity mechanisms to acquire iron from the host proteins during infection.

1.5 Heme uptake mechanisms by bacterial pathogens

The largest reservoir of iron in humans is heme. Pathogenic bacteria employ high-affinity heme scavenging proteins to capture and import heme from circulating host hemoproteins or protein that are released by hemolysis and tissue damage during infection [21]. The mechanism of heme uptake is better understood in Gram-negative bacteria. These pathogens often use hemophores (e.g., *Pseudomonas aeruginosa*, *Yersinia pestis*, and *Hemophilus influenza*, [22-24]) and / or outer membrane receptors (e.g., Neisseria species and *Vibrio Cholerae*, [25-27]) to remove heme from host hemoproteins. In both cases, the seized heme is transported through the outer membrane. In the periplasm, ligand-binding proteins capture the heme and deliver it to a cognate ABC transporter for translocation through the inner membrane and into the cytosol. The energy required for the outer membrane transports comes from the proton motive force, *via* the TonB ExbB and ExbD system. ATP hydrolysis (by the transporter ATPase) energizes the import across the inner membrane. Gram-positive bacteria also use hemophores and or heme receptors to capture heme from the host. Nevertheless, protein relay systems are often used to shuttle the heme through the thick peptidoglycan of Gram-positive bacteria. Like with Gram-negative organisms, dedicated

ABC transporters transport the heme into the cytoplasm. [28]. In many Gram-positive bacteria, the proteins that participate in heme relay across the cell wall use a common protein domain, named NEAT (NEAr-iron Transporter). The NEAT protein module shares a common fold but exhibits a significant sequence and functional diversities [29]. The ligands different NEAT domains interact with include, heme, hemoglobin, and various ECM components [30]. The Isd machinery used by *Staphylococcus aureus* is the best described NEAT-based heme acquisition system [28].

1.6 Heme uptake in GAS

GAS utilizes surface receptors that contain NEAT domains to obtain heme and transfer it through the cell wall. The best-studied heme acquisition pathway in GAS is the Sia system, which is encoded by a ten-gene operon named *sia (*streptococcal iron acquisition) [31]. MtsR (metal transport repressor), a global regulator that controls iron homeostasis in GAS, represses the *sia* operon in an iron-dependent manner. [31]. The first five genes of the *sia* operon, encode Shr (streptococcal hemoprotein receptor), Shp (streptococcal heme-binding protein), and the ABC transporter, SiaABC. Shr is a 145 kDa protein with a unique N-terminal region (NTR) followed by two NEAT domains, separated by a leucine-rich repeat region [29]. Shr binds to hemoglobin via its NTR that harbors two copies of a unique domain (aka DUF1533). Recently the structure of one of the Shr DUF1533 domains has been resolved and renamed HID (Hb-interacting domain) because of its hemoglobin-binding capacity [32]. Following binding to hemoglobin, NEAT1 captures and transfers the heme to NEAT2 or Shp, the second receptor in the pathway. Kinetic studies suggest that two NEAT domains of Shr are functionally distinct. NEAT1 is involved in heme uptake and delivery, whereas NEAT2 serves as temporary heme storage. According to the proposed model, in the presence of a high concentration of heme, holo-NEAT1 rapidly relays heme to Shp and also delivers heme to apo-NEAT2. In low heme concentration, heme stored in NEAT2

is transferred back to NEAT1 and then to Shp [33]. A rapid and affinity-driven mechanism is involved in the transfer of heme from Shp to SiaA [34]. Finally, heme is transported into the cytoplasm via the SiaBC proteins. The function of the proteins encoded by the remaining genes in the *sia* operon is unknown. A second iron-complex transporter has been described in GAS, SiuADBG/FtsABCD, shown to involve in ferrichrome [35] and heme [36] import. The redundancy in heme uptake protein highlight the importance of heme iron as a nutrient for GAS.

1.7 Dissertation objectives and significance

The research project aims to expand the current understanding of bacterial heme uptake mechanisms and to explore if heme uptake proteins could be targeted for the development of new therapies. Work focused on GAS, a critical human pathogen. This research endeavor facilitated the discovery of a new surface receptor encoded outside of the *sia* operon, which is conserved in GAS and the related group B streptococcus (GBS or *S. dysgalactiae*). The investigation also revealed a novel heme transporter, encoded by the *si*a operon, which is found in other Gram-positive pathogens. The role of the new components in heme acquisition in bacterial physiology and disease process was described. Research efforts also yielded proof of concept for targeting heme uptake proteins for the development of new modalities for prevention and therapy.

2 CHAPTER I: TRANSCRIPTOMIC ANALYSIS OF STREPTOCOCCUS PYOGENES COLONIZING THE VAGINAL MUCOSA IDENTIFIES HUPY, AN MTSR-REGULATED ADHESIN INVOLVED IN HEME UTILIZATION

2.1 Introduction

Streptococcus pyogenes (Group A Streptococcus, GAS) is an important primary pathogen causing severe infections like necrotizing fasciitis and toxic shock syndrome, but it also colonizes mucosal surfaces, often asymptomatically. Mucosal carriage of GAS in the throat [37-39], gastrointestinal tract [40], and recto-vaginal tract [41, 42] can serve as principal reservoirs for community infections. Although the rate of transmission from carriers is lower than in acutely infected individuals, this reservoir is important on a population level as rates of carriage greatly eclipse rates of acute infections in the community [43].

Vaginal mucosal colonization by GAS is associated with vulvovaginitis in prepubertal girls with studies reporting 11-20% of swabs collected from girls with vulvovaginitis contained GAS [44-46]. A recto-vaginal carrier state has been demonstrated in adult women [42, 47] and although the level of vaginitis is lower in adults, it has been reported in the literature [40, 48]. A murine vaginal colonization model has been developed for GAS based on a similar model used for the related *Streptococcus agalactiae* (Group B Strep, GBS) [49-51]. Not only does this model allow for examination of GAS vaginal colonization, but it also provides an easily accessible model for colonization of host mucosal surfaces. Here, we describe the transcriptome of GAS during murine vaginal carriage. This work, in conjunction with previous research describing transcriptional profiles during vaginal colonization by GBS [52], provides an important framework for the genetic changes streptococcal pathogens undergo during mucosal carriage.

The environment encountered in mucosal surfaces is vastly different from liquid laboratory culture, which is reflected in the large number of genetic changes observed via RNASeq. One set of genes that was highly differentially expressed during GAS vaginal colonization is known to be under the regulation of MtsR (Spy49_0380c), a master regulator of iron homeostasis and virulence in GAS and related streptococci [53-55]. In iron-replete conditions, MtsR acts as a negative regulator of over 40 genes in GAS including the ribonucleotide reductase operon *nrdF.2IE.2* operon (*spy49_0339-0341*) and many genes involved in heme metabolism such as *shr* (*spy49_1405c*), *shp* (*spy49_1404c*), *siaABC* (*spy49_1401c-1403c*), and *hupZ* (*spy49_0662*) [54, 56, 57].

HupZ was recently described as a novel enzyme involved in GAS heme biotransformation. HupZ binds and degrades heme to generate free iron in vitro [56]. As a cytoplasmic enzyme, HupZ does not have access to extracellular heme and thus depends on GAS uptake machinery for heme supply. Heme acquisition in Gram-positive bacteria typically involves surface receptors that capture heme from the host and deliver it through the peptidoglycan layers to dedicated ABC transporters in the membrane for import into the cytoplasm [58]. The only receptors for hemoproteins and heme described in GAS are Shr and Shp, which together consist of a heme relay system that shuttles heme from the extracellular environment to the SiaABC heme transporter (also known as HtsABC) [30, 33, 34]. Here we report that the gene adjacent to HupZ, *spy49_0661* now renamed *hupY*, is highly upregulated during vaginal carriage and is not only important for mucosal colonization but also plays a role in heme utilization in GAS.

HupY, previously known as LrrG, is a leucine rich repeat protein with homologs in other species of streptococci, including GBS (SAK_0502). These proteins have previously been described as LPXTG-anchored cell surface proteins in GAS and GBS that are involved in binding

epithelial cells. Immunization against LrrG was protective in a mouse model of GAS infection, and it was also shown to be expressed during a macaque model of acute pharyngitis [59-61]. Genetic location and co-regulation indicate that the function of HupZ and HupY may be related. We hypothesize that HupY serves as both an adhesin and receptor that facilitates the capture and uptake of heme into GAS during colonization and infection of the host.

2.2 Materials and methods

2.2.1 Bacterial strains, media, plasmids, and primers

Bacterial strains and plasmids used in this work are listed in Table S2 (Appendix A.2), and primer sequences are shown in Table S3 (Appendix A.3). BH10C *Escherichia coli* were grown in Luria-Bertani medium (LB) and GAS strain NZ131 and its derivatives were grown in Todd-Hewitt medium supplemented with 2% (w/v) yeast extract (THY) or chemically defined medium [62]. Antibiotics were added at the following concentrations when needed: *E. coli* chloramphenicol (Cm), 10 μg ml^{-1}; kanamycin (Kan) 150 μg ml^{-1}, spectinomycin (Spec), 100 μg ml^{-1}; GAS chloramphenicol (Cm), 3 μg ml^{-1}; kanamycin (Kan) 150 μg ml^{-1}; spectinomycin (Spec), 100 μg ml^{-1}. Plating of murine lavage fluid was done on CHROMagar StrepB agar plates (DRG, CHROMagar).

2.2.2 Mouse model of vaginal colonization

Experiments were performed as previously described [50, 63, 64]. Female CD1 mice aged 6-10 weeks were used for all experiments. Briefly, mice were administered an intraperitoneal (IP) injection of 0.5 mg β-estradiol valerate (Acros Organics) suspended in 100 μL filter-sterilized sesame oil (Sigma). IP estradiol synchronizes the estrus cycle of the mice. 24 h later, mice were

inoculated with 10^7 CFU of bacteria in 10 µL PBS intravaginally using a pipet tip. On days 1, 2, 3, and 5, the vaginal lumen was washed with 50 µL sterile PBS using a pipet tip to flush the liquid into the vaginal vault 6-8 times. Vaginal lavage fluid was then collected and put on ice for no more than 30 minutes prior to performing serial dilutions in PBS. Dilutions were plated on CHROMagar StrepB plates, which allow the growth of GAS with a purple hue.

2.2.3 RNA collection

RNA collection from the murine vaginal tract was done as previously described [52]. 50 µL of vaginal lavage fluid from ten colonized mice for 48 hours was combined (500 µL total) and put into a tube containing 1 mL Trizol LS Reagent (Ambion) and placed on ice for no more than 30 minutes. Samples were centrifuged at 14,000 x g for 1 minute and the Trizol Reagent was removed. The Ambion RiboPure Bacteria Kit (Thermo Fisher AM1925) was used to purify total RNA from the resulting pellets according to the manufacturer protocol. For lysis, the pellets were resuspended in 250 µL of RNAWiz and mixed with glass beads. The samples underwent 10 minutes of bead beating in a MiniBeadbeater (BioSpec) set to homogenize. DNA was removed from the total purified RNA using DNaseI treatment for 30 minutes at 37º C. For the preparation of total RNA from planktonic cultures, bacteria were grown overnight in THY medium. Cultures were diluted 1:50 in freshly prepared CDM medium and grown to an OD_{600} of 0.3-0.6. Cultures were centrifuged at the same OD_{600} and RNA was prepared and treated with DNaseI as described above for vaginal lavage without the addition of Trizol LS Reagent.

2.2.4 Detection of eukaryotic and ribosomal RNA from total RNA

Vaginal total RNA samples were depleted of both eukaryotic and ribosomal RNA and planktonic samples were depleted of only ribosomal RNA as previously described [52]. Eukaryotic

RNA was depleted using the MICROBEnrich kit (Thermo Fisher AM1901) and ribosomal RNA was depleted using the MicrobExpress kit (Thermo Fisher AM1905) according to the manufacturer instructions. Depletion of eukaryotic and ribosomal RNA as well as RNA quality was determined using a TapeStation 2200 (Aglient) and a Qubit RNA High Sensitivity fluormeter (MBL) by the DNA Services Facility at the University of Illinois at Chicago Center for Genomic Research. If analysis showed remaining high quantities of ribosomal RNA, the MicrobExpress kit protocol was repeated to retreat samples.

2.2.5 Preparation of cDNA libraries for RNASeq

cDNA RNASeq libraries were prepared as previously described [52]. Because of the small amount of input RNA, cDNA libraries were generated with 10-400 ng of input RNA using the KAPA Stranded RNA-Seq library (KAPABiosystems, KR0934) according to manufacturer instructions. Briefly, eukaryotic and ribosomally-depleted RNA samples were fragmented in fragmentation buffer at 94º C for 6 minutes. Random primers were used to synthesize the first strand cDNA before second sd synthesis, marking, and the addition of a poly-A tail. Illumina adapters were ligated to the fragments and the subsequent library was cleaned up using DNA purifier magnetic beads (101 Bio, P920-30). The library was amplified for 10 cycles followed by an additional magnetic bead cleanup. Libraries underwent quality control and quantification on the Tapestation 2200 (Agilent) as above. 20 µL of 50 nM libraries were sequenced and analyzed at the University of Chicago Genomic Facility with 8 samples multiplexed per RNASeq lane.

2.2.6 RNA sequencing analysis

The quality of reads was assessed using FasQC v0.11.2 (www.bioinformatics.babraham.ac.uk/projects/fastqc/) and reads were mapped to the

Streptococcus pyogenes NZ131 genome. Samtools v0.1.19 [30] was used to down-sample all *in vitro* mapped samples. Cufflinks v2.2.1 [31] was used to assembly and quantify transcripts to the NZ131 genome and assemblies were merged using Cuffmerge and wrapped in nCufflinks v2.2.1. Quantification of transcripts was done using Cuffquant and featureCounts [32]. Differentially expressed genes (DEGs) with a false discovery rate (FDR) corrected p-value of 0.05 or less and at least a two fold change were identified using FPKM-based Cuffdiff and count-based edgeR methods [33].

2.2.7 Creation of mutant and complemented NZ131 strains

NZ131 ΔhupY::aphA3 creation. The NZ131 Δ*hupY*::*aphA3* strain was created as described previously [52]. Briefly, approximately 1000 bp upstream (primers LC149 *Pst* / LC150) and downstream (primers LC151/LC152 *NotI*) of *spy49_0661* (*hupY*) were amplified by PCR. Amplification products were fused in a subsequent PCR reaction using outside primers LC149 *PstI* and LC152 *NotI*. The fusion product and temperature sensitive pJC159 (Cm^R) vector were digested with *PstI* and *NotI* restriction enzymes and ligated together. Using inverse PCR, the plasmid was replicated (primers LC153 *MluI* / LC154 *MluI*. The *aphA3* kanamycin resistance gene was amplified from pOSKAR using primers JC292 *MluI* /JC304 *MluI*. The resulting linear fragments were digested with *MluI*, ligated together and electroporated into competent BH10C *E. coli* cells. Colonies were screened on LB plates supplemented with Cm and Kan at a permissive temperature (30° C). Plasmid was collected and sequenced to ensure correct assembly and then electroporated into competent NZ131 cells. A temperature-dependent selection process that has been previously described was used to isolate NZ131 Δ*hupY*::*aphA3* cells [65]. Cells containing the deletion plasmid were grown at 30° C and then shifted to a higher temperature (37° C) and plated on Cm/Kan THY plates to select for plasmid integration. Following integration, cells were

passaged in antibiotic free THY at 30° C twice daily for 4 days to allow for plasmid excision. Mutants were then selected on THY Kan at 37° C and screened for loss of Cm resistance. Colonies that grew at 30° C in Kan but not Cm were sequenced to confirm the proper genotype. *pLC007 complementation plasmid.* The complementation plasmid pLC007 was created by amplifying the *hupY* gene from NZ131 genomic DNA using primers LC184 / LC185. Plasmid pJC303, which contains a constitutive *recA* promoter digested using *NotI* and *BamHI*. The digested plasmid and amplified *hupY* genes were combined in a Gibson assembly reaction using 2x NEBuilder Hifi DNA Assembly mix. The assemble plasmid, pLC007, was electroporated into BH10C *E. coli* cells and plated on LB plates containing spectinomycin. Plasmid was purified, sequenced, and electroporated in competent NZ131 Δ*hupY*::*aphA3* cells and the resulting cells were plated and propagated on THY Kan, Spec plates.

2.2.8 HupY cloning, purification and heme binding

The construction of HupY-His expression vectors was accomplished by TOPO® directional cloning according to the manufacturer instruction (Invitrogen, K101-01). The *hupY* gene was amplified from GAS NZ131 chromosome using the ZE435/ZE436 primer set (Table S3, Appendix A.3) and introduced into the pET101/D-TOPO vector (Table S2, Appendix A.2). The resulting plasmid, pZZ1, codes for a HupY-His tag fusion protein expressed from the T7 RNA polymerase promoter. The recombinant HupY protein was produced and purified from *E. coli* as previously described [56]. Briefly, cells were harvested and resuspended in 20 mM Tris-Cl, 100 mM NaCl, 0.1% Triton X-100, pH 8.0, with the addition of 0.5 mg/mL lysozyme and protease inhibitor (Complete mini-EDTA-free, Roche), and lysed by sonication. The cell debris was removed by centrifugation and the cleared lysate was applied to a HisTrap HP affinity column (GE Healthcare) and purified using a FPLC. Heme titration and differential spectroscopy of HupY-heme complex

was conducted as described [30]. In short, haemin chloride (in DMSO) was added in increasing concentrations to 17 µM apo-HupY (in PBS), the solution was allowed to incubate at room temperature for five minutes prior to UV-visible scan. PBS with equal amounts of heme served as the blank. The differential UV–visible absorption spectrum was acquired at room temperature by UV-Vis spectrophotometer (Beckman Coulter, DU730).

2.2.9 GAS growth in the presence of streptonigrin or using human serum or hemoglobin as iron source

Sterptonigrin killing assays: Streptonigrin stock solutions (Sigma, 2mg/ml) were prepared in chloroform and methanol at 1:1 (v/v) and kept in -20° C up to six months. In each experiment, overnight GAS cultures grown in THYB were used to inoculate fresh broth (OD_{600} of 0.01) containing streptonigrin in various concentrations. The culture optical density was determined after 20 hours incubation at 37° C. *Serum and hemoglobin use assays*: New 1M Dipyridyl (2,2' Dipyridyl, Acros Organics) prepared in absolute ethanol and 1mM human hemoglobin (Sigma) prepared in saline (and filter sterilized) were used in all experiments. Fresh THYB containing 3 mM Dipyridyl and increasing amounts of pooled normal human serum (Innovative Research) or human hemoglobin were inoculated with overnight GAS cultures grown in THYB (OD_{600} of 0.01). The culture optical density was determined after 20 hours incubation at 37° C. In all experiments, bacteria were grown statically in 6 ml broth in 15 ml screw cap Falcon tubes. The WT and *ΔhupY* strains were grown in THYB without antibiotics as the strains were observed to be stable without selection in antibiotics (unpublished data and Table S2). The complemented strain (*ΔhupY/pLC007)* was cultivated with spectinomycin (100 µg /ml) during the first overnight growth. The presences of the antibiotic markers (kanamycin for *ΔhupY* and spectinomycin for the

complementation plasmid) was confirmed by viable counts using the appropriate antibiotics at the end of each experiment.

2.2.10 qRT-PCR

Quantitative reverse transcriptase PCR was done to validate RNASeq data and test the polarity of the Δ*hupY* GAS and GBS mutants on the downstream *hupZ* gene. qPCR primers are listed in Table S3, Appendix A.3. RNA was collected and treated with DNaseI as above. cDNA was then prepared using the iScript cDNA synthesis kit (Bio-Rad) according to manufacturer's instructions. cDNA was amplified using random hexamers and diluted 1:5 prior to qPCR. For GAS, the *proS* (primer pair LC082/LC083) gene and for GBS, *gyrA* (primer pair LC060/061), were used as housekeeping reference genes. Amplification was done using iTaq Universal SYBR Green Supermix or SSoAdvanced Universal SYBR Green Supermix (Bio-Rad) in a CFX96 Real Time Detection System (Bio-Rad). Samples were run in triplicate technical replicates and at least duplicate biological replicates.

2.2.11 Ethics statement

All mouse experimentation was approved by the University of Illinois at Chicago Animal Care and Use Committee (ACC) and IACUC under protocol #16-068. All animal work was carried out using accepted veterinary standards in accordance with the Animal Care Policies of the University of Illinois at Chicago Office of Animal Care and Institutional Biosafety Committee and IACUC. This institution has Animal Welfare Assurance Number A3460.01 on file with the Office of Laboratory Animal Welfare, NIH.

2.3 Results

2.3.1 Extensive transcriptional remodeling

Mice were vaginally inoculated with GAS strain NZ131 and, after 48 hours of colonization, vaginal lavage samples containing GAS cells were collected for RNASeq analysis. Vaginal carriage samples were compared to log-phase NZ131 bacteria grown statically at 37 ºC in chemically defined laboratory medium (CDM). Of the 1686 NZ131 genes with transcripts detected, 581 genes, were differentially expressed with a False Discovery Rate (FDR) corrected *p* value of ≤ 0.05. Of those, 491 genes had a fold change of ≥2-fold (**Table S1, Appendix A.1**) and **Figure 1**). To validate RNASeq findings, qualitative Real-Time PCR was done on two genes shown to be downregulated in the vaginal tract (**Figure S1, Appendix B.1**).

Like the previously published transcriptome of GBS in the murine vaginal tract [52], there are extensive changes in metabolic pathways associated with host colonization in GAS. Similar to GBS, GAS cells significantly down-regulated the fatty acid biosynthesis *fab* operon (*spy49_1359c-1371c*), ostensibly resulting in increased long-chain fatty acids. In other species of streptococci including *Streptococcus gordonii* and *S. salivarius*, an increase in long-chain and mono-unsaturated fatty acids was observed in response to acidic pH and hypothesized to be an adaptive response to acidic environments [66] (**Table S1, Appendix A.1)** and [52]).

Both GAS and GBS also highly upregulated homologous phosphotransferase systems essential for the import of a variety of sugars such as ascorbate (*spy49_0154-1055* and *sak_1833-*183), mannose (*spy49_0834-0836* and *sak_1908-1910*), maltose (*spy49_1028-1030* and *sak_1475-1477*), and galactose and fructose (*spy49_1327c-1329c* and *sak_1893-1895*). Genes and operons involved in degradation of sugars such as ascorbate (*spy49_0156-0158, 0160* and

sak_1820, 1830-1832), galactose (*spy49_0673, 1322c-1323c, 1325, 1326c* and *sak_0345-346, 1878-1890*), and malate (*spy49_0864, 0865c* and *sak_1651 and 1878*) were often also upregulated in both organisms (**Table S1, Appendix A.1)** and [52]).

Not all homologous metabolic pathways were similarly regulated between GAS and GBS. During GBS colonization, genes involved in the *de novo* purine biosynthetic pathway *purCLFMNH (sak_0057, sak_0059-0061, sak_0063)* and *purDEKB (sak_0076-0078* and *sak_0080)* were upregulated between 2 and 25 fold [52]. Interestingly, the purine biosynthesis pathway in GAS *(spy49_0020-0025, spy49_0027-0029, and spy49_31)* was significantly down-regulated during colonization compared with log-phase growth in the same medium (**Table S1, Appendix A.1**). Although GAS and GBS are closely related species that both colonize mucosal surfaces, their metabolic profiles, while similar, demonstrate some distinct transcriptional changes associated with vaginal colonization. Growth phase is an important factor determining transcriptional profiles. Growth in the vaginal tract does not equate to log phase growth in liquid culture, which likely explains some of the observed large-scale transcriptional shifts. Some genes highly upregulated during stationary phase in liquid culture are also upregulated in the vaginal tract. *speB* and *mf* for example, are known to be upregulated during stationary phase liquid growth and expressed at lower levels during other phases of growth [67]. In the vaginal tract compared to log-phase growth, *speB* and *mf* expression are highly upregulated (**Table S1, Appendix A.1**). In contrast, there are also genes like *clpE*, that have previously been shown to be upregulated during stationary phase compared to log phase growth [68] but are down-regulated during growth in the vaginal tract compared to liquid growth (**Table S1, Appendix A.1**). This indicates that cells colonizing mucosal surfaces cannot be characterized by typical liquid growth phases. This was previously observed for mucosal colonization in GBS as well, where colonization of the vaginal

tract showed some genetic signatures of stationary phase growth but some characteristics of different phases of liquid growth [52].

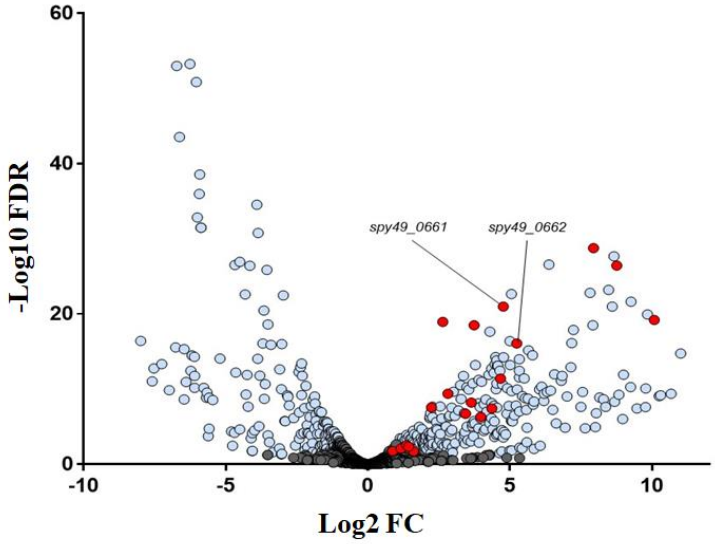

Figure 1 Differentially expressed genes during GAS growth in vivo

Volcano plot showing transcriptomic changes in GAS genes during growth in liquid versus colonizing the murine vaginal tract with – Log_{10} False Discovery Rate (FDR) adjusted *p* value on the y axis and Log_2 fold change during murine vaginal growth on the x axis. Genes in blue were significantly differentially expressed with an FDR adjusted *p* value of < 0.05 and a fold change of >2. Genes known to be regulated by the metal regulator MtsR are shown in red and *hupY (spy49_0661)*/*hupZ (spy49_0662)* are specifically marked.

Table 1 Genes repressed by MtsR with differential regulation in the vaginal tract

Gene	Name	Description	Fold change[a]	P value[b]
spy49_0247	pbp7	D-Alanyl–D-alanine carboxypeptidase	2.4	0.00565
spy49_0339	nrdF.2	Ribonucleotide reductase	432.03	3.60E 27
spy49_0340	nrdI	Ribonucleotide reductase stimulatory protein	1079.15	6.20E 20
spy49_0341	nrdE.2	Ribonucleotide diphosphate reductase	245.77	1.80E 29
spy49_0381	mtsA	Metal ABC transporter, substrate binding	6.23	1.10E 19
spy49_0382	mtsB	Metal ABC transporter, ATP binding	1.83	0.00791
spy49_0383	mtsC	Metal ABC transporter, permease	2.24	0.0007
spy49_0661	hupY	Adhesion and heme receptor	27.26	1.10E 21
spy49_0662	hupZ	Enzyme, heme degradation	37.69	8.40E 17
spy49_1159c	manB	Phosphoglucomutase, phosphomannomutase	13.35	3.20E 19
spy49_1374c	dnaK	Chaperone protein	3.05	0.01803
spy49_1395c	siaH	ECF transporter, A component	2.56	0.00283
spy49_1396c	siaG	ECF transporter, T component	2.7	0.00464
spy49_1397c	siaF	ECF transporter, S component	4.71	2.70E 08
spy49_1398c	siaE	Putative ABC transporter	7.03	4.10E 10
spy49_1400c	siaD	Putative ABC transporter	12.49	6.10E 09
spy49_1401c	siaC	Heme ABC transporter, ATP binding	15.68	4.90E 07
spy49_1402c	siaB	Heme ABC transporter, permease	10.82	1.90E 07
spy49_1403c/ 1404c[c]	siaA/shp	Heme ABC transporter, substrate binding/streptococcal heme-associated protein	20.58	3.80E 08
spy49 _1405c	shr	Streptococcal hemoprotein receptor	25.46	4.10E 12
spy49_1687c	prsA	Foldase	144.61	7.43E 17

[a]*Fold upregulation in the vaginal tract compared to liquid growth.*

[b]*False discovery rate-corrected P value.*

[c]*Annotation of NZ131 incorrectly lists spy49_1403c (siaA) and spy49_1404c (shp) as a single fused gene product rather than two distinct genes.*

2.3.2 The MtsR regulon of both GAS and GBS

Notably, some of the most highly upregulated genes during vaginal carriage include those previously shown to be directly regulated by MtsR. MtsR regulates genes involved in iron and heme metabolism and this regulation is dependent on the concentration of iron and manganese. The MtsR regulon includes the metal transporter *mtsABC (spy49_1554-1556)* and the 10 gene streptococcal iron acquisition locus (*sia*), which includes *shr (spy49_1405c*), *shp* (*spy49_1404c*), and *siaA-siaH (spy49_1395c-1398c, 1400-1403c)* [53, 69], all of which are significantly upregulated between 2.5 and >25 fold during growth in the vaginal tract (**Table 1 and Figure 1**). Annotation of NZ131 incorrectly lists *siaA* and *shp* as a single fused gene product, although they are actually separate genes [57]. Because of the annotation error, gene upregulation for *shp* and *siaA* were measured together over the course of the single transcript, which was highly upregulated. Because the genes are separate but coregulated, the upregulation of *shp* is inferred from RNASeq data.

In addition, MtsR has been shown previously to directly repress genes such as the *nrdF.2IE.2* operon *(spy49_0339-0341*), which is upregulated over 200-fold during vaginal colonization (**Table 1 and Table S1**) but does not regulate the related *nrdHEF* genes which are slightly repressed in the vaginal tract [54]. In total, at least 20 genes, about half of those previously shown to be repressed by MtsR, were significantly upregulated in our RNASeq data (**Table 1**).

Mining previously published transcriptomic data shows that GBS homologs of genes in the GAS MtsR regulon including *mstABC* (*sak_1554-1556*) and *nrdF.2IE.2 (sak_499-501)*, were similarly upregulated during vaginal colonization and contain putative MtsR promoter DNA binding sites (**Figure 2B** and [52]). Consensus promoter sequences match previously published

known MtsR binding sites [54]. It is likely that the MtsR regulon in GBS is similar to GAS and previous transcriptomic data [52] as well as this study suggest that the regulon is de-repressed during streptococcal host colonization (**Table 1 and Figure 1**).

Transcription of MtsR-regulated *spy49_0662*, also known as *hupZ*, as well as the gene immediately upstream, *spy49_0661*, are both increased during vaginal colonization (**Figure 1, Figure 2A, and Table 1**). Previous RNASeq data from GBS strain A909 colonizing the vaginal tract also showed significant upregulation of the homologous *hupYZ* gene pair [52] and a putative MtsR binding site is located upstream of *spy49_0661* in both organisms (**Figure 2B**). In addition, the MtsR-regulated *nrdF.2IE.2* operon is located adjacent to the homologous gene pair in GBS (**Figure 2A**).

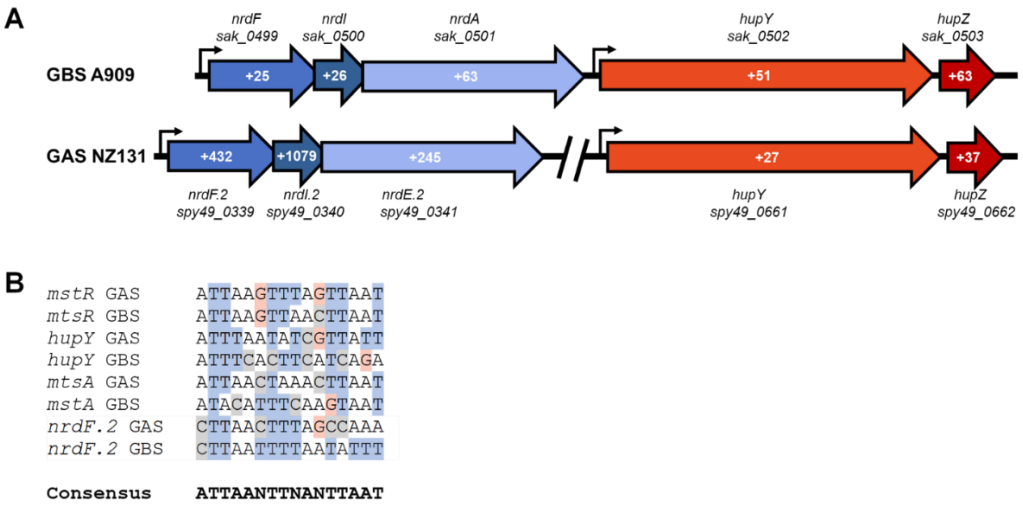

Figure 2 Differential regulation of MtsR-regulated operons in GAS and GBS and MtsR-regulated promoter alignment

(**A**) Select MtsR-regulated operons of GAS and GBS are shown. Red genes are *hupYZ* homologs and blue genes are *nrdF.2I.2E.2* homologs. Fold change during *in vivo* growth is shown in white.

Values from GBS A909 were previously reported [52]. (**B**) Promoter alignment of select MtsR-regulated genes in both GAS and GBS.

2.3.3 HupY protein binds heme in vitro

spy49_0661 had previously been designated *lrrG* in GBS [59] because of its leucine rich repeat region. GAS and GBS LrrG homologs have been demonstrated to be important adhesins that play a role in infection [59, 60]. HupZ can degrade heme and thus may free iron from heme inside the GAS cell [56] but, as it is a cytoplasmic protein, it does not have the ability to import heme on its own. To begin testing if Spy49_0661 contributes to heme metabolism in GAS, we cloned and purified the protein. HupY did not exhibit significant absorption other than at 280 nm (**Figure 3**, 0 μM heme) indicating it was purified from *E. coli* in the apo form. *In vitro* heme binding was tested by titration of the apo protein with increasing amounts of free heme. A growing absorbance band with maximum at 414 nm appeared in the resultant solution with incremental addition of heme (**Figure 3**). The absorption maximum at the Soret region (390–430 nm) demonstrated by HupY following incubation with heme is characteristic of protein-bound heme and is distinguishable from that of free heme in solution [56]. Plotting the differential absorbance at the Soret peak as a function of heme concentration (**Figure 3**) indicated that heme-binding was dose dependent, saturable and with a stoichiometry of 3:1 (protein to heme) indicating that Spy49_0661 can bind heme *in vitro*. We designate this gene *hupY* (heme utilization protein Y) based on its proximity to *hupZ* and its role in heme utilization.

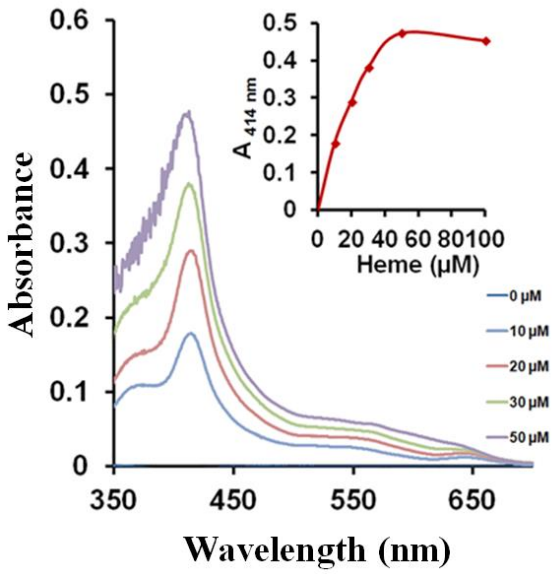

Figure 3 Differential absorption spectroscopy of heme-HupY complex

An increase of heme bound to HupY (17 µM) as increasing concentrations of heme were added to the protein is shown by the sharp peak at 414 nm. The insert displays the changes in absorbance at 414 nm plotted against heme concentration. The data are representative of at least two independent spectroscopic analyses, 0 µM line at axis.

2.3.4 ΔhupY cells have lower intracellular concentrations of iron and impaired ability to use human serum and hemoglobin as sole iron sources compared to wildtype (WT) cells

To test the role of HupY in iron metabolism *in vivo*, a deletion of *hupY* was created in GAS strain NZ131. Strains were tested for their ability to resist killing by streptonigrin, an antibacterial whose potency depends on the levels of intracellular iron [53, 70]. The *hupY* mutant was able to grow to an OD_{600} of 1.0 in the presence of high levels (3.5 µM) streptonigrin. At these concentrations, little to no growth was observed in WT NZ131. The addition of *hupY* on a plasmid under a constitutive promoter was able to partially restore the killing phenotype seen in WT cells

(**Figure 4**). This indicates that the Δ*hupY* mutant strain has lower intracellular iron concentrations than the WT strain when grown in THYB.

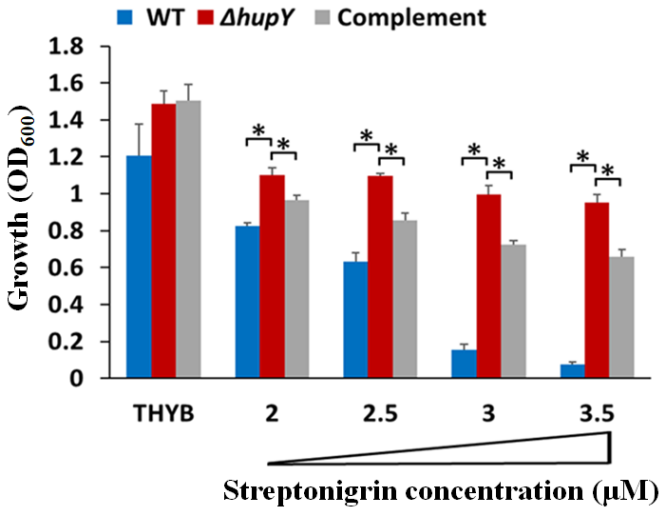

Figure 4 HupY affects intracellular iron concentrations

Growth (20 h) of an NZ131 wildtype (blue), Δ*hupY* mutant (red) and complemented (Δ*hupY/pLC007*, gray) strains in THYB or in THYB containing streptonigrin. The data are from two independent experiments done in technical triplicates with standard deviation shown. The asterisk indicates significance (p <0.05, Student's t-test, equal variance).

To test if HupY contributes to the use of heme iron by GAS, THYB medium was treated with dipyridyl, a liposoluble iron chelator. Human serum or hemoglobin were then added to the medium and the ability of GAS strains to grow in these media was tested. Addition of human serum restored the growth of WT NZ131 in the dipyridyl-containing THYB. This ability was significantly decreased in the Δ*hupY* mutant strain and could be complemented (**Figure 5A**). This indicates that the Δ*hupY* strain is impaired in its ability to obtain iron from human serum. Similarly,

human hemoglobin was able to support the growth of WT GAS while the Δ*hupY* mutant had a severe growth defect when growing in hemoglobin as the sole iron source (**Figure 5B**).

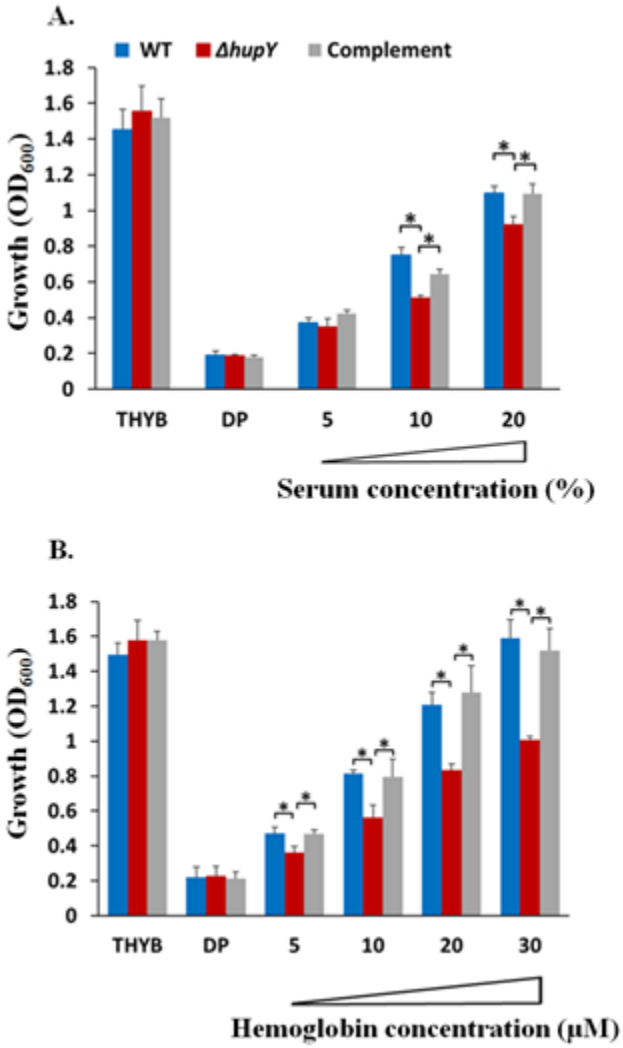

Figure 5 *ΔhupY* mutants are impaired in growth with serum or hemoglobin as the sole iron source

Growth (20 h) of an NZ131 wildtype (blue), Δ*hupY* mutant (red) and complemented (Δ*hupY/pLC007*, gray) strains in THYB, THYB with dipyridyl (DP), or THYB-DP supplemented with human serum (5-20 % final volume, (**A**) or human hemoglobin (**B**). The data are from two

independent experiments done in technical triplicates with standard deviation shown. The asterisk indicates significance (p <0.05, Student's t-test, equal variance).

2.3.5 HupY plays an important role in vaginal colonization by both GAS and GBS

HupY homologs were previously suggested to serve as adhesins with important roles in binding to epithelial cells [59]. We hypothesized that HupY would be important for mucosal colonization of the murine vaginal tract. To test this, mice were inoculated with WT NZ131, an isogenic Δ*hupY* mutant and a mutant strain containing pLC007, a plasmid containing a copy of NZ131 *hupY* under the control of a constitutive promoter. Initial inoculation and day 1 colonization levels were not statistically different between these strains. By day 2 of colonization, the mutant strains were impaired in colonization and by days 3 and 5, the mutant strains colonized the mice at significantly lower levels than the WT or complemented strains (**Figure 6A**).

Because the *hupY* homolog in GBS is closely related and also upregulated in the vaginal tract [52], we hypothesized that this gene would also play a role in colonization of the vaginal tract by GBS. Like GAS, a GBS Δ*hupY* mutant is impaired in colonization of the vaginal tract. The mutant strain was able to be complemented, at least partially, using the GAS *hupY* gene (pLC007), indicating that the heme binding and/or attachment phenotype is likely conserved between GAS and GBS (**Figure 6B**).

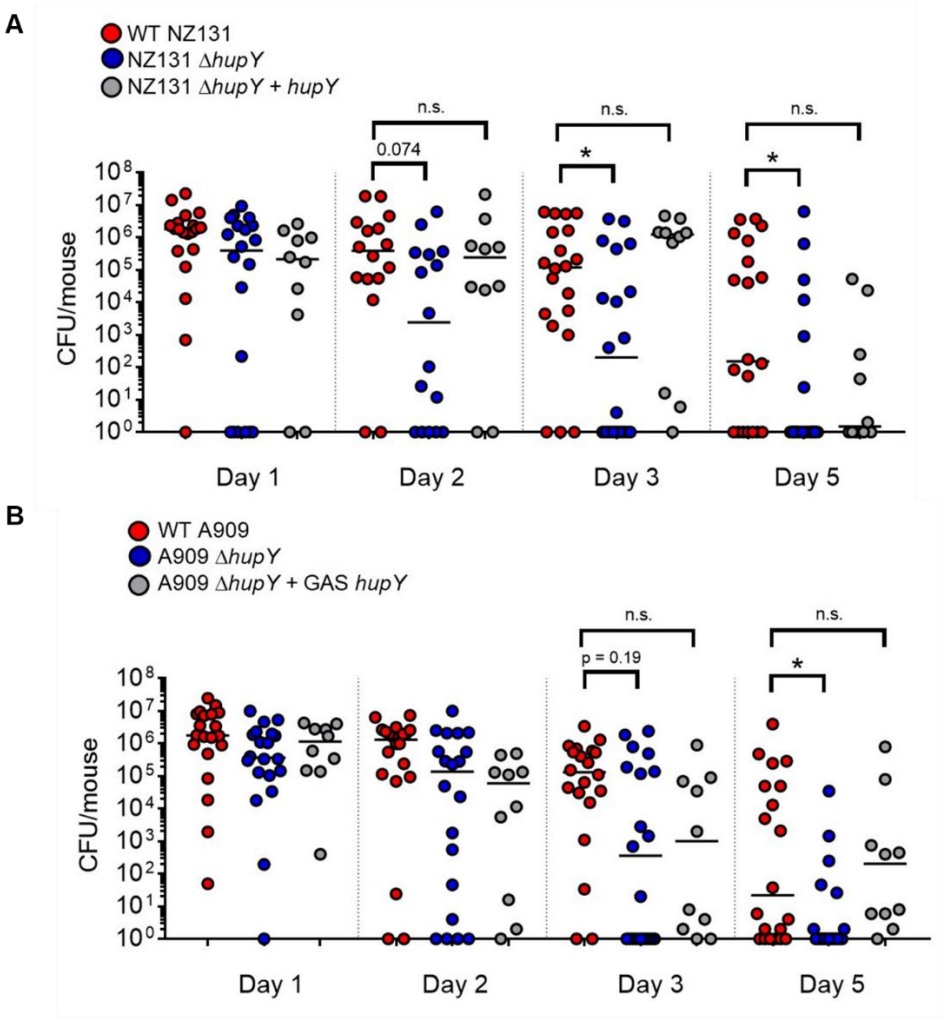

Figure 6 *ΔhupY* mutants in both GAS and GBS are impaired in their ability to colonize the murine vaginal tract

WT and isogenic Δ*hupY* mutants in GAS (**A**) or GBS (**B**) were used to colonize the murine vaginal tract. In both cases, the GAS *hupY* gene was used to complement the mutant strains. Both NZ131Δ*hupY* and A909Δ*hupY* mutants were attenuated for vaginal colonization compared to WT GAS and GBS and both mutants were able to be at least partially complemented by the addition of GAS *hupY* on a plasmid. Statistical significance was assessed using a one-way ANOVA and non-parametric Kruskal Wallis test; the asterisk indicates significance (p <0.05), n.s. not significant.

2.4 Discussion

Bacteria must alter transcriptional programs to survive and adapt to changing environments. In this study, we analyzed the transcriptome of GAS colonizing the murine vaginal tract. These data provide a new and important look at the genetic regulation of various metabolic and virulence pathways in GAS during mucosal carriage. With over one quarter of the genome differentially expressed during mucosal carriage compared to liquid culture, clearly transcriptional remodeling during colonization is extensive.

Comparing the GAS vaginal transcriptome to the recently published GBS vaginal transcriptome offers much insight into the similarities and differences in the way these two related organisms adapt to a mucosal environment. While many genes and pathways involved in metabolic processes were similarly regulated in GAS and GBS there were also many pathways such as purine biosynthesis, that were upregulated in one species and down regulated in the other (**Table S1 (Appendix A.1)** and [52]). These two species obviously share many similarities in terms of adapting to the vaginal environment, but some distinct transcriptional differences are also observed. Comparing transcriptomic profiles from organisms collected from the same model system provides important insight into the differing colonization rates and infections caused by these organisms at the vaginal mucosa.

One striking observation from this data is that many genes in the MtsR regulon are highly activated during GAS colonization of the murine vaginal tract (**Table 1**). MtsR, an important regulator of metal homeostasis, mediates repression of metal acquisition genes in GAS including genes involved in heme utilization and iron and manganese transport. Although GBS also contains an MtsR homolog, much less is known about MtsR regulation in GBS. Examining the previously

published vaginal transcriptome, homologous genes with potential MtsR binding sites are also de-repressed during GBS colonization (**Figure 2** and [52]).

MtsR was first described as a DtxR family regulator repressing expression of the streptococcal iron acquisition (*sia*) operon in the presence of high levels iron and manganese [53]. It was later shown that MtsR controls the expression of 64 genes in GAS including many that impact iron and heme metabolism. MtsR mutants have been shown to be attenuated for virulence in zebrafish infection models [53] and MtsR has also been shown to affect transcription of important GAS virulence factors including *mga*, *emm49*, and *ska* via direct binding to promoter regions [54].

Iron is an essential nutrient and heme is a major source of iron for organisms growing in the human host. To use heme as an iron source, bacteria must be able to bind, transport, and utilize the iron present in heme. In GAS, the surface receptor Shr is important for iron uptake as it binds to heme-containing proteins like hemoglobin and myoglobin, sequesters the heme and transfers it to another surface receptor, Shp and then to the SiaABC ABC transporter system for internalization (**Figure 7** and [30, 53, 71-73]). Both Shr and Shp contain NEAT (near iron transporter) heme binding domains found in heme binding proteins of other Gram-positive bacteria such as the iron-regulated surface determinant (Isd) proteins of *Staphylococcus aureus* [58]. In Shr, NEAT1 and NEAT2 are separated by a leucine rich repeat domain [30]. *shr*, *shp*, and the *siaA-H* genes are all present in a single operon controlled by MtsR and all were found to be de-repressed during colonization of the vaginal tract by GAS.

In iron-complete medium, *shr* is expressed more highly during log phase growth in liquid culture and expression is decreased during stationary phase, (Eichenbaum, unpublished results).

Starving the cells for iron, however, increases further *shr* transcription during log phase due to MtsR depression [54]. In our data, *shr* expression is higher on the mucosal surface than during log phase growth in liquid culture, consistent with iron limitation conditions in the mucosal surfaces. Thus, it is likely that the observed up-regulation of these genes is associated with iron availability in the mucosa rather than the difference in growth phase of the two conditions being compared by RNASeq.

spy49_0661, here renamed *hupY*, and the gene immediately downstream of it, *hupZ*, are also negatively regulated by MtsR in GAS and a putative MtsR binding site is found upstream of *hupYZ* in both GAS and GBS (**Figure 2B** and [54]). *hupYZ* are both significantly upregulated during vaginal colonization by both GAS and GBS (**Figure 2** and [52]). HupZ was recently described as a novel GAS enzyme that binds heme and is involved in heme biotransformation *in vitro*. Interestingly, HupZ which belongs to a group of atypical heme degrading enzymes, does bind and degrade heme although it is missing key residues found in this protein family [56, 74]. As a small cytoplasmic enzyme, HupZ does not appear able to transport heme into the cell and would thus rely on other heme binding and transport proteins. Although complementation indicates that the observed phenotypes can be attributed to HupY, because *hupYZ* appear to be under the control of a single promoter, we tested whether the allelic exchange of *hupY* with *aphA3* (Kan^R) affected expression of *hupZ*. qRT-PCR data showed no significant change in the expression of *hupZ* between the WT GAS or GBS and the *ΔhupY* strains (Figure S2).

HupY (Spy49_0661 in NZ131 GAS and SAK_0502 in A909 GBS), previously referred to in the literature as LrrG, was initially identified as a leucine rich repeat protein and putative surface adhesin. The protein sequences of the Spy49_0661 and SAK_0502 homologs in GAS strain NZ131 and GBS strain A909 are 72% identical and both contain an LPXTG motif and surface

localization has been observed in both GAS [60] and GBS [59, 75] homologs. Both have 15 22-amino acid leucine rich repeat regions matching the consensus sequence for bacterial leucine rich repeat proteins (LRRs) [59, 76]. The proteins are related to the internalins InlA and InlB from *Listeria monocytogenes,* which are important for bacterial adhesion to host surfaces via the E-cadherin receptor and subsequent invasion into host cells [77-79]. Because of their similarity to internalins and because LRRs are generally involved in protein-protein interactions, previous studies on the LrrG homologs focused mainly on their adherence properties.

SAK_0502 has been shown to bind to fixed HEp-2 lung epithelial cells and ME180 cervical epithelial cells although with a stronger preference for cervical cells over lung cells [59]. Subsequent studies demonstrated binding to the human scavenger receptor gp340 by both GAS and GBS HupY homologs [80]. gp340 is expressed by immune cells and epithelial cells including genital tract cell lines such as VK2E6E7 vaginal epithelial cells and HEC1A endometrial carcinoma cells and has been shown to be important for HIV transmission in the genital epithelium [81]. Based on this data, it is likely that HupY serves an adhesive function in the vaginal tract. HupY homologs have also been proposed as potential vaccine candidates as they are highly conserved and surface-expressed proteins [59, 60, 80]. Immunization against the HupY homologs protected against lethal challenge with GAS, GBS, and *Streptococcus equi* ssp. *epidemicus* species [59, 60, 82].

Adhesins have been known to have alternative functions as in the case of the GBS protein Lmb that is involved in both adherence to human laminin [83] and invasion into brain endothelial cells [84] as well as zinc uptake [85]. Similarly, Shr enhances GAS attachment to laminin in addition to its function in heme uptake [86]. Based on the genetic relationship with *hupZ* and direct

repression by MtsR, we hypothesized that HupY may have a dual role in adherence and heme uptake and degradation as well.

Data presented here show that HupY is able to bind heme *in vitro* (**Figure 3**), providing evidence that it may serve as a heme receptor that helps transfer heme inside the cell to HupZ for degradation. In addition, NZ131Δ*hupY* cells are killed less efficiently by streptonigrin, an antibacterial compound that is preferentially toxic to cells with higher levels of intracellular iron, indicating that NZ131Δ*hupY* cells have less intracellular iron than WT and complemented strains (**Figure 4**). This provides evidence that HupY may not only bind heme but may also play a role in transporting it into the cell for use as a bacterial iron source. GAS cells were also tested for their ability to grow using hemoglobin or serum as a sole iron source. Δ*hupY* mutants had impaired growth under these conditions, indicating that HupY contributes to the ability of GAS to obtain heme iron from serum and hemoglobin.

Because *hupY* was highly upregulated in the vaginal tract and because of its observed properties as an adhesin, we tested the ability of GAS and GBS Δ*hupY* mutants to colonize the murine vaginal tract. Both GAS and GBS Δ*hupY* mutants were significantly impaired in their ability to colonize the vaginal tract. Complementing the mutation using the GAS *hupY* homolog restored the colonization phenotype in both GAS and GBS, indicating similar functions in both organisms (**Figure 6**). Although it appears that HupY is necessary for vaginal colonization, some questions remain to be answered. We have not yet elucidated whether decreased colonization levels are due to decreased adherence to mucosal surfaces or decreased survival due to inability to acquire iron from the host. In addition, this mucosal colonization has only been tested in the vaginal tract and remains to be examined at other mucosal sites streptococci are known to colonize such as the nasopharynx. In GBS the HupY homolog, SAK_0502, was found to bind preferentially to

cervical cell lines over lung cell lines [59]. It is possible that its role as an adhesin is host mucosal site-specific, while its role in heme binding and utilization is more universal. Further experiments to determine the potential interplay between the adhesion and iron homeostasis functions of HupY are currently underway.

Unlike heme receptor proteins like Shr and Shp that contain recognized NEAT domains, HupY does not contain any known heme binding domains. Leucine rich repeat domains are found in both HupY and Shr and could play a role in heme binding by a novel unknown mechanism. A full analysis of the protein structure and domains involved in binding both the host and heme is an important next step and will allow determination of whether these binding sites are localized to the same regions of the protein.

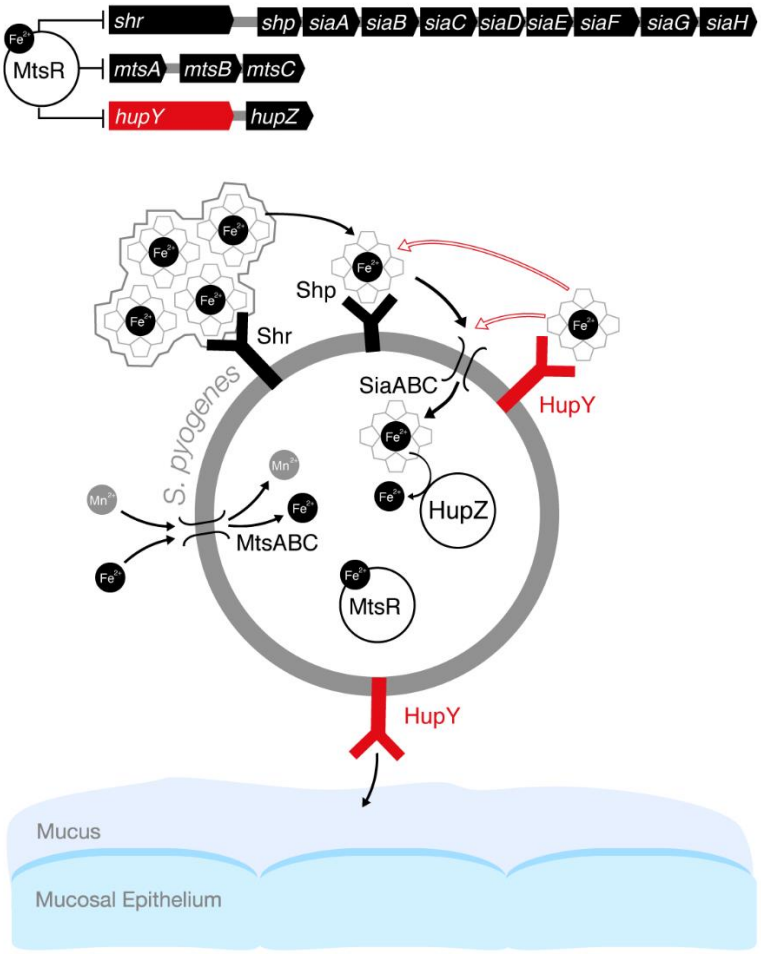

Figure 7 Model of the role of HupY in GAS colonization and heme utilization on mucosal surfaces

In the presence of high levels of iron, iron-bound MtsR represses a large number of genes including the *sia* operon which includes the genes for the *siaABC* heme importer as well as *shr*, and *shp* heme binding proteins. In addition, MtsR represses the manganese and iron *mtsABC* transporter, *hupZ* and *hupY*. MtsR also downregulates the *mtsABC* gene cluster in a manganese dependent manner ([69], not shown in the model). In iron deplete conditions such as on mucosal surfaces, MtsR repression is relieved, leading to upregulation of these operons. Shr captures heme (from host hemoproteins or the environment) and delivers it to Shp and subsequently to the SiaABC for import into the cell. Once inside the cell, iron can be liberated from heme by the HupZ enzyme.

HupY, coregulated with HupZ, is a surface protein that has the ability to bind heme. We propose that HupY binds heme to allow transport to HupZ, either through the Shp/SiaABC heme import pathway or another mechanism. Open arrows indicate possible heme transfer pathways. HupY also plays a role in mucosal colonization, possibly as an adhesin important for binding to host cells.

It also remains to be tested whether HupY plays a role in iron acquisition and utilization in GBS as well as GAS although all evidence would point to this. The presence of an MtsR binding site upstream of GBS *hupYZ*, the genetic neighborhood of the genes (**Figure 2**), and the fact that GAS *hupY* can complement the *in vivo* mutant phenotype in GBS (**Figure 6**) strongly indicate that these genes have similar functions in GAS and GBS.

Here we have identified a gene, *hupY*, previously thought to encode an adhesin in GAS and GBS, which serves additional functions important for GAS colonization including heme binding. Both *hupY* and *hupZ* as well as other members of the MtsR regulon are highly de-repressed during *in vivo* mucosal colonization in both GAS and GBS. Likely in conjunction with its co-regulated neighboring gene, *hupZ*, HupY acts as a heme binding protein involved in regulating intracellular iron levels.

3 CHAPTER II: A NOVEL HEME TRANSPORTER FROM THE ECF FAMILY IS VITAL FOR THE GROUP A STREPTOCOCCUS COLONIZATION AND INFECTIONS

3.1 Introduction

Group A Streptococcus (GAS) is a significant pathogen and a leading cause of human morbidity and mortality. The Gram-positive GAS is the etiological agent of common infections such as pharyngitis and impetigo. These simple episodes can lead to immune-based complications in susceptible individuals with severe outcomes, such as acute rheumatic fever, rheumatic heart disease (RHD), and post-streptococcal glomerulonephritis. GAS also produces rare but life-threatening conditions, including bacteremia, necrotizing fasciitis, and Streptococcal Toxic Shock Syndrome [1, 87]. Altogether, GAS is responsible for several million cases globally and claims approximately 500,000 lives annually [2]. RHD and invasive infections are the primary culprits in GAS related mortality [3, 7]. The development of a vaccine against GAS has met serious challenges due to hypervariability and cross-reactions with host epitopes. Hence, the control of GAS infections continues to rely on conventional antibiotics. Still, resistance to macrolides and clindamycin, which are used as an alternative [9] or together with β-lactams [10], is on the rise.

The establishment of infection requires pathogens such as GAS to successfully compete with the host for iron [88, 89]. GAS cannot obtain iron from the host ferric proteins, transferrin, or lactoferrin [89]. But, this β-hemolytic pathogen thrives on heme iron, and can readily remove heme from hemoglobin and other host hemoproteins [89]. The best-characterized heme uptake system in GAS is encoded by the 10-gene Sia operon [72]. The Sia mechanism consists of two surface proteins, Shr and Shp, and the heme ABC transporter, SiaABC. The remaining *siaDEFGH* genes

are yet to be described. Shr binds to hemoglobin on the surface, extracts the heme, and delivers it through the cell wall to Shp, using a shared heme-binding module named NEAT [30, 33]. A rapid and affinity-driven mechanism then mediates the transfer of heme from Shp to SiaA, the substrate-binding component of the SiaABC transporter, for import into the cytoplasm [34, 90, 91]. Shr, the first protein in the Sia heme-relay system, is important for virulence [57, 86] and serves as a protective antigen in both passive and active vaccination models [92]. The bicistronic operon, *hupYZ*, also contributes to GAS growth on heme iron. HupY is a cell-wall receptor that binds heme *in vitro* [93]. A *hupY* deletion mutant is impaired in the use of serum or hemoglobin as a source of iron and exhibits lower iron content when cultivated *in vitro*. The mechanism by which HupY captures heme from the surface and delivers it into the cytoplasm remains unknown. HupZ is a cytoplasmic enzyme that binds and degrades heme *in vitro* [56, 74]. The *sia* and the *hupYZ* operons are both negatively regulated by iron availability *via* the metal responsive regulator, MtsR [94]. Besides SiaABC, the only other iron-complex transporter reported in GAS is the SiuADBG/FtsABCD system. The SiuADBG/FtsABCD proteins consist of an ABC transporter that was implicated in the uptake of ferrichrome [35] as well as heme [36] and thus may exhibit broad specificity for iron compounds. In summary, three surface proteins and two conventional ABC transporters function in heme capture and import in GAS. This redundancy highlights the essentials nutritional role heme iron plays in GAS.

The energy-coupling factor (ECF) transporter family, is an unusual type of ABC importers that is widespread among Gram-positive bacteria [95]. ECF transporters are comprised of a small membrane-embedded protein that provides substrate specificity (S component/EcfS) and an ECF module consisting of a transmembrane protein (T component/EcfT), and a pair of similar or identical cytosolic ATPases (A component/EcfA) [96, 97]. The suggested import mechanism by

these non-canonical ABC transporters involves the toppling and repositioning of the S protein to facilitate substrate capture at the extracellular side and its release into the cytoplasm [95]. Hence, the S component is the only ECF component suggested to interact with the ligand. Twenty-seven different S families have been identified, each for a separate micronutrient (e.g., various vitamins, amino acids, queuosine, or trace metals, not including iron or iron complexes) [96, 98]. The ECF family is categorized into two groups. In Group I, a single S-component interacts with a specific ECF module, whereas, in the Group II system, multiple S components of unrelated sequence and various ligands, can form a complex with the same ECF module [95, 96]. Some S components, referred to as Solitary, do not have a recognized ECF module [99]. The genetic organization suggests that GAS *siaFGH* genes code for a Group I ECF system, in which all of the components are co-expressed and work exclusively together. The *siaFGH* genes are expressed in response to iron deprivation as part of the *sia* operon and along with the rest of the MtsR regulon. We hypothesize that *siaFGH* genes encode a novel heme import system that is imperative for the establishment of GAS infection.

3.2 Materials and methods

3.2.1 Strains, media, and growth conditions

The strains and plasmids used in this study are listed in Table 2, and primers are listed in Table 3. *Escherichia coli* (*E. coli*) were used for cloning and grown aerobically in Luria-Bertani (LB) medium at 37° C with shaking. GAS cells were grown statically at 37 °C in Todd-Hewitt broth (THY, Difco Laboratories) with 0.2% w/v yeast extract (THYB) or Chemically Defined Medium (CDM; SAFC Biosciences) [36]. When necessary, 100 μg/mL ampicillin, 100 μg/mL spectinomycin, 70 or 300 μg/mL kanamycin (for *E. coli* and GAS, respectively), or 500 μg/mL

erythromycin was added to the medium. All of the constructed chromosomal mutations are stable. Hence, antibiotics were used for strain construction and only when the strains were recovered from glycerol stocks.

3.2.2 Nucleic acid methods

We used the PureLink Genomic DNA Mini Kit (Invitrogen) to extract chromosomal DNA and the Wizard Plus Minipreps DNA Purification System (Promega) for plasmid DNA. DNA was amplified by PCR using the AccuTaq^{TM} LA DNA Polymerase (Sigma). DNA fragments were purified from agarose with the S.N.A.P. UV-free gel purification kit (Invitrogen). T4 DNA ligase (Roche) was used for ligation reactions. Restriction enzymes and DNA modifying enzymes were purchased from NEB and used according to the manufacturer's recommendations. Transformation and all molecular and genetic manipulations were performed according to the manufacturer's instructions and standard protocols [100, 101].

3.2.3 Plasmid construction

The plasmids and strains used in this study are described in Table 2 and the primers in Table 3. *Plasmid pHNG7*: A DNA fragment with the *siaFGH* genes and ~ 1Kb flanking region was amplified from NZ131 chromosome, with the primers ZE480/ZE481, and fused to pCR-XL-TOPO using the TOPO TA Cloning kit (Invitrogen) [102]. *Plasmid pHNG10:* A DNA fragment generated by inverse PCR from pHNG7 was cut with *Nhe*I and ligated to a PCR fragment encoding *aad9* gene (spectinomycin resistance), amplified from pJRS525 with the primers ZE408/ZE409 and digested with *Nhe*I. *Plasmid pHNG12:* A DNA fragment with the Δ*siaFGH::aad9* allele was amplified from pHNG10 with primers ZE451/ZE452, cut with *Cla*I, and ligated into pJRS700 [31, 36] linearized with *Cla*I. *Plasmid pNC111*: The *siaFGH* genes were amplified from NZ131

chromosome using the primers ZE836/ZE837 digested with *Pst*I, and ligated into pMSP3535 [103] cut with *Pst*I.

3.2.4 Construction of ΔsiaFGH mutant and complemented strains

GAS mutants were constructed by homologous recombination using a temperature sensitive shuttle vector and establish protocols. *ZE4950 (ΔsiaFGH::aad9 in NZ131):* Mutant construction involved the following steps: 1) Introduction and propagation of pHNG12 in NZ131 under the permissive conditions (i.e., growth at 30 °C with spectinomycin); 2) Selection for GAS clones with a chromosomally integrated pHNG12 on kanamycin at 37 °C; and 3) A screen for clones with a second homologous recombination using passages in broth at 30 °C followed by plating on kanamycin at 37 °C. Mutants were identified by replica plating. The mutation in clones with the kanamycin sensitive and spectinomycin resistance phenotype were confirmed by PCR analysis. The complemented ZE4952 strain was created by transforming pNC111 into ZE4950 background. *ZE151 (ΔsiaFGH::aad9 in MGAS5005) and ZE152 (wildtype rescue):* Plasmid pHNG12 was introduced into MGAS5005 and the mutant was selected as described for ZE4950. To isolate the wild type rescue strain, GAS was plated at 37 °C without antibiotics following the passages at 30 °C (Step 3 above), and cells that are sensitive to both kanamycin and spectinomycin were identified by replica plating. The genotypes of the mutant and the wildtype rescue strains were confirmed by PCR analysis.

3.2.5 Growth assays for streptonigrin sensitivity and use of hemoglobin iron

Streptonigrin sensitivity: Streptonigrin (Sigma) stock solutions (2 mg/mL) were prepared in chloroform and methanol at 1:1 (v/v) and stored at -20° C. In each experiment, fresh THYB

containing 0 - 5µM streptonigrin was inoculated with overnight cultures (starting OD_{600} = 0.01). The culture optical density was determined following 20 h incubation at 37°C. *GAS use of hemoglobin iron:* New 1 M 2,2' dipyridyl (DP, Acros Organics) stock solution prepared in absolute ethanol and 1 mM human hemoglobin (Sigma) prepared in saline (and filter sterilized) were used in all experiments. In each experiment, fresh THYB containing 3mM DP and hemoglobin (0 - 20 µM) were inoculated with overnight GAS cultures (starting OD_{600} = 0.01). The culture optical density was determined following 20 h incubation at 37°C.

3.2.6 Iron uptake assays

Iron uptake assays were performed as previously described with small modification [36]. Fresh CDM prepared without iron (and thus contains only trace iron levels) was inoculated with GAS cells and the culture was allowed to grow to the mid-exponential phase (~35 Klett units) at 37 °C. 1.3 µM $^{55}FeCl_3$ (Perkin Elmer, specific activity: 18.55 mCi/mg, concentration: 38.80 mCi/mL) prepared in 1 mM sodium ascorbate (ferrous uptake) or 0.0075 M HCl (ferric uptake) was added to 1.4 mL culture. Samples (200 µL) were drawn every 30 minutes and washed twice with 500 µL of CDM with 2 mM DP. Radioactivity (counts per minute, c.p.m) was measured for 5 minutes using a ^{3}H standard with a Beckman LS6500 scintillation counter. The sample optical density was also determined using a Beckman DU730 UV/Vis Spectrophotometer. ^{55}Fe incorporation was standardized by cell quantity by dividing c.p.m in the cell pellet by the culture OD_{600}.

Table 2 Lists of strains and plasmids used in this study

Strain name	Characteristics	References
S. pyogenes		
NZ131	M49 serotype	Lab stock
ZE4950	NZ131 derivative with the ΔsiaFGH::aad9 mutation	This study
ZE4952/pNC111	ZE4950 with pNC111 expressing the siaFGH genes	This study
ZE4952/pMSP3535	ZE4950 with pMSP3535 (empty vector)	This study
MGAS5005	M1 serotype	Lab stock
MGAS151	MGAS5005 derivative the ΔsiaFGH::aad9 mutation	This study
MGAS152	Wildtype rescue of MGAS151	This study
E. coli		
JM109	*endA1 glnV44 thi-1 relA1 gyrA96 recA1 mcrB+ Δ(lac-proAB) e14- [F' traD36 proAB+ lacIq lacZΔM15] hsdR17(rK-mK+)*	Lab stock
DH5α	*F– endA1 glnV44 thi 1 recA1 relA1 gyrA96 deoR nupG purB20 φ80dlacZΔM15Δ(lacZYA-argF)U169, hsdR17(rK–mK+), λ–*	Lab stock
TOPO 10	*endA1recA1F- mcrA Δ(mrr-hsdRMS-mcrBC) Φ80lacZΔM15 Δ lacX74 araD139 galU galK Δ(araleu)7697 rpsL (StrR) nupG*	Invitrogen
Plasmids		
pCR-XL TOPO	TOPO Cloning vector, Kan^R	Invitrogen
pHNG7	pCR-XL TOPO derivative with the siaFGH region, Kan^R	This study
pHNG12	pHNG12 derivative with the ΔsiaFGH::aad9 allele, Kan^R	This study
pMSP3535	pAMβ1 (from pIL252), ColE1 replicon, Erm^R, *nisRK*, P*nis*A	[103]
pNC111	pMSP3535 with the siaFGH gens under P*nis*A	This study
pJRS525	Broad host-range vector, $Spec^R$	Lab stock [104]
pJRS700	pVE6037 derivative, Kan^R, TmS	Lab stock [105]

3.2.7 Inductively Coupled Plasma-Mass Spectrometry (ICP-MS) analysis

Fresh THYB containing 0.5 µg/mL Nisin and 80 µM $FeCl_3$ (Fisher Scientific) were inoculated with GAS from overnight culture (starting OD_{600} = 0.01) and incubated at 37°C for 20 h. Culture samples (5mL, OD_{600} = 0.8) were washed three times with phosphate-buffered saline (PBS) prior to collection. Cell pellet was digested and analyzed (Center for Applied Isotope Studies, University of Georgia, Athens, GA) as described [106, 107].

3.2.8 Determination of cellular heme content and accumulation

Fresh THYB containing 20 µM of hemoglobin with or without 0.5 µg/mL nisin was inoculated with overnight GAS cultures (initial OD_{600} =0.01) and incubated at 37°C for 20 h. Culture samples (standardized according to cell density) were collected, washed 5x with PBS, resuspended in 2 mL of DMSO and subjected to sonication (20 % amplitude for 30 s.). Cellular heme amount was determined using acidified chloroform extraction as described [108, 109]. Briefly, 2 mL of 50 mM glycine buffer (pH 2.0), 0.1 mL of 4 N HCl (pH 2.0), 0.2 mL of 5 M NaCl (pH 2.0) and 2mL chloroform were added to the experimental samples and standard heme solutions and mixed vigorously by vortex. The reactions were incubated at room temperature for 1 min prior to centrifugation (20,000 x g, 20 min at 4 °C). The absorbance of the organic phase at 388, 450 and 330 nm was fed into the correction equation $Ac= 2 \times A388 - (A450+A330)$. Heme content was estimated from the plot of Ac corrected for standard heme concentrations. *Heme accumulation assays:* cells were grown in THYB and 20 µM of hemoglobin. Nisin (0.5 µg/mL) was added to the culture at the early logarithmic phase (20-30 Klett units), to induce the *siaFGH* expression. Samples (standardized according to cell density) were collected at the 0, 1, 2 and 3 h time points and cellular heme content was determined as described above.

3.2.9 Mouse model of vaginal colonization

Eight-to-ten-week old female outbred CD-1 mice were acclimated and randomly distributed into experimental groups. Experiments were performed as described [64, 93, 110-112]. Briefly, mice were estrus-synchronized by an intraperitoneal administration of 0.5 mg of β-estradiol valerate (Acros Organics) suspended in 100 µL of filter-sterilized sesame oil (Sigma) 24 hours prior to inoculation. NZ131 and ZE4950 strains were grown to OD_{600} of 0.3-0.5 in THYB and concentrated to 10^9 CFU/mL in PBS. Mice were intravaginally inoculated with 10^7 CFU of GAS culture in 10 µL of PBS. On days 1, 2, 3, and 5 post-inoculation, the vaginal lumen was gently washed with 50 µL PBS. The bacteria in the resulting vaginal lavage were enumerated by viable counts using StrepB selective plates (CHROMagar).

3.2.10 Mouse model of systemic GAS infection

CD-1 female mice (weight, 20–22 g, Charles River Laboratories) were acclimated and randomly distributed into experimental groups. Culture of *ZE151 (*Δ*siaFGH::aad9 in MGAS5005)* and ZE152 (wildtype rescue) grown in THYB were harvested at the mid-logarithmic phase ($O.D._{600}$ = 0.7), washed, and resuspended in saline. Mice were infected intraperitoneally with 0.1 mL of cell suspension at 1.4 x 10^8 CFU. The animals were observed 4 times per day after challenge, and mice exhibiting signs of severe distress were euthanized and counted as dead.

3.2.11 In silico methods

SiaF ribbon structure was predicted using I-TASSER (https://zhanglab.ccmb.med.umich.edu/I-TASSER/) [113] and visualized using molecular visualization software Pymol. FASTA sequence of each protein was retrieved from the NCBI

database and then analyzed in the BLASTP server (https://blast.ncbi.nlm.nih.gov/) for the comparative analysis.

3.2.12 Ethics statement

All mouse experimentation was conducted according to the approved protocol by the Institutional Animal Care and Use Committee of Georgia State University and Binghamton University.

Table 3 Lists of primers used in this study

Primers Name	**Sequence (5'-3')**	**Restriction site**
ZE389	CCTATTTGTACAGCAATATTGTCTGCAGG	NheI
ZE393	AAAACTGCAGGCGCTTGCTTATACTCTG	NheI
ZE408 (*spec*)	TTTGCTAGCGGTCGATTTTCGTTCGTGAATACATG	
ZE409 (*spec*)	GGGGCTAGCCGAAAGTCTATGCAAGGGTTTATTG	
ZE451	GGGAAATCGATACAGCAATATTGTCTGCAGG	ClaI
ZE452	CAAATGCGCATCGATTTCAAAAGCTG	ClaI
ZE480 (*siaFGH*)	ATGATAACAGGCGCATTTGC	
ZE481 (*siaFGH*)	CACTACTTAGAAGTTCTTCATCATGTG	
ZE691 (*siaF*)	CACCAAACAGTTAACAATAAAAGATATT	
ZE692 (*siaF*)	TCATGATAACAATCCTGATT	
ZE836 (*siaFGH*)	AAAGGATCC TTCCCTAAAAGAGGTG	BamHI
ZE837 (*siaFGH*)	CCCTGCAG CTATTATACAAGAGTTCC	PstI
SpecFw	GTGAGGAGGATATATTTGAATACATACGAA	
SpecRev	GTCCATTCAATATTCTCTCCAAGATAACTA	

3.3 Results

3.3.1 The siaFGH genes encode a putative ECF importer

In silico analysis suggested that the SiaFGH proteins consist of the Group I ECF family of transporters [95], with *siaFGH* respectively encoding the substrate-binding S component (EcfS), the transmembrane T component (EcfT), and the energy-coupling A component (EcfA, **Figure 8A)**. Based on the substrate-binding component, SiaF, the SiaFGH transporter belongs to the HtsTUV ECF subgroup, whose ligands are unknown [96]. SiaF is predicted to be an α only protein with both the N and C terminals in the cytosol (data not shown) [114]. Six distinct helices make up the transmembrane domains, and an extended extracellular loop connects two of the helices in SiaF [115]. The predicted SiaF ribbon-structure **(Figure 8B)** is highly similar to the overall fold and membrane topology shared by EcfS units with one exception; the large extracellular loop that typically connects helices 1 and 2 in EcfS proteins, joins helices 5 and 6 in SiaF. This difference is intriguing since this loop is proposed to serve as a lid over the binding site. The SiaFGH proteins are highly conserved in GAS isolates and the related *S. dysgalactiae* and *S. equi*, both of which encode the entire *sia* operon. (**Table 4).**

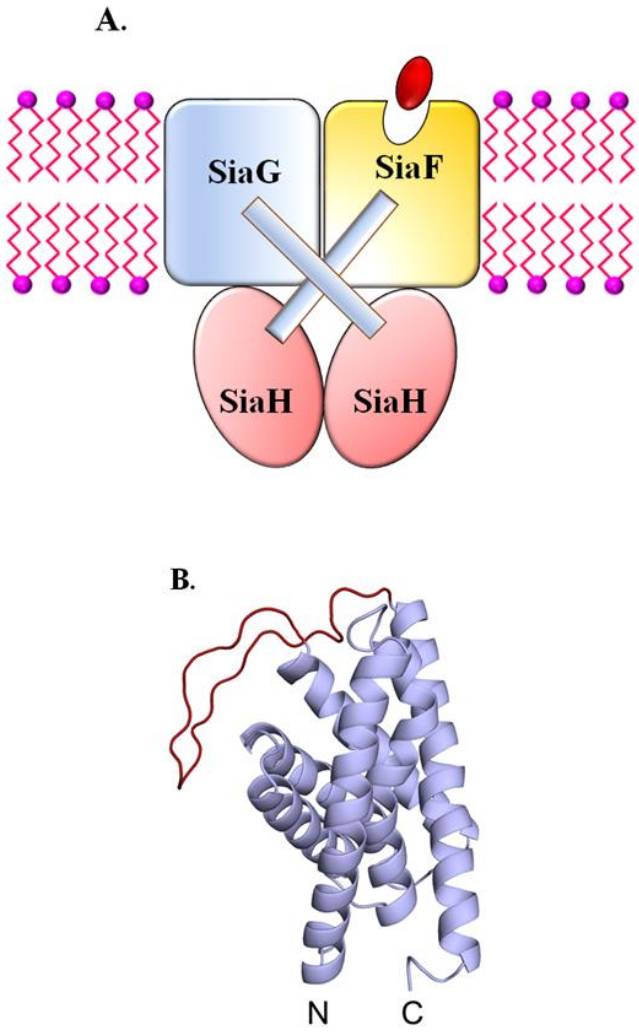

Figure 8 The *siaFGH* genes encode an ECF transporter

A. Schematic representation of the SiaFGH ECF transporter. SiaFGH proteins belong respectively to the subgroups 3.A.1.31.1; 3.A.1.25.4; and 3.A.1.25.6, in the transporter classification (TC) database (http://www.tcdb.org) [116]. The red oval indicates the substrate. **B.** SiaF structural model (I-TASSER [113]) based on *Bacillus subtilis* EcfS (PDB#5delA).

Table 4 In silico analysis suggests SiaFGH system is conserved in streptococcal strains

	Percent identity to GAS SiaFGH proteins		
	SiaF (ACI61675)	**SiaG** (ACI61674)	**SiaH** (WP_136048563.1)
S. dysgalactiae	86.80% (WP_129556215.1)	66.37% (WP_111717518.1)	85.66% (WP_143928109.1)
S. equi	75% (WP_043040123.1)	64.6% (WP_165626339.1)	77.42% (WP_043026841.1)
S. canis	86.80% (WP_003045124.1)	74.34% (WP_164227913.1)	85.66% (WP_164405649.1)
S. castoreus	79.19% (WP_027969907.1)	68.37% (WP_027969908.1)	79.21% (WP_027969709.1)
S. phocae	73.10% (WP_054278834.1)	65.74% (WP_054278835.1)	78.85% (WP_037595860.1)
S. ictaluri	74.62% (WP_008086912.1)	59.11% (WP_008087003.1)	78.06% (WP_008087568.1)

NCBI accession number is in parenthesis

3.3.2 Deletion of the siaFGH genes results in higher streptonigrin resistance and impaired use of hemoglobin iron

Expression of Group I ECFs is often regulated according to ligand requirement; hence, the repression of the *siaFGH* genes by iron and heme [31, 94] suggests that the SiaFGH substrate is related to iron metabolism. To test this hypothesis, we constructed a deletion mutant in M49 NZ131 background and examined the impact on GAS physiology. The parental NZ131 and the isogenic Δ*siaFGH* (ZE4950) grew equally well in THYB **(Figure 9)**, but the mutant was more

resistant to the antibiotic streptonigrin (LD_{50} > 3.5 μM for ZE4950 and 3 μM for NZ131). Iron potentiates bacterial killing by streptonigrin [70]. Hence, increased resistance suggests the Δ*siaFGH* strain has lower levels of cellular iron compared with the parental NZ131. We next tested if the function of the *siaFGH* genes is related to heme uptake, similarly to that of the neighboring, *shr*, *shp,* and *siaABC* genes. We examined the wildtype and the mutant strains when cultivated in iron-depleted medium (THYB with DP) supplemented with hemoglobin. Deletion of the *siaFGH* genes impaired growth on low concentrations of hemoglobin (2.5 - 10 μM, **Figure 10A**). But the addition of hemoglobin at higher levels resulted in similar growth by both strains. These data support the hypothesis that SiaFGH is a high-affinity heme importer, and consistent with the redundancy of heme uptake mechanisms in GAS. The *siaFG genes* are integral membrane proteins, and thus are difficult to clone under a constitutive promoter. Thus for complementation analysis, we cloned *siaFGH* under the nisin dependent promoter, P_{nisA} [89]. Inducing *siaFGH* expression with nisin improved the ability of the mutant harboring the complementation plasmid to grow on hemoglobin iron compared with the mutant carrying an empty vector **(Figure 10B)**. Therefore, *siaFGH* expression *in trans* complements the defect in the use of hemoglobin as an iron source. Complementation is partial, however, and is observed only with 10 μM hemoglobin and above.

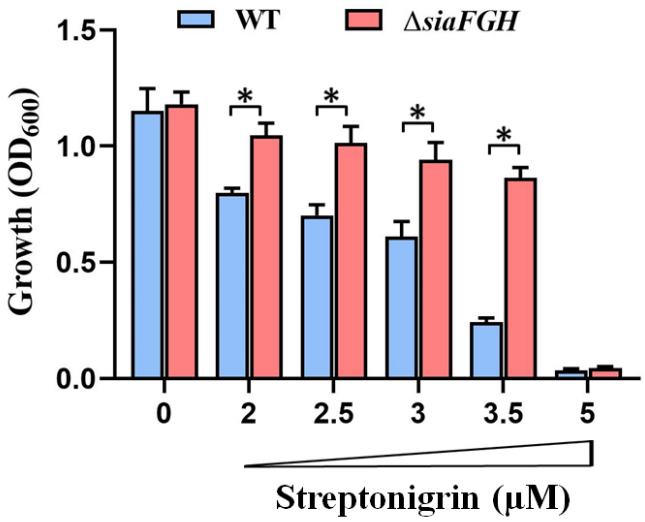

Figure 9 The SiaFGH importer impacts intracellular iron levels

Growth (20 h) of NZ131 (wildtype) and ZE4950 (Δ*siaFGH*) in THYB with increasing concentrations of streptonigrin at 37 °C. The data are from two independent experiments done in technical triplicates, with SD shown. * indicate significance ($P < 0.05$, Student's t test, equal variance).

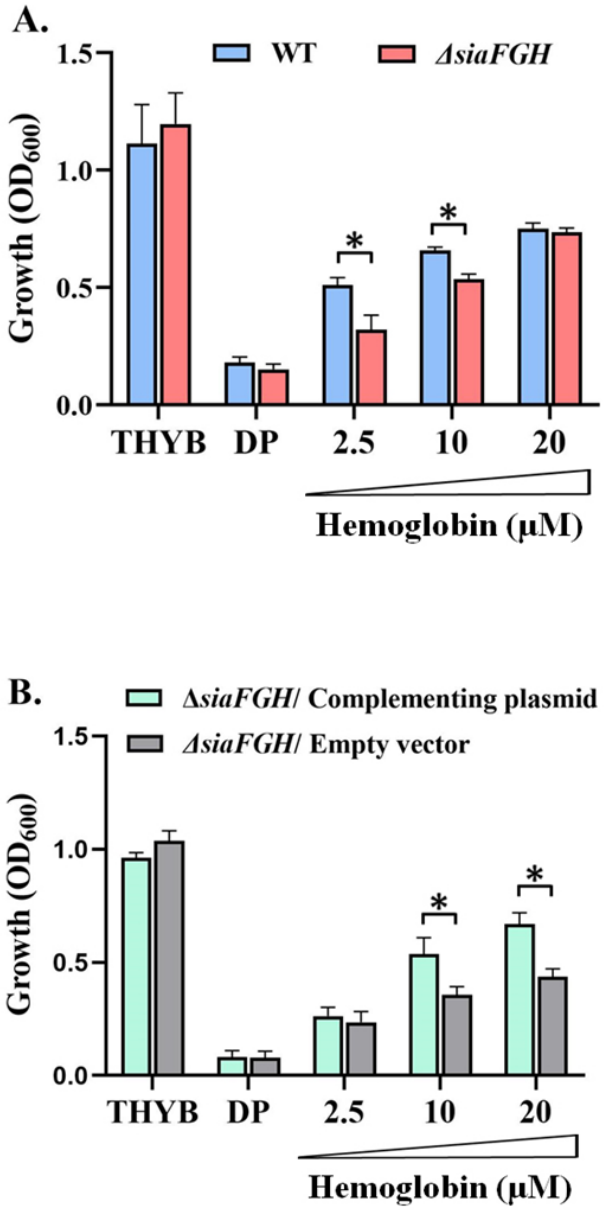

Figure 10 The SiaFGH transporter impact the use of hemoglobin iron

Shown is growth (20 h) of NZ131 (wildtype) and ZE4950 (Δ*siaFGH*), (**A**) or ZE5950/pNC111(complement) and ZE4950/ pMSP3535 (empty vector), (**B**). Cells were grown in THYB with 3 mM DP with or in THYB-DP with hemoglobin. Data are derived from three experiments done in triplicates. * indicate significance (Student's *t* test, $P < 0.05$).

3.3.3 The SiaFGH proteins import heme but not iron ion

To investigate if the SiaFGH system takes up heme, we studied heme accumulation in the mutant and complemented pair. GAS was grown overnight in THYB and 20 µM hemoglobin with or without nisin. The cellular heme levels in culture samples of equal cell density were determined as previously described [108, 109]. The complemented strain accumulated 90% more heme in response to nisin, and about twice as much compared with the mutant **(Figure 11A)**. Therefore, the induction of the *siaFGH* gene expression results in increased heme import. The complemented strain accumulated more heme even in the absence of nisin, indicating some basal level of P_{nisA} activity. To study heme uptake over time, we grew cells in THYB with hemoglobin and added nisin to the culture at the early logarithmic phase. Heme content in samples collected at 0, 1, 2, and 3 hours after induction was determined **(Figure 11B)**. While we observed a slow increase in heme levels over time in the mutant strain (harboring an empty vector), the addition of nisin to the complemented strain resulted in a much faster heme uptake. Together, these observations establish that the SiaFGH promotes heme uptake in GAS.

To test if SiaFGH imports iron ions in addition to heme, we monitored radioactivity accumulations in cells grown in iron-deplete CDM supplemented with ^{55}Fe in the ferrous **(Figure 12A)** or the ferric **(Figure 12B)** form. Interestingly, both strains incorporated radioactivity at a faster rate when supplied with reduced iron compared to the oxidized form. The deletion of the *siaFGH* genes, however, did not affect import of the metal in either state significantly. We also compared iron accumulation between in a Δ*siaFGH* strain carrying an empty vector, and a mutant harboring the complementation plasmid. The mutant and complemented pair were grown in THYB supplemented with 80 µM iron and nisin, and we determined the iron content in cell samples collected after overnight growth using ICP-MS **(Figure 12C)**. Similar amounts of iron were found

in both strains, indicating that the induction of the *siaFGH* genes did not result in enhanced uptake of the metal iron.

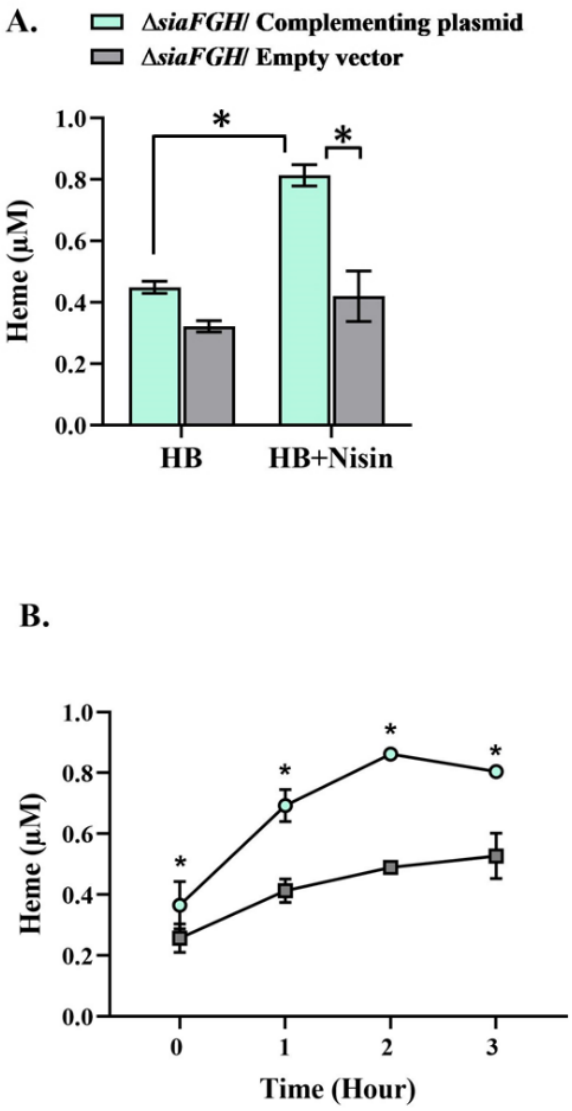

Figure 11 The SiaFGH transporter promotes heme uptake

A. Cultures of ZE4950 (Δ*siaFGH*) harboring plasmid pNC111(complement) or pMSP3535 (empty vector) were grown overnight in THYB supplemented with 20 μM hemoglobin with or without nisin. Cells were harvested, washed, and were subjected to chloroform extraction. UV-

visible spectra (250–700 nm) of the collected organic phases were recorded and the concentrations of heme in the test samples were calculated as described [108]. **B.** The same as in A, only that nisin was added to the cultures at the early exponential phase, and the heme content was determined in samples collected at 0, 1, 2, and 3 h post nisin addition.

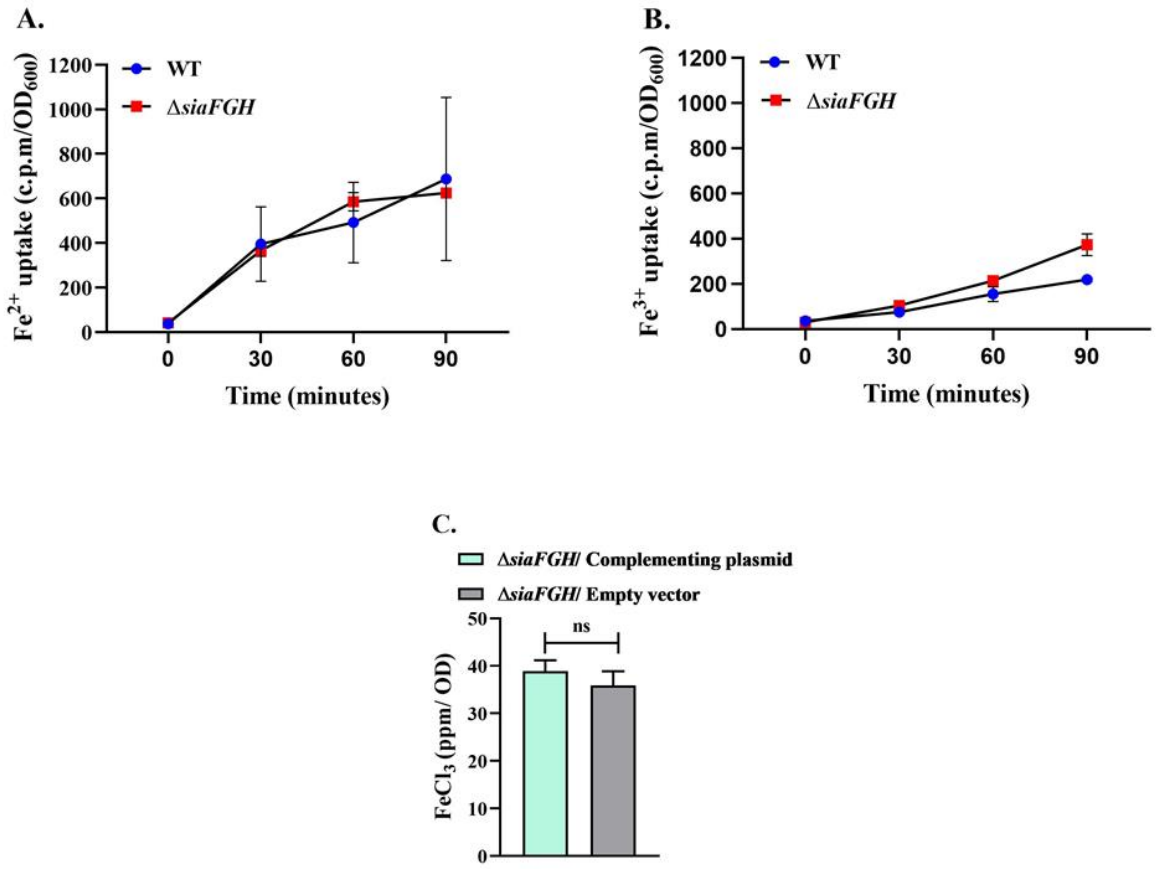

Figure 12 Inactivation of the SiaFGH genes did not influence metal iron uptake

Shown is the uptake of ferrous iron (A) or ferric iron (B) by NZ131 (wildtype) and ZE4950 (Δ*siaFGH*) grown in iron-deplete CDM supplemented with ^{55}Fe. The data is derived from two experiments done in duplicates; SD is shown (error bars). Total iron content in ZE151 (wildtype)

and ZE152 (complemented) strains grown overnight in THYB supplemented with 80 µM $FeCl_3$ and nisin, as determined ICP-MS **(C)**. The data are derived from two independent experiments.

3.3.4 SiaFGH contributes to GAS mucosal colonization as well as systemic infection

We recently observed that the entire *sia* operon is induced during vaginal colonization in mice [93]. We, therefore, used this infection model to test the role of the SiaFGH transporter in GAS colonization of the mucosa **(Figure 13)**. Estrus-synchronized mice were inoculated intravaginally with the M49 NZ131 (wildtype) or ZE4950 (Δ*siaFGH*) strain, and the colonization rate was followed for five days. Although there was an obvious trend of higher colonization in the mice inoculated with the wildtype strain immediately, we observed no statistical significance between the wildtype and the mutant strain in the first day of the experiments. A significant colonization defect, however, was exhibited by the *siaFGH* mutant on the second day. Colonization remained much lower than that of the wild type strain through the third day, but it was lost on day 5 for both the wild type and the mutant strain. To test if the SiaFGH system also impacts GAS invasive disease, a Δ*siaFGH* mutant (ZE151) and a wildtype rescue strain (ZE152) were constructed in the virulent M1 MGAS5005 background and examine in a murine model for systemic infection **(Figure 14)**. Mice were infected intraperitoneally, and survival was recorded for five days. Infection by the wild type strain (ZE151) caused a rapid and lethal infection (resulting in a 20% survival rate in day 2). Mice infected with the mutant strain, however, exhibited a slower disease with a lower mortality rate (50% final survival rate). Together, data shows that the *siaFGH* genes are imperative for mucosal colonization as well as systemic infection.

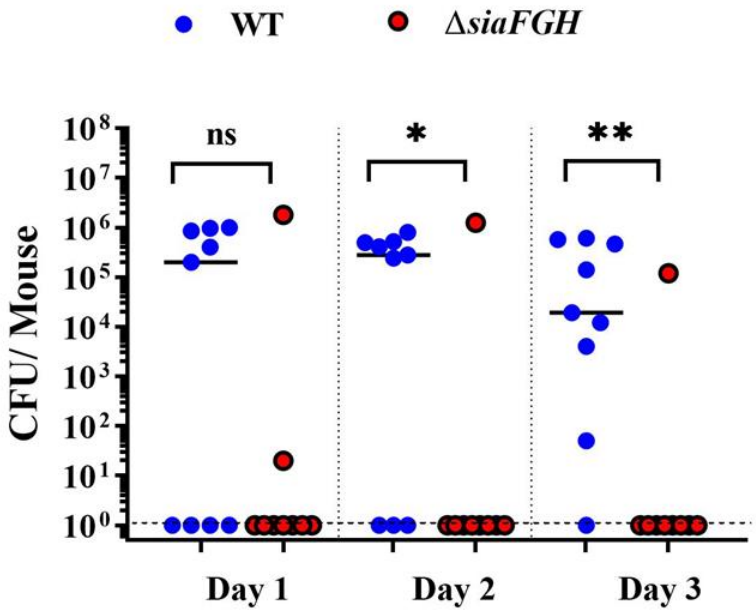

Figure 13 Inactivation of siaFGH attenuate GAS vaginal colonization

NZ131 (Wildtype) and ZE4950 (Δ*siaFGH*) were inoculated into the vaginal vault of mice, and colonization rates were determined. Significance was assessed on daily samples using a Mann Whitney test. * p value < 0.05, ** p value < 0.005.

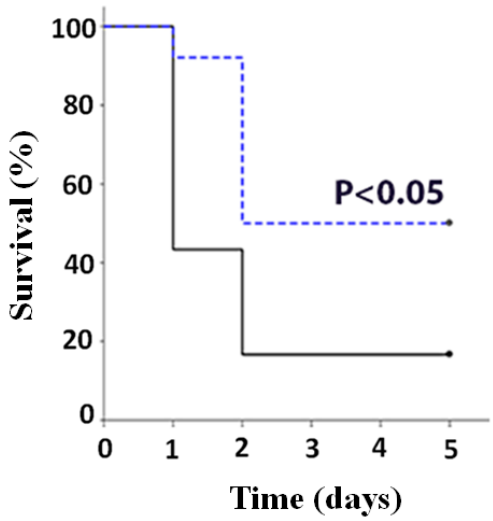

Figure 14 Survival of CD-1 mice from systemic GAS infection

Kaplan-Meier survival curve is shown for mice following intraperitoneal infection (1.4 x 10^8 CFU) with ZE150 (wildtype rescue, solid line) or ZE152 (Δ*siaFGH* (dash line). The data are pooled from two independent experiments (log-rank test, $P < 0.05$, $n = 30$).

3.4 Discussion

The 10 gene *sia* operon belongs to the core genome in GAS, *S. dysgalactiae*, and *S. equi*, which are chief human and animal pathogens. We and others have elucidated the structure/function of *shr*, *shp*, and *siaABC*, and established their role in heme acquisition, adherence, and virulence in multiple serotypes [30, 33, 34, 57, 72, 86, 90-92, 117-119]. However, the *sia* operon has five additional genes (*siaDEFGH*) that are yet to be described. The data in this study show that the last three genes, *siaFGH*, encode a novel ECF transporter that imports heme and promotes GAS colonization and infection. Notably, heme uptake in bacteria was described so far only with conventional ABC transporters. In GAS, the two typical ABC systems that import heme are SiaABC and the SiuADBG (which may also take up ferrichrome). This is the first heme ECF

system to be described. Hence the finding of a new heme transporter in the *sia* operon from the ECF system family, expands the paradigm of heme uptake not only in GAS but also in the related *S. dysgalactiae* and *S. equi* and in bacteria overall.

SiaFGH belongs to one of the few ECF families whose ligand was unknown [96]. Inactivation of the *siaFGH* resulted in decreased sensitivity to streptonigrin **(Figure 9)**. Streptonigrin binding to metal iron leads to structural changes that facilitate a transition from a partially active form into a fully functioning state [120, 121]. Therefore, the difference in streptonigrin susceptibility suggests the Δ*siaFGH* mutant accumulates lower levels of total iron when cultivated in normal THYB. THYB is a beef heart infusion supplemented with the iron/heme rich yeast extract and contains both metal iron and heme. The observed changes in iron levels in the *siaFGH* mutant grown in THYB could therefore result from a reduction in uptake of either free iron or heme. Growth experiments, however, suggested that the *siaFGH* imports heme, since the mutant did not grow as well as the wildtype in iron-deplete THYB (THYB-DP) supplemented with hemoglobin (≤ 10 μM, **Figure 10A**). Expressing *siaFGH* in trans complemented the mutant phenotype **(Figure 10B)**. The observation that the mutant phenotype was lost when the cells grew with 20 μM hemoglobin implies that, like other ECF systems, the SiaFGH is a high-affinity importer whose role becomes redundant in the presence of a higher amount of hemoglobin. This redundancy is likely due to the activity of additional transporters, such as SiaABC and SiuADBG.

We used direct heme import assays to test the suggestion that heme serves as a ligand for the SiaFGH proteins **(Figure 11)**. The expression in trans of the *siaFGH* genes (from P_{nisA}) resulted in heme accumulation by the complemented strain when grown overnight with hemoglobin **(Figure 11A)**. Furthermore, the activation of *siaFGH* genes in exponentially growing cells (in THYB with hemoglobin) triggered a pronounced heme uptake in cells harboring the

complementation plasmid **(Figure 11B)**. The noticeable amount of heme that was present in the *siaFGH* mutant, even in the absence of the complementation plasmid, likely resulted from the activity of other heme transporters. We also noted some basal activity of P_{nisA}. Together the data identify the *siaFGH* as a heme importer.

To examine if the SiaFGH system also imports metal iron, we conducted iron uptake and accumulation assays using ^{55}Fe **(Figure 12)**. We did not observe any impact on the import of ferric or ferrous iron in the deletion mutant **(Figure 12A & B)**. Also, the induction of the *siaFGH* genes did not promote more iron intake in the cells grown on THYB supplemented with ferric iron. Hence the SiaFGH importer is specific for heme. We noted, however, that both the wildtype and the mutant cells import ferrous iron more readily compared to the oxidized ferric state. As acid-forming bacteria, GAS might create a reduced microenvironment during growth, and its import systems might be better adapted for the uptake of reduced iron.

Inactivation of the *siaFGH* impaired GAS growth on hemoglobin as the sole source of iron **(Figure 10)** and the pathogen's ability to import heme from hemoglobin **(Figure 11)**. Hemoglobin is too large to diffuse through the cell wall and reach the membrane SiaFGH transporter. Gram-positive pathogens typically use surface receptors to capture heme from hemoglobin or other host sources on the bacterial surface and shuttle it through the cell wall to a membrane transporter [28, 72]. In GAS, Shr, Shp, and SiaABC together create such a heme relay system [30, 33, 34, 72, 90, 91]. It seems possible that SiaF also interacts with one or more of the heme relay components encode by the *sia* operon. SiaF may receive the heme also from the recently described heme receptor, HupY [93]. Alternatively, small amounts of heme that are released by hemoglobin arrived at the membrane and reach SiaF. Additional studies are required to examine these possibilities and to describe the mechanism of heme capture by the SiaFGH transporter.

GAS is not able to obtain the iron it needs for growth from the ferric glycoproteins, lactoferrin, or transferrin [36, 89]. To survive and cause infection, the beta-hemolytic pathogen metabolizes the heme it sequesters from hemoglobin and other host hemoproteins. Examination of the *siaFGH* mutant in a murine model for mucosal colonization revealed the transporter is critical for GAS establishment in the vaginal track in mice; the mutant colonized only one mouse (out of nine) comparing to the 8 animals that were colonized by the wildtype strain (day 3 $P < 0.005$, **Figure 13**). The strong activation of the MtsR regulon in this infection model [93], suggests the transporter plays a key role in GAS adaptation to the vaginal mucosa, and indicates that highly restricted iron availability confronts bacteria attempting to colonize this niche. Notably, the *siaFGH* mutant is also attenuated in a murine model for systemic GAS infection **(Figure 14)**. The attenuation of virulence by the mutant strain is less dramatic compared to the mutation impact in the model for colonization. This tempered reduction in virulence implies that iron availability might be less limiting during systemic growth (compared to the mucosal surfaces).

This study identifies the SiaFGH system as a novel transporter that imports heme in high affinity, and a new virulence factor in GAS. Homologs of this new heme transporter are found in the chromosome of additional bacteria. For example, in addition to GAS, the related *S. dysgalactiae* and *S. equi*, harbor the entire *sia* operon (including the *siaFGH* genes). We also identified homologs of *siaFGH* next to siaDE-like genes in *Streptococcus gordoni* and *Eggerthella lenta* or near iron-dependent repressors in the Group B streptococcus and *Enterococcus faecalis*. Finally, while this manuscript was under preparation, a study describing a heme ECF system from *L. lactis* was published in the Preprint service for Biology (Verplaetse E et al., not peer reviewed). *In silico* analysis also suggest that ECF- type transporters mediate siderophore import. Zoe Heather *et al*., described a novel non-ribosomal peptide synthetase (NRPS) system in *S. equi* that produce

the siderophore, equibactin [122]. The *eqbHIJ* genes in this gene cluster, which are predicted to import iron-equbactin complex, also belongs to the ECF family (NCBI-Protein ID: EqbH/EcfS CAW93973, EqbI/EcfT: CAW93972, EqbJ/EcfA CAW93970). Therefore, transporters from the new ECF family may import other types of iron-complexes in addition to heme.

In summary, multiple bacteria, including dangerous pathogens, carry a SiaFGH-type heme transporter. Hence, describing the mechanism of this new import system and its role in bacterial pathophysiology may facilitate future methods for prevention and treatment with broad applicability.

4 CHAPTER III: NATIVE HUMAN ANTIBODY TO SHR FROM GROUP A STREPTOCOCCUS PROTECTS FROM INVASIVE INFECTION

4.1 Introduction

The bacterial pathogen GAS is the ninth leading infectious source of human morbidity and mortality, with a global burden estimated to exceed 500,000 deaths annually [123, 124]. GAS commonly colonizes the mucosal surfaces and skin, frequently causing pharyngitis and impetigo. These infections can lead to severe immune sequelae, such as acute rheumatic fever and glomerulonephritis [123]. Timely treatment with antibiotics can mitigate GAS infections and their complications, but resistance to penicillin alternatives are on the rise [9, 10, 123]. The frequency of GAS diseases has increased in the past two decades, reaching 7-10 cases per 100,000 in the US and Canada [6, 7]. A large number of circulating serotypes pose a significant challenge for the vaccine approach, with none approved to date [125, 126]. Without a vaccine, the burden of GAS sequelae and invasive diseases is extreme, and the need for improved means to prevent and manage infections is high.

GAS is an iron-requiring pathogen that mostly relies on heme-iron to satisfy its need for the metal [89]. Proteins involved in heme capture and import are critical for GAS survival in the host. The *sia* operon encodes a key heme acquisition pathway in GAS, including two surface receptors and an ABC transporter, which capture heme from the host (*shr*) shuttle it across the cell wall (*shp*) and through the cytoplasmic membrane (*siaABC*) [30, 33, 34, 71, 72]. Shr, the first receptor in the *sia* heme relay, binds to hemoglobin and other host hemoproteins [72]. It is a 145 kDa surface protein with a unique N-terminal region (NTR) followed by two near–iron transport (NEAT) domains [30]. Shr binds to hemoglobin using a novel mechanism through a domain

(DUF1533) that appears twice in its NTR; this new hemoglobin binding module was named HID for Hemoglobin-interacting domain [30, 32]. Following binding to hemoglobin, NEAT1 captures and transfers the heme to either NEAT2 or Shp [33, 127]. Inactivation of *shr* impairs the bacteria's ability to grow on hemoglobin as a sole source of iron [30] or in human blood [86]. In addition to its contribution to the iron acquisition, Shr binds fibronectin and laminin in vitro [57], and deletion mutants show reduced binding to fibronectin or laminin in a strain-dependent manner [57, 86, 128]. Shr knockout mutants are attenuated in both zebrafish [57], and mouse models for invasive GAS infections [86].

The essential role Shr plays in GAS pathophysiology raised the possibility of targeting this protein for the development of antibacterial strategies. Immunizing mice intraperitoneally with the purified protein or intranasally with Shr-expressing *Lactococcus lactis* protects from an invasive GAS infection [92]. Moreover, rabbit Shr-antiserum administrated prophylactically also defends against GAS in a mouse model for passive immunity [92]. In this study, we used a B-lymphocyte screen to identify two native human monoclonal antibodies (TRL96 and TRL186) to Shr. Here, we show that TRL186, but not TRL96, aids in the clearance of systemic GAS infections in both prophylactic and therapeutic mouse models and elucidate its defense mechanism.

4.2 Materials and methods

4.2.1 Strains and growth conditions

The strains and plasmids used in this study are listed in **Table 5**. *Escherichia coli* were grown aerobically in Luria-Bertani broth at 37°C. GAS and *Streptococcus dysgalactiae* subsp. *equisimilis* (SDSE) were grown statically at 37°C in Todd-Hewitt broth (Difco Laboratories) with

0.2% w/v yeast extract. When necessary, ampicillin (100 μg/mL), or kanamycin (70 μg/mL) was added to the medium.

Table 5 Strains and plasmids used in this study

Name	Description	Reference
Strains		
E. coli BL21 Star™DE3	Host for pCB1 and pEB11	Invitrogen
E. coli One shot Omni Max2-TI	Host for pHSL2 and pYSH6	Invitrogen
GAS MGAS5005	M type 1,	Lab stock
ZE491	M type 49, mtsR-	Lab stock
S. dysgalactiae subsp. equisimilis		ATCC# 12388
Plasmids		
pCB1	Expresses His6-Xpress-ShrGAS from P_{BAD}	[72]
pEB10	Expresses Strep-tag-NTR from P_{tet}	[30]
pHSL2	Expresses Strep tag-NEAT2 from P_{tet}	[33]
pYSH6	Expresses His6-MBP-NEAT1 from P_{tac}	[33]
pYSH9	Expresses His6-Shrdys from P_{T7}	[129]

4.2.2 Single B-lymphocyte mAb discovery technology

Blood samples were collected from anonymized donors under informed consent approved by the Institutional Review Board of Stanford University (Stanford Blood Center, Stanford, CA), and peripheral mononuclear cells were prepared as described. Using the CellSpot platform (Trellis Bioscience, Redwood City, CA) [130], memory B cells were stimulated to proliferate and differentiate into plasma cells. The secreted IgG footprint (100 fg/cell over a 5-h period) of individual cells was probed with fluorescent nanoparticles of distinguishable types conjugated with full-length recombinant Shr protein, the NEAT1 and NEAT2 domains, and BSA (counter-screening bead). Over 30 mAbs have been cloned based on their binding profiles. The V regions

from mRNA of single B-cells of interest were cloned onto an IgG1 constant region, which was then expressed by transient transfection in HEK293 cells.

4.2.3 Enzyme-linked immunosorbent assays (ELISA)

4.2.3.1 ELISA with Shr proteins

Full-length Shr from GAS (Shr_{GAS}) or SDSE (Shr_{dys}), and Shr_{GAS} fragments (NTR, NEAT1, or NEAT2) were expressed in *E. coli* and purified using affinity chromatography as previously described [30]. Antibody binding to the target was evaluated by ELISA using 96-well EIA/RIA microplates (Corning™ Costar™). Microplates were incubated overnight at 4°C with 25 µg/mL bait protein in PBS (10 mM phosphate-buffered saline, 100 nM NaCl, pH 7.4). Wells coated with BSA, and uncoated wells served as controls for nonspecific interactions. Plates were washed with PBS and 0.05% Tween (PBST), blocked with 5% soymilk (in PBST) for one hour at 37°C and washed again. TRL186 (2 µg/mL in PBST) was allowed to react with the bait for one hour at 37°C. Antibody binding was detected using alkaline phosphatase (AP) conjugated anti-human IgG (Sigma). The absorbance at 405 nm was measured after 30 min incubation at room temperature after the addition of p-nitrophenyl phosphate hexahydrate disodium salt (pNPP) tablets dissolved in diethanolamine buffer solution (KPL). For affinity testing, TRL186 (in PBST) was added to a plate coated with Shr_{GAS}. Binding was detected using horseradish peroxidase-conjugated anti-human IgG.

4.2.3.2 ELISA with synthetic peptides

A library of overlapping peptides (15-mers with an offset of three amino acids) encompassing Shr_{GAS} NTR (Mimotopes, Melbourne Australia) were screened for interactions with

TRL186 by ELISA similar to that done with Shr proteins. Biotinylated peptides dissolved in 80% DMSO (5-15 mg/mL) were diluted 1/200 in PBST and immobilized onto Pierce streptavidin-coated high capacity plates (Thermo Scientific™). TRL186 (2 µg/mL in PBST) was allowed to interact with the coated wells for 30 minutes at room temperature, and binding was detected using AP-conjugated anti-human IgG.

4.2.3.3 ELISA with immobilized bacteria

Overnight grown cultures (5 mL of OD_{600} 0.9) of GAS or SDSE were harvested, washed with PBS (5 mL), and used to coat microplates (50 µL) overnight at 4°C. After blocking, TRL186 was allowed to interact with the coated wells for one hour at 37°C and binding was detected as above.

4.2.3.4 ELISA with Shr_{GAS} and hemoglobin

Human hemoglobin (Sigma) was biotinylated using the EZ-Link™Sulfo-NHS-SS-Biotinylation Kit (Thermo Scientific™) according to manufacturer's instruction. Microplates were coated overnight at 4°C with purified Shr or control proteins. Plates were washed and blocked as above, and biotinylated hemoglobin (50 nM in saline) was allowed to react with the coated wells during overnight incubation at 4°C. Hemoglobin binding was detected with streptavidin-conjugated AP (Sigma). The same assay was used to study the impact of TRL186 on Shr's binding to hemoglobin, only that mAb in increasing concentrations was allowed to interact with the coated wells for 1 hour at 37°C, before the addition of the biotinylated hemoglobin.

4.2.4 GAS growth in hemoglobin and mAb

THYB containing 3 mM 2,2' dipyridyl (DP, Acros Organics) with 5 µM hemoglobin and 20 µg/mL antibody (TRL186 or TRL96) were inoculated with overnight GAS cultures (starting OD_{600} 0.01). The culture optical density was determined following 20-hour incubation at 37°C.

4.2.5 Growth and differentiation of HL60 cells

HL60 promyelocytic leukemia cells were purchased from the American Type Culture Collection (CCL240); they were maintained, passaged, and differentiated into granulocytes (with 100 mM dimethylformamide [DMF]) as described [131]. The viability of the differentiated cells was assessed using trypan blue exclusion and was considered acceptable if more than 90% of the cells excluded the azo dye. HL60 cells were used for opsonophagocytic assay at day five post-differentiation as long as the expression of CD35 (complement receptor 1) was up-regulated by ≥ 55% of the cell population and that of CD71 (transferrin receptor) was down-regulated by ≤ 15% of the cell population, as determined by flow cytometry (BD LSRFortessa^{TM}) [132, 133].

4.2.6 Opsonophagocytosis Killing Assay (OPKA)

GAS opsonization was evaluated using a previously described method [131, 134]. Briefly, mAbs diluted in Hanks balanced salt solution containing 0.1% gelatin (OPA buffer) was added to a 96-well microplate (10 µL/well). 20 µL of GAS culture (50 CFU/µL) and 10 µL of 50% baby rabbit serum or normal rabbit sera (NRS, control group) were added to wells, and the plates were incubated at 37 °C for 30 minutes on an orbital shaker at 200 rpm. 40 µL of differentiated HL60 cells ($1x10^4$/µL) freshly prepared in OPA buffer was added, and the plates were incubated at 37 °C for an additional 45 minutes with shaking. 40 µl from each reaction was mixed with 360 µL of

0.9% NaCl and plated on THYA plates (100 µL/ plate) to enumerate the colony number. Opsonophagocytic killing was calculated as following equation: (CFU [control] - CFU [mAb])/ CFU [control]) * 100.

4.2.7 Passive vaccination and GAS infection model

MGAS5005 cells were harvested at the mid-logarithmic phase (OD_{600} 0.7), washed, and resuspended at the desired density in 0.9% saline. Bacterial concentration was determined by microscopic counts and verified by plating. CD-1 mice (20–22 g, Charles River Laboratories) were infected by intraperitoneal (IP) injection of 0.1 mL cell suspension. Mice were weighed and administrated IP with a single dose of TRL186 (15 mg/kg) or with PBS (mock vaccination) one hour before challenge with 5×10^7 CFU (prophylactic model) or four hours after infection with 1 x 10^8 CFU (therapeutic model). Fifteen mice were used in experimental groups with at least one repeat. Mice were observed four times per day after the challenge. Morbid animals were euthanized according to protocols approved by the Georgia State University Institutional Animal Care and Use Committee.

4.2.8 Structural Prediction

The DUF1 domain was modeled with Modeller [135]. The structure of DUF2 domain (PBD: 6DK) was used as a template [32]. RAMPAGE was used to verify that structural residues resided primarily in the favored region (98%), with only a few in the allowed region (2%) and that no residues resided in the outlier region [136].

4.2.9 Statistical Analysis

Data presented are averaged from experiments repeated at least twice (Student's *t*-test, $P < 0.05$). The survival curve was analyzed by Kaplan-Meier plots.

4.3 Results

We selected two lead candidates, TRL96 and TRL186, based on high specificity and affinity to Shr and investigated their efficacy in protection against GAS infection.

4.3.1 TRL96 and TRL186 bind to GAS surface and enhance opsonization

To examine if TRL96 and TRL186 interact with GAS surface, we performed a whole-cell ELISA, where GAS cells were used to coat the microtiter plates and allowed to react with the mAbs (**Figure 15A**). Both mAbs generated specific and significant binding with *S. pyogenes* cells with a stronger signal for TRL186 (OD_{405} 0.7), providing nearly half the signal as the positive control polyclonal antibodies, anti-Shr and anti-GAS. Since both mAbs interacted with whole cells, it indicates that the epitopes for TRL96 and TRL186 on Shr were accessible on the GAS surface.

Next, we performed OPKA to measure the ability of the mAbs to opsonize GAS cells. There was a marked reduction in GAS survival in the presence of both antibodies; in contrast, no killing was observed while using the normal rabbit serum (NRS) control. The mAbs enhanced opsonophagocytic killing by 44% for TRL96, and 35% by TRL186 (**Figure 15B**).

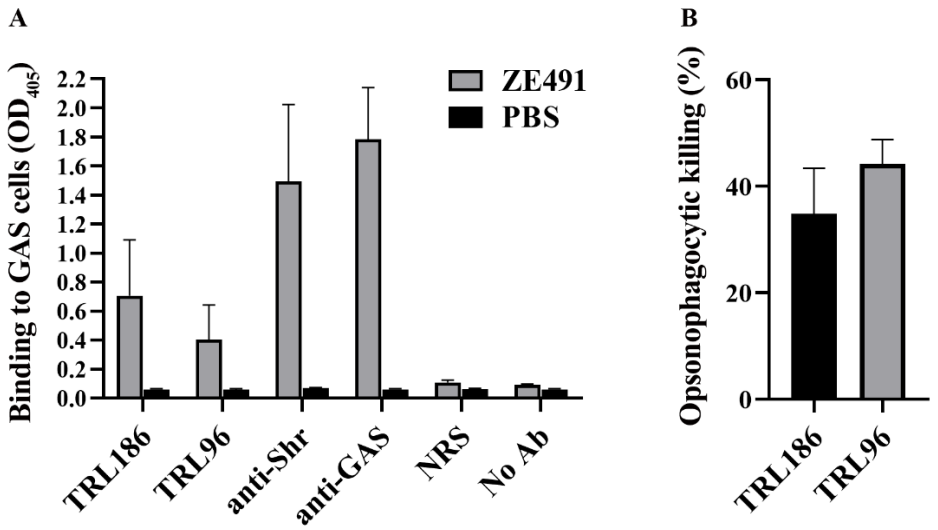

Figure 15 TRL96 and TRL186 bind to whole-cell and enhance opsonization

A. Microtiter wells coated with ZE491 strain of GAS were reacted with mAbs and antibody binding was detected. Data are from two experiments done in triplicates **B.** GAS cells (1000 CFU) preincubated with mAbs or NRS in 50% baby rabbit serum were added to HL60 cells. GAS survival after 30 min incubation was determined by measuring colony forming units. Data were derived from three experiments. The standard deviation (SD) is represented by the error bars.

4.3.2 TRL186 protects mice from invasive GAS infection

We evaluated the *in vivo* efficacy of the mAbs in a prophylactic model against systemic GAS infection (**Figure 16A**). A single dose of each mAb (15 mg/kg) was administered intraperitoneally into the mice of the experimental groups, while the control groups received the same volume of PBS. After one hour, we infected the mice with a mid-dose of MGAS5005 (10^7 CFU), and then monitored survival for five days. TRL186 conferred 100% protection to the mice. In contrast, mice receiving TRL96 were as susceptible as the control group. This observation implicates TRL186 in GAS protection while eliminating TRL96 from further analysis.

To explore the protection conferred by TRL186, we tested the therapeutic effectiveness **(Figure 16B**). CD-1 mice were first infected with a lethal dose of MGAS5005 (10^8 CFU), and the mAb was injected four hours after exposure. We observed a rapid progression of GAS infection in the control mice, which resulted in only 27% survival after five days. In contrast, mice that received TRL186 had a 73% survival rate. Together, the immunity conferred by TRL186 in both infection models suggests its potential utility in infection treatment.

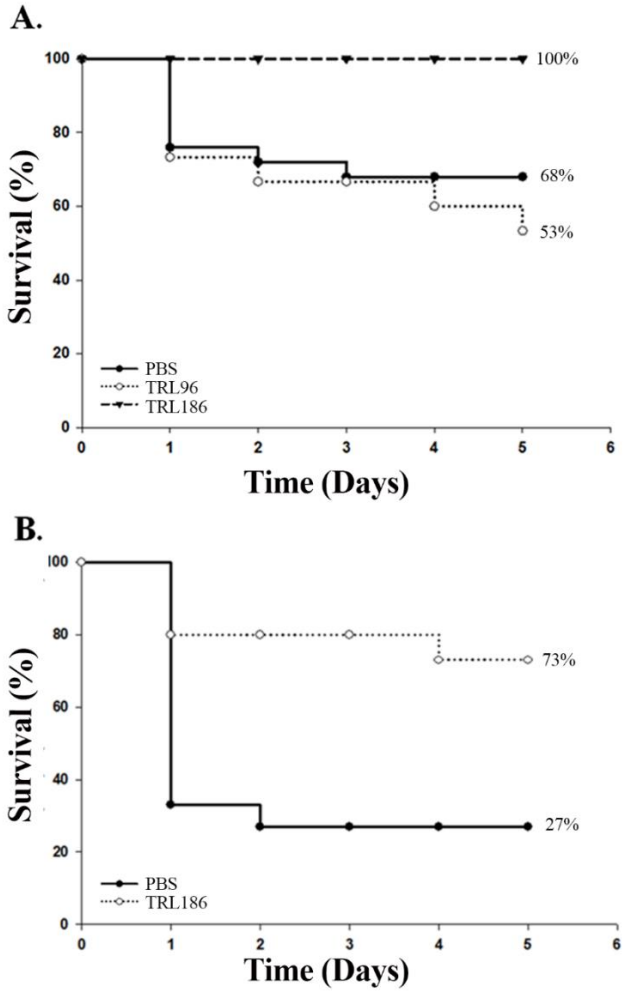

Figure 16 TRL186 protects mice from GAS infection

A. Prophylaxis of TRL96 and TRL186, **B.** Therapeutic efficacy of TRL186. Mice (N=15) were injected intraperitoneally with mAb (15 mg/kg) one hour before infection (**A**, $5x10^7$ CFU) or four

hours after infection (**B**, $1x10^8$ CFU) with MGAS5005. The data shown are pooled data from two independent experiments.

4.3.3 TRL186 interacts with a short segment in the NTR of Shr

An ELISA with immobilized Shr showed that TRL186 binds to the full-length Shr with high potency (K_D is in the 100 pM range, **Figure 17A**). We next performed an ELISA with Shr fragments to identify the binding site of TRL186. The Shr variants include recombinant proteins with just the NTR, the NEAT1 domain, or the NEAT2 domain **(Figure 17B)**. TRL186 generated a strong binding signal with the NTR fragment similar to the positive control, full-length Shr, while only background signals were recorded from the wells containing NEAT1 or NEAT2. To define the epitope region on the NTR recognized by TRL186, we constructed a series of overlapping peptides covering Shr-NTR comprising biotin-labeled 15-mers peptides with 12 overlapping amino acids in each peptide. Among 109 peptides covering the Shr-NTR region, only two peptides (#33 and #34) exhibited significant reactivity with TRL186 in an ELISA (**Figure 17C**). This analysis identified a short Shr segment (IKKGDKVTFISA) located at the end of the first DUF1533/HID region in the interaction with TRL186, which we mapped onto the predicted ribbon structure **(Figure 17D)**.

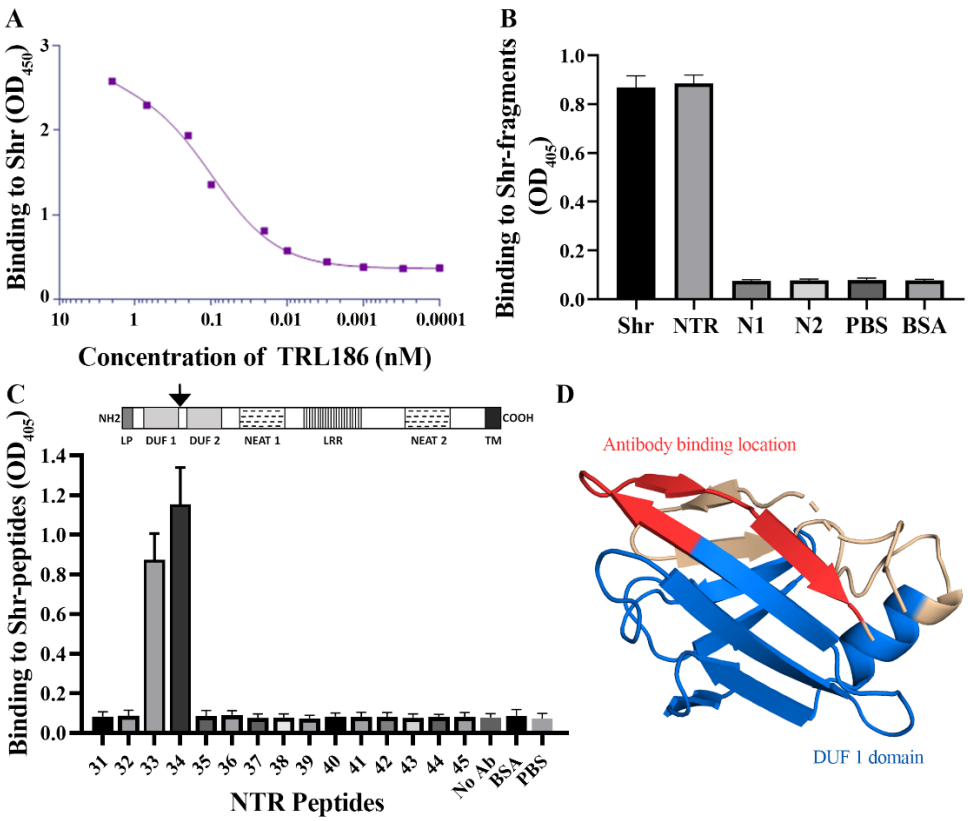

Figure 17 TRL186 affinity and binding site

A. TRL186 binds to Shr with high affinity. Microtiter plate wells coated with Shr were allowed to react with TRL186 in serial dilution starting at 5 ug/ml (30 nM). Antibody binding was plotted as a function of TRL186 concentration. **B**. **TRL186 binding is localized to Shr-NTR**. TRL186 was allowed to interact with wells coated with the full length Shr, NTR, NEAT1 (N1), or NEAT2 (N2)**. C. TRL186 binds to peptides from Shr-NTR**. TRL186 was allowed to react with immobilized peptides derived from NTR. The reaction in wells without antibody (no Ab), uncoated wells (PBS), or BSA coated wells (BSA) is shown. The data are pooled from three independent experiments. Error bars represent SD. The top panel in C shows a schematic representation of Shr. The black arrow indicates the TRL186 binding site. **D. Ribbon diagram of predicted DUF 1533 structure**. The first DUF1533 region is shown in blue, and the TRL186 binding location is in red.

4.3.4 TRL186 interferes with NTR-hemoglobin binding and hemoglobin-dependent growth of GAS

Since the NTR region is known to interact with hemoglobin, we examined the Shr-hemoglobin interaction in the presence of TRL186 in an ELISA. After optimizing the hemoglobin binding by purified NTR protein (**Figure 18A**), we evaluated the NTR-hemoglobin binding in the presence of increasing concentrations of TRL186. Hemoglobin binding by NTR was inhibited in a dose-dependent manner by TRL186 **(Figure 18B).** The maximum inhibition (43%) was achieved at 2 µg/mL concentration. The partial inhibition indicates that TRL186 did not block the entire region on the NTR that interacts with the hemoglobin.

Next, we tested if TRL186 impacts the bacteria's use of hemoglobin as a sole source of iron **(Figure 18C)**. We added TRL186 in THYB chelated with DP and supplemented with hemoglobin. Overnight-grown GAS cells (starting OD_{600} 0.01) were then added to investigate the antibody-mediated inhibition in heme iron uptake. We used TRL96 as a negative control since it binds to the NEAT1 domain (data not shown), which does not interact with hemoglobin [30]. 5 µM hemoglobin was sufficient for partial restoration of the GAS only culture and the TRL96 control. However, cultures grown with TRL186 did not exhibit restoration. Our data suggest that TRL186 prevents streptococci from interacting with hemoglobin and utilizing it as an iron source.

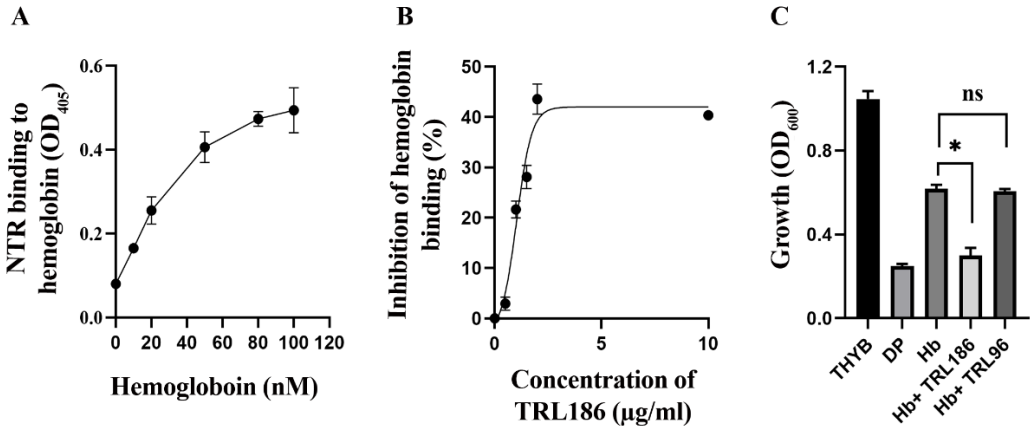

Figure 18 Impact of NTR-hemoglobin binding and hemoglobin-dependent growth in the presence of TRL186

NTR was allowed to react with biotin-labeled hemoglobin in the absence **(A)** or presence **(B)** of TRL186. AP-conjugated streptavidin was used to detect the Shr/hemoglobin interaction at 405 nm. Inhibition of hemoglobin binding (%) is plotted as a function of TRL186 concentration. **C.** NZ131 GAS cells were inoculated into THYB, iron-chelated THYB (DP), or THYB-DP supplemented with hemoglobin (Hb) with and without TRL186 or TRL96. Growth was monitored at 600 nm. Data are from two independent experiments done in duplicates. Error bars represent SD.

4.3.5 *TRL186 interacts with whole-cell and purified Shr of S. dysgalactiae*

Shr from GAS and SDSE have almost identical sequences in the TRL186 binding region **(Figure 19A)**. Therefore, we investigated the interaction of TRL186 in a whole-cell ELISA with SDSE (**Figure 19B**) and recombinant Shr_{SDSE} similar to that done with GAS cells and Shr_{GAS} **(Figure 19C)**. We recorded a strong binding signal in both cases, which suggests that the mAb also recognized Shr on the SDSE surface.

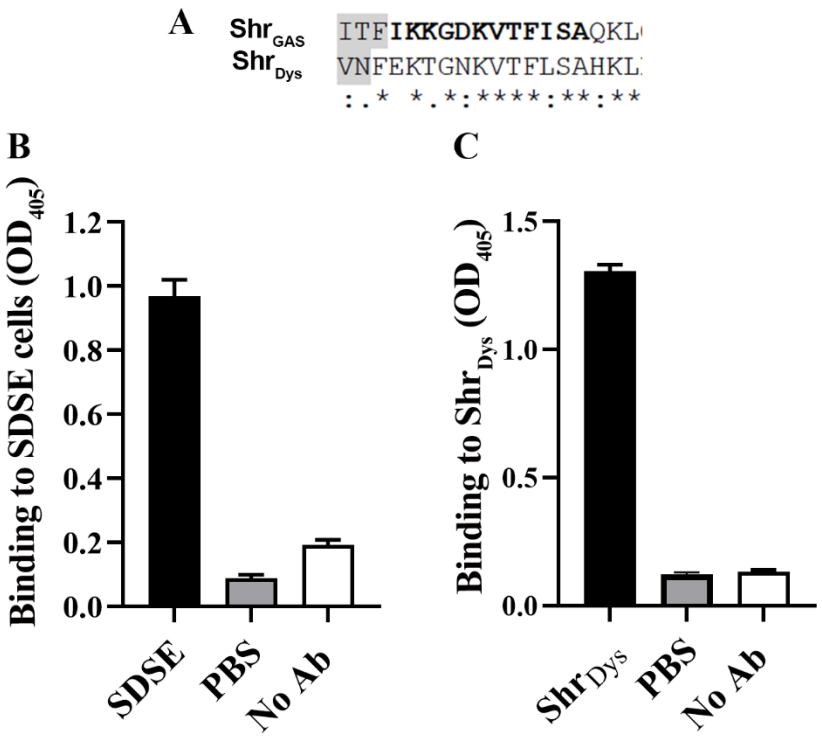

Figure 19 TRL186 interacts with SDSE cells and Shr protein

A. Sequence alignment of TRL186 binding site in Shr_{GAS} (WP_010922617.1) and Shr_{Dys} (BAH82346.1). The grey area indicates the border of the first DUF 1533. Microtiter plate wells coated with SDSE **(B)** or Shr_{DYS} protein **(C)** were allowed to react with TRL186, and antibody binding was detected. The reaction in wells without antibody (no Ab) or uncoated wells (PBS) is shown. Each bar represents an average of three repeats, and SD is represented by the error bars.

4.4 Discussion

Herein, we report a high-affinity mAb against Shr, which protects from systemic GAS infection in mice. This is the first human mAb described against a protein involved in GAS heme acquisition. In this study, we used a single B-lymphocyte technology to isolate a pool of mAbs

against GAS-Shr. Based on affinity to Shr, we selected two lead candidates (TRL96 and TRL186) for further characterization.

Shr is exposed on the streptococcal surface [57]. Our whole-cell ELISA with mAbs revealed that the epitopes on Shr are accessible on the surface and recognized by the mAbs (**Figure 15A**). Opsonophagocytic killing is a potent mechanism by which many bacterial surface-specific mAbs act to reduce bacterial load [137]. We previously showed that Shr antiserum evokes opsonizing antibodies that facilitate phagocytosis [92]. In a complement-mediated opsonization reaction, we observed both TRL96 and TRL186 enhanced GAS clearance, which suggests their potential in treatment (**Figure 15B**). Next, we investigated the ability of each mAb to protect mice in a prophylactic analysis. Prophylaxis with TRL96 conferred no protection to mice infected with GAS, while, TRL186 bestowed 100% protection (**Figure 16A**). Since TRL96 did not aid in protecting from GAS infection, we only tested TLR186 for its therapeutic value (**Figure 16B**). Mice that were given TRL186 four hours after exposure to GAS were almost 50% more likely to survive than mice given PBS. These protection data are encouraging since protection by antibody administrated after a challenge can be more difficult to achieve compared to a pre-challenge vaccination especially, in a model for aggressive systemic infection, as we used in this study. Prophylaxis with a human mAb to the hemoprotein receptor IsdB of *Staphylococcus aureus*, for example, confers significant protection in a lethal sepsis model, but not when given after the challenge [138]. Notably, the same IsdB mAb is protective in a staphylococcal catheter colonization model when administrated either pre- or post-infection. Together, the opsonic efficacy and protective potential suggest utility for TRL186 in the antibody-mediated treatment against the GAS disease.

Shr is a large surface protein that belongs to the GAS core genome. To better understand the mechanism of TRL186 *in vivo* protection, we investigated the antibody binding region. An ELISA indicated that the antibody binds the NTR (**Figure 17B**). The region was further narrowed using overlapping peptide sequences to identify a short sequence (IKKGDKVTFISA) at the end of the first DUF1533 region (**Figure 17C**). Using the protein prediction software, Modeller, we generated a ribbon structure of this region (**Figure 17D**). The antibody binding location appears to be at the end of the antiparallel β-sheet directly, a region that was recently recognized for interacting with hemoglobin [32].

The interactions between bacterial receptors and host hemoproteins consist of the first step in the process of heme uptake, in the case of Shr, this step is mediated by its NTR. A recent study extends the hemoglobin-capture mechanism by showing that two domains of unknown function (DUF1533) in the NTR, now named hemoglobin-interacting domains, bind hemoglobin independently [32]. Based on TRL186 binding region, it is reasonable to assume that the mAb is blocking Shr interaction with hemoglobin. We tested the ability of hemoglobin to bind to purified Shr in the presence of the mAb, and found that TRL186 inhibited NTR-hemoglobin binding in a concentration-dependent manner (**Figure 18B**). This observation raised the possibility that TRL186 interferes with heme uptake. The addition of hemoglobin or hemoglobin with TRL96 (control), to medium containing DP, which chelates free but not heme iron [139], restored GAS growth. In contrast, with TRL186, GAS growth remained inhibited, similarly to the DP only group (**Figure 18C**). These observations indicate that at least a part of TRL186 protection is due to the iron-starvation of the bacteria. Together, these data suggest that TRL186 offers protection by interfering with the heme intake. Notably, TRL96, which could not defend from GAS infection, had no impact on heme uptake. TRL186 may also offer protection against the recently recognized

emerging pathogen *S. dysgalactiae*, as the mAb showed specific reactivity with both whole-cells and purified Shr_{SDSE} (**Figure 19**).

Because of the central role of iron in infection, the iron uptake machinery is an attractive vaccination target. Cattle vaccination against a siderophore receptor, for example, reduced the load of *E. coli 0157* in feces and the rectoanal mucosa [140, 141]. Heme acquisition satisfies the iron requirement for GAS, and each of the heme uptake components characterized in GAS contributes to virulence [36, 57, 86, 93, 142, 143]. Therefore, an antibody-mediated treatment impacting heme intake may offer a promising treatment strategy. Blocking heme uptake is a significant part of the protection mechanism against *S. aureus* provided by human mAbs against the heme receptor, IsdA [144]. Redundancy often limits protection by an antibody that targets a single antigen [145], and using an antibody cocktail improved efficacy and strain coverage in several models for staphylococcal infections [146]. Hence, a combination therapy that consists of several mAbs that may include the heme receptors Shp [71] and HupY [93], and the binding protein SiaA (HtsA) [72] might increase the protection observed with TRL186.

Altogether, the data show that TRL186 elicited significant protection in mouse models, achieved by both opsonization and heme-blocking. Because TRL186's target antigen, Shr, belongs to the core genome of GAS and a few additional streptococci [30], it could be a therapeutic candidate with broad efficacy. The prevalence of antibiotic resistance places an urgent demand for new antimicrobial means. The recent strides in antibody discovery and engineering enabled the isolation of therapeutic antibodies candidate to treated infection by major bacterial pathogens, including *S. aureus*, *Bacillus anthracis*, and *Clostridium difficile* [145, 147-149]. Only a few protective mAbs were described in GAS. One recent example includes a mAb to the Platelet-Activating Factor Acetylhydrolase, SsE. Prophylaxis with an anti-SsE mAb increased neutrophil

infiltration, reduced lesion size, and systemic spread in mice challenged subcutaneously with the invasive MGAS5005 GAS strain [150]. To the best of our knowledge, TRL186 is the first mAb that increases mouse survival rate in a model for systemic GAS infection in a therapeutic mode. This study serves as a proof of concept for using mAbs that target heme uptake in GAS for immunotherapy.

5 CONCLUSIONS

GAS causes a wide variety of clinical manifestations through its arsenal of virulence factors and the ability to evade the host immune system. Incidence of antibiotic resistance and the emergence of new virulent strains further complicate the prevention and control of GAS infections. This dissertation intended to improve the understanding of heme uptake and its implications on bacterial physiology and disease. The investigations focused on GAS and related Gram-positive pathogens. The knowledge gained could then be used and for the development of new prevention and therapy.

Iron requiring pathogens employ different strategies for scavenging the metal from the host's restricted iron environment to survive and mount an infection. Previous studies from this lab showed that iron is essential for GAS growth, and heme satisfies most of its iron requirement as GAS is unable to utilize transferrin and lactoferrin [89]. This research group and others have established that Sia heme-relay proteins are involved in GAS virulence [30, 33, 34, 36, 57, 72, 86, 90-92, 117-119]. These findings demonstrate that the components of the heme acquisition pathways are critical virulence factors in the β-hemolytic GAS. This dissertation identified a new receptor and importer that are needed for GAS heme uptake and delineate their contribution in pathophysiology. The study also described human monoclonal antibodies that target the hemoprotein receptor, Shr, their efficacy, and protection mechanism.

The gene we named in this study, *hupY*, encodes a cell surface receptor that belongs to the core genome of GAS and the related vaginal colonizer and pathogen GBS [144]. Similar proteins promote adherence in other bacteria. Previous studies in GBS and GAS demonstrate that HupY is a protective antigen and that GAS expresses the *hupY* gene during infection [59-61]. This

dissertation describes the function of HupY and its role in GAS biology. The data identified receptor HupY as a new heme receptor, which promotes the acquisition of iron from hemoglobin and heme. HupY does not have a NEAT domain or any of the canonical motifs usually found in heme-binding proteins. HupY LRR (Leucine-rich repeat [80]) is the only common element it shares with some heme receptors, such as Shr (GAS) [30], IlsA (*B. cereus*) [151] and Hal (*B. anthracis*) [152]. Hence, HupY mediates heme capture by a novel mechanism. Additional studies are needed to determine how the cell-wall protein, HupY, transfer the heme into the cell. HupY may deliver its heme to one or more of the receptor proteins or the heme transporters encoded by the *sia* operon. It is also possible that HupY uses an independent pathway. Experiments in a murine model demonstrated that HupY serves a significant role in GAS and GBS colonization of the vaginal track. Together, these observations illustrate the important part of the iron and heme uptake proteins in the establishment of infection investigations in GAS, and related pathogens.

Shr, Shp, and SiaABC together play a significant role in heme capture and relay in GAS, but the function of the remaining *siaDEFGH* genes in the 10-gene *sia* operon was not described before this work. This investigation elaborated on the role of the last three genes, *siaFGH*, in iron homeostasis and virulence in GAS. The data established that SiaFGH is a new type of heme importer that contributes to GAS growth on heme iron and that this importer is imperative for both bacterial colonization and invasive infections. The SiaFGH proteins are highly conserved in GAS isolates, and the related *S. dysgalactiae* and *S. equi*, and homologous systems can be found in the genomes of additional Gram-positive bacteria, including important pathogens. Hence, the description if the SiaFGH function has broad impactions on bacterial physiology overall. Furthermore, conventional ABC transporters are the only type of heme importers that were described up to date [36, 72, 153]. The findings of an ECF heme transporter in this dissertation are

therefore novel and expands the paradigm of heme transport in bacteria overall. This investigation did aim at the import mechanism of the SiaFGH system, and additional studies are needed to examine this.

Shr, the first protein in the *sia* operon, is the only GAS protein shown to scavenge heme from host proteins. This dissertation used murine infection models to investigate the efficacy of human monoclonal antibodies (mAbs) against Shr. The experiments identified the monoclonal antibody, TRL186, as a high-affinity antibody that protects from invasive GAS infections. The data show that TRL186 binds near the hemoglobin-binding region of Shr and intervenes with hemoglobin binding by the purified receptor and in heme uptake by whole GAS cells. TRL186 is the first human mAb described against GAS protein involved in heme uptake. Shr (with the entire *sia* operon) is highly conserved among GAS isolates and Streptococci spices that harbor the operon. Hence, targeting Shr may avert the strain-diversity and cross-reactivity problems found with the M- based vaccines, and could facilitate protection against also from related streptococci.

In summary, this dissertation elaborates on the mechanisms for heme uptake, and their role in bacterial physiology and infection in GAS and related pathogens. The investigations demonstrated that targeting heme uptake proteins has the premise of yielding an effective treatment with broad protection for Streptococcal diseases.

Disclaimer: I, Nilanjana Chatterjee, conceived and contributed to the design and implementation of the research described in this dissertation. We wrote three manuscripts based on these findings with consultation with Dr. Zehava Eichenbaum and additional co-authors. In chapter one, I was responsible for investigating HupY binding to heme and the receptor role in GAS iron hemostasis and heme uptake. In Chapter II, constructed the complemented strain and conducted the experiments investigating the role of the SiaFGH proteins in GAS use of hemoproteins as an iron source and in heme import. In Chapter III, I determined TRL186 binding site, the antibody impact on hemoglobin binding by Shr and the use of hemoglobin iron by GAS, and its interactions with the *S. dysgalactiae* cells and proteins.

APPENDICES

Appendix A: Supplemental Tables

Appendix A.1 (Table S1: Differentially expressed genes (FDR <0.05) between WT NZ131 GAS grown in liquid culture (CDM) to bacteria colonizing the murine vaginal tract (Mouse))

Locus	Name	Description	WT_Mouse/ WT_CDM Fold change	WT_Mouse/ WT_CDM: FDR
spy49_0020	purC	Phosphoribosylaminoimidazole-succinocarboxamide synthetase	-17.79689279	3.9252E-27
spy49_0021	purL	Phosphoribosylformylglycinamidine synthase	-14.96843173	2.97204E-35
spy49_0022	purF	Amidophosphoribosyltransferase	-12.64638665	3.59039E-21
spy49_0023	purM	Phosphoribosylglycinamide cyclo-ligase	-12.26483359	2.11743E-11
spy49_0024	purN	Phosphoribosylglycinamide formyltransferase	-8.577561355	2.34114E-13
spy49_0025	purH	Bifunctional purine biosynthesis protein PurH	-12.95265693	8.39393E-17
spy49_0027	purD	Phosphoribosylamine-glycine ligase	-11.7123065	1.3817E-26
spy49_0028	purE	Phosphoribosyl carboxyaminoimidazole mutase	-10.62375203	1.32574E-16
spy49_0029	purK	Phosphoribosylaminoimidazole carboxylase	-11.45309502	2.47934E-19
spy49_0030		Hypothetical	-2.647293277	0.026089987
spy49_0031	purB	Adenylosuccinate lyase	-2.618810105	8.84673E-05
spy49_0032	comR	Cro/CI family transcriptional regulator	-2.440317465	0.017118775
spy49_0038	adhE	Bifunctional acetaldehyde-CoA/alcohol dehydrogenase	40.12663315	2.72862E-12
spy49_0039	adhP	Alcohol dehydrogenase	94.85044562	1.03862E-12
spy49_0044	rpsJ	SSU ribosomal protein S10p	-1.855981459	0.045601753
spy49_0046	rplD	LSU ribosomal protein L4p	-1.699724911	0.033931423
spy49_0059	rplE	LSU ribosomal protein L5p	-1.598571362	0.0434377

spy49_0067	rplO	LSU ribosomal protein L15p	-1.63057787	0.034983464
spy49_0068	secY	Preprotein translocase secY	-1.533273042	0.035611777
spy49_0069	adk	Adenylate kinase	-1.843282338	0.005791335
spy49_0073	rpsK	SSU ribosomal protein S11p	-1.798205748	0.015699409
spy49_0075	rplQ	LSU ribosomal protein L17p	-1.801846444	0.04175526
spy49_0078		4-diphosphocytidyl-2-c-methyl d-erythritol kinase	-2.841871511	0.000144147
spy49_0079		4-diphosphocytidyl-2-c-methyl d-erythritol kinase	-2.118752295	0.010434288
spy49_0083c		Histidine triad protein	3.493505965	0.035513787
spy49_0089		Dipicolinate Synthase, DNA binding protein	-4.213243931	7.59761E-05
spy49_0092	comYC	Putative competence protein	-16.71045907	0.016579383
spy49_0100	proC	Pyrroline-5-carboxylate reductase	2.241261205	0.008183834
spy49_0110c	hslO		-2.291765805	0.004435282
spy49_0111	nra	Regulatory protein	4.628441583	0.002364207
spy49_0112	cbp	Putative collagen binding protein	28.8277752	0.000101273
spy49_0113	lepA-1	Putative signal peptidase I	27.6303236	4.76209E-05
spy49_0114	cpa	Hypothetical, pilin related, sortase B signal domain	128.5972146	9.6656E-10
spy49_0116	srtB	NPQTN specific sortase B	22.87148797	0.000114638
spy49_0117	cpa	Hypothetical	40.38676901	9.06581E-08
spy49_0122c		Transcriptional regulator	263.0986236	1.54749E-07
spy49_0126c		Transcriptional regulator	6.058603003	8.01847E-07
spy49_0127		Translation initiation inhibitor	9.566704208	2.89342E-11
spy49_0128	sloR	Hypothetical, regulatory protein	23.16943635	1.50834E-14
spy49_0129		Hypothetical	313.6976398	2.18755E-09
spy49_0130	ntpI	ATP synthase subunit I	150.3667367	1.35913E-18
spy49_0131	ntpK	V-type ATP synthase subunit K	313.6976398	2.35748E-08
spy49_0132	ntpE	V-type ATP synthease subunit	114.1300285	1.69506E-12
spy49_0133	ntpC	V-type ATP synthase subunit C, oxidative phosphorylation	69.38875564	4.58367E-11
spy49_0134	ntpG	ATP synthase subunit F	56.18408362	1.2191E-08
spy49_0135	ntpA	V-type ATP synthase alpha chain	40.10153977	1.013E-14
spy49_0136	ntpB	V-type ATP synthase beta chain	55.30885223	3.20593E-15
spy49_0137	ntpD	V-type ATP synthase subunit D	40.23104119	3.68502E-13
spy49_0138c		Toxic anion resistance protein	3.033703084	0.000899301

spy49_0139c		Hypothetical	3.103681	0.012784526
spy49_0142		ABC transporter	-2.765488792	3.33971E-06
spy49_0151	metB	Cystathionine beta-lyase	3.73154311	2.02844E-05
spy49_0153	sgaT	Putative transport protein SgaT	606.9991739	5.42321E-11
spy49_0154	sgaB	PTS ascorbate transporter subunit IIB	33.37336365	1.35964E-06
spy49_0155	ptsN, ptxA, ulaC	PTS ascorbate transporter subunit IIA	35.70261679	2.98188E-07
spy49_0156	sgbH ulaD	3-keto-L-gulonate-6-phosphate decarboxylase	410.1262563	4.89557E-09
spy49_0157	sgaU, ulaE	L-xylulose 5-phosphate 3-epimerase	57.40443854	4.54118E-09
spy49_0158	araD, ulaF	L-ribulose-5-phosphate 4-epimerase	86.22549306	1.58141E-10
spy49_0160		L-ascorbate 6-phosphate lactonase	22.51462851	5.25408E-15
spy49_0161	opuAA	L-proline glycine betaine ABC transporter ATP-binding protein ProV	-5.833824633	0.003122534
spy49_0162	opuABC	L-proline glycine betaine ABC transporter ATP-binding protein ProW	-5.09235192	9.29565E-05
spy49_0169		Hypothetical	2.131357095	0.005961916
spy49_0189c	rofA.1	RofA family transcriptional regulator	4.789738816	0.000220758
spy49_0199	dut	Putative deoxyuridine 5-triphosphate	-2.97990095	7.48104E-06
spy49_0200	radA	RadA-like DNA repair protein	-2.683417358	2.92959E-06
spy49_0201		Carbonic anhydrase	-5.035620936	3.87769E-14
spy49_0211	nanE	N-acetylmannosamine-6-phosphate 2-epimerase	17.77032209	2.38442E-09
spy49_0212	ugpB	Sugar ABC transporter substrate-binding protein	14.96071212	5.90162E-12
spy49_0213	ugpA	Acetylneuraminate ABC Transporter permease	13.30723644	1.79798E-06
spy49_0214	ugpE	Sugar ABC transporter permease	7.78110658	2.57923E-05
spy49_0215		Hypothetical	13.56989279	3.65965E-06
spy49_0216	nanH	N-actylneuraminate lyase	16.02702835	1.05476E-11
spy49_0217		Glucose kinase	14.76841001	7.97692E-09
spy49_0235c		Hypothetical	256.8005765	1.12348E-05
spy49_0242	sufC	Iron-sulfur cluster assembly ATPase SufC	-3.557084614	2.3767E-07
spy49_0243	sufD	Iron-sulfur cluster assembly protein SufD	-3.987508443	1.66502E-08
spy49_0244		Cysteine desulfurase	-3.433696287	9.07E-05
spy49_0245	iscU	Iron-sulfer cluster assembly scaffold protein IscU	-3.544303086	1.66629E-06

spy49_0246	sufB	Iron-sulfur cluster assembly protein SufB	-4.962278409	1.73095E-12
spy49_0247	pbp7	D-alanyl-D-alanine carboxypeptidase	2.404750289	0.005649303
spy49_0248c	dacA	Penicillin-binding protein 7 precursor (PBP-7)	2.577022024	0.000123799
spy49_0259		Hypothetical	-1.84699643	0.040912596
spy49_0263		Ubiquinone/menaquinone biosynthesis methyltransferase	-1.774885871	0.017791308
spy49_0266	atmA	ABC transporter substrate-binding protein	-4.40073042	6.17997E-06
spy49_0276	lemA	Putative cytoplasmic membrane protein	-1.929674868	0.021429456
spy49_0285	snf	Putative SNF helicase	-1.960588728	0.004339213
spy49_0294		Hypothetical	-1.70055663	0.026351913
spy49_0307	ypaA	Riboflavin transporter YpaA	5.589643132	0.042798679
spy49_0315	fhuG	Ferrichrome transport system permease protein	2.778052575	0.003898829
spy49_0316	fhuB1	Ferrichrome transporter system permease protein	4.805916585	5.61368E-05
spy49_0317c	fhuD	Ferrichrome-binding periplasmid protein	4.654451381	0.000282152
spy49_0318	fhuC1	Ferrichrome transport ATP-binding protein	3.754058259	0.000789101
spy49_0333		Arsenate reductase	2.296610224	0.031503076
spy49_0335	lctO	L-Lactate oxidase	10.65140536	5.03718E-05
spy49_0336	prtS/spyCEP	Putative cell envelope proteinase	-3.180660552	0.004038505
spy49_0337		Hypothetical	6.757159823	9.34231E-06
spy49_0339	nrdF.2	Ribonucleotide reductase of class Ib (aerobic) beta subunit	432.0269702	3.57468E-27
spy49_0340	nrdI	Ribonucleotide reductase stimulatory protein	1079.152582	6.23852E-20
spy49_0341	nrdE.2	Ribonucleotide-diphosphate reductase subunit alpha	245.7685672	1.7568E-29
spy49_0356c		Hypothetical	-8.262593067	0.048523277
spy49_0357c		Hypothetical	-16.78897341	0.017320633
spy49_0367c		Hypothetical	-8.139490927	0.040423558
spy49_0374	glpT	Glycerol-3-phosphate transporter	5.846010406	2.07713E-08
spy49_0381	mtsA	Metal ABC transporter substrate-binding	6.225597117	1.13969E-19
spy49_0382	mtsB	ATP-binding protein MtsB	1.827231797	0.016788616
spy49_0383	mtsC	Integral membrane protein MtsC, ABC transporter	2.242106502	0.007912867
spy49_0390	pyrH	Uridylate kinase	-2.006082652	0.000703334

spy49_0392		S1 RNA binding domain	-2.074646658	0.000199685
spy49_0398		Myosin-cross-reactive antigen	3.047540798	0.019125795
spy49_0399	phoH	Putative phosphate starvation-induced protein	-1.989138114	0.002280657
spy49_0422	vacB	Putative exoribonuclease R	-2.010225372	0.001037552
spy49_0429c	gloA	Lactoylglutathione lyase	2.122292641	0.011968273
spy49_0430c		NAD(P)H-flavin oxidoreductase	2.029883409	0.033945217
spy49_0431c	pepQ	Putative Xaa-Pro dipeptidase	1.852149736	0.048568566
spy49_0432	ccpA	Catabolite control protein A	2.389637168	0.001379918
spy49_0436	tagH	Teichoic acid export ATP-binding protein TagH	12.78393915	8.83258E-06
spy49_0437		Hypothetical	4.852984544	0.003439383
spy49_0438		Hypothetical	4.858786638	0.001798229
spy49_0447	rnc	Ribonuclease III, dsRNA-specific ribonuclease	-2.324807158	0.013422537
spy49_0448	smc	Putative chromosome segragation SMC	-2.088613951	0.01056393
spy49_0484	bglG	Putative transcription antiterminator	3.991470691	0.012679178
spy49_0485		Putative PTS system, beta-glucosides-specific IIABC component	5.426753754	0.002361019
spy49_0487	bglA	Putative beta-glucosidase	4.739245828	0.000345994
spy49_0494	ptsK	HPr kinase phophorylase	-1.772587802	0.013037954
spy49_0495	lgt	Prolipoprotein diacylglyceryl transferase	-1.751382547	0.011828264
spy49_0508c		Endolysin, phage associated	3.385651366	0.019482521
spy49_0509		ABC transporter, permease subunit of cbiOQ-type, hypothetical	-7.513391597	1.83805E-06
spy49_0510		Hypothetical	-2.852711513	0.019125795
spy49_0513	ppc	Phosphoenolpyruvate carboxylase	-1.680603992	0.033751335
spy49_0525c	agaD	Putative PTS dependent galactosamine IID	7.466091353	0.034597322
spy49_0526c	agaW	Putative PTS dependent N-acetyl-galactosamine IIC componenet	7.500027807	0.024671471
spy49_0528c	ugl	Putative unsaturated glucuronyl hydrolase	4.646690433	0.034731292
spy49_0533	kdgA	4-hydroxy-2-oxoglutarate aldolase/2-dehydro-3-deoxyphosphogluconate aldolase	4.01709345	0.035225821
spy49_0540	fabG	Acetoin reductase	2.499154266	0.010360527
spy49_0541	dinG	DNA polymerase III, epsilon subunit/ATP-dependent helicase	1.806011875	0.044914097

spy49_0548	pepD	Probable dipeptidase A	2.302864213	0.020088445
spy49_0549	adcA	Zinc-binding protein adcA precursor	10.70996959	0.001727165
spy49_0550		GntR family transcriptional regulator	1.972463719	0.036814652
spy49_0551	agaS	Putative tagatose-6-phosphate aldose/ketose	2.934968062	0.000319433
spy49_0559		Phosphoglycolate phosphatase	-1.840691557	0.00349562
spy49_0564c		Transposon	5.878670267	9.22313E-05
spy49_0565c		Transposase	3.76663936	0.024020115
spy49_0566c		RofA family transcriptional regulator	7.266108739	4.90031E-07
spy49_0568	sagA	Streptolysin S associated protein SagA	32.15204399	6.25566E-14
spy49_0569	sagB	Streptolysin associated protein SagB	21.60066817	7.06213E-13
spy49_0570	sagC	Streptolysin associate protein SagC	22.18914609	4.90734E-14
spy49_0572	sagD	Streptolysin associated protein SagD	23.53155986	8.19461E-14
spy49_0573	sagE	Streptolysin associated protein SagE	26.66151094	2.50249E-11
spy49_0574	sagF	Streptolysin associated protein SagF	20.47607079	1.84002E-13
spy49_0575	sagG	SLS export ATP-binding protein SagG	13.77946268	6.25566E-14
spy49_0576	sagH	SLS export transmembrane protein SagH	19.05169381	1.29496E-12
spy49_0577	sagI	SLS export protein SagI	19.64803067	2.27917E-18
spy49_0582		F0F1 ATP synthase subunit C	-2.333301581	0.013057482
spy49_0583		F0F1 ATP synthase subunit A	-2.062037626	0.001848147
spy49_0584		F0F1 ATP synthase subunit B	-1.747488406	0.021019874
spy49_0587		F0F1 ATP synthase subunit Gamma	-1.785796558	0.024878338
spy49_0588		F0F1 ATP synthase subunit Beta	-1.731788201	0.027174456
spy49_0593	endA	DNA-entry nuclease fragment	-2.20039985	0.024816975
spy49_0594		Pseudogene	-2.139981014	0.031310712
spy49_0596	pheS	Phenylalanyl-tRNA synthetase alpha chain	-1.954764996	0.046662575
spy49_0600		Hypothetical	-3.036551696	0.002364207
spy49_0601		ABC transporter ATP-binding protein	-3.671097568	9.80299E-10
spy49_0607c	mscL	Putative large conductance mechanosensitive channel	-2.321413584	0.034983464
spy49_0638c	folC.2	Deihydrofolate synthase/folylpolyglutamate synthase	2.403523837	0.001170307
spy49_0642		Hypothetical	1.872334713	0.018284724
spy49_0646		Capsular polysaccharide biosynthetsis regulatory protein	-2.20048541	0.014963993
spy49_0651	pyrP	Putative uracil permease	2.320597814	0.000331948
spy49_0652	pyrB	Aspartate carbamoyltransferase	2.088415886	0.013841151

spy49_0653	carA	Carbamoyl-phosphate synthase small chain	1.863465029	0.007522449
spy49_0661	hupY	Cell surface protein, MtsR repressed	27.25598866	1.07219E-21
spy49_0662	hupZ	Regulatory protein, heme utilization protein, MtsR-repressed	37.6885773	8.39393E-17
spy49_0669	pfoR	Putative regulatory protein, possible toxin regulator	2.296115394	0.000614135
spy49_0671	apbA	2-dehydropantoate 2-reductase	2.608263631	0.000408468
spy49_0672	fruR	Putative transcipriotnal repressor	3.83192317	0.002044836
spy49_0673	fruK	Tagatose-6-phosphate kinase 1-pohsphofructokinase	4.422714519	0.000789101
spy49_0674	fruA	PTS system, fructoase-specific IIABC component	3.035252732	0.004176921
spy49_0686c		5-nucleotidase	-5.323517253	1.27582E-07
spy49_0689		Two component sensor histidine kinase	1.894947547	0.011582364
spy49_0690	mvaK1	Mevalonate kinase	-1.595389928	0.042419206
spy49_0696	thyA	Thymidylate synthase	-1.749802494	0.034983464
spy49_0697	dyr	Dihydrofolate reductase	-1.851828525	0.00977296
spy49_0701	engB	GTP-binding protein EngB	-1.659524049	0.031188118
spy49_0712	pyrF	Orotidine 5-phosphate decarboxylase	5.354968508	0.003379324
spy49_0713	pyrE	Orotate phosphoribosyltransferase	4.376429356	0.001210992
spy49_0715		ABC trasnporter	-3.628258265	8.11082E-09
spy49_0716	yckA	Amino acid ABC transporter permease yckA	-3.269312297	8.74686E-08
spy49_0717	ung	Uracil-DNA glycosylase	-1.913304699	0.017909501
spy49_0722	bcaT	Branched-chain amino acid aminotransferase	-2.105047717	0.007891447
spy49_0725c		Hypothetical	-7.116583756	6.75192E-10
spy49_0726		Hypothetical	-6.088512285	7.22378E-07
spy49_0727		Hypothetical	-4.766727359	6.43354E-05
spy49_0735	recJ	Single stranded DNA specific exonuclease recJ	-1.628379165	0.038274324
spy49_0737	dnaD	DNA replication protein	-1.874747386	0.005084225
spy49_0738	nth	Endonuclease III	-1.635075702	0.042419206
spy49_0746c		Prophage ps2 integrase	4.205086167	0.010665396
spy49_0747c		Hypothetical	5.715224159	0.000258304
spy49_0748c		Phage-associated protein	2.761791092	0.018956537
spy49_0749c		Repressor phage associated	3.086746726	0.010666067

spy49_0750		Hypothetical	-15.86305232	3.18298E-05
spy49_0751c		Hypothetical	2.960409688	0.033945217
spy49_0752		Phage DNA-binding anti-repressor protein	-48.0403898	1.8283E-05
spy49_0753		Phage excisionase	-8.616417275	0.007461577
spy49_0755		Hypothetical protein	-10.14593276	0.024671471
spy49_0756		Hypothetical	-11.42452997	0.000137999
spy49_0759		Phage associate protein, hypothetical	-18.51940234	2.17911E-08
spy49_0760		Phage-associated protein	-19.08183987	1.29496E-12
spy49_0761		Phage associate protein, hypothetical	-12.46355741	1.93284E-09
spy49_0762		Bacteriophage-type DNA polymerase	-43.99589661	2.85587E-09
spy49_0763		DNA primase/helicase Phage associated	-19.52280751	5.16224E-10
spy49_0765		Phage associated helicase	-47.94535003	1.40334E-09
spy49_0766		Hypothetical	-11.03377912	0.001164427
spy49_0767		Phage associated transcriptional activator	-25.86810101	6.28156E-05
spy49_0768		Phage terminase small subunit	-27.15730197	0.003444264
spy49_0769		Phage terminase large subunit	-72.65214123	3.31639E-15
spy49_0770		Phage portal protein	-25.09495611	6.21429E-13
spy49_0771		Phage associate protein, hypothetical	-254.4361957	3.97929E-17
spy49_0772		Putative phage associated protein	-184.7148826	1.74276E-13
spy49_0773		Phage scaffold protein, hypothetical	-88.12464903	4.836E-16
spy49_0774		Hypothetical phage, major head protein	-108.6673651	2.86999E-16
spy49_0775		Hypothetical phage protein	-88.17792193	2.289E-09
spy49_0776		Hypothetical phage protein	-127.04592	1.39206E-10
spy49_0777		Hypothetical	-68.91028783	4.94274E-15
spy49_0778		Hypothetical phage protein	-192.1943446	9.1468E-12
spy49_0779		Hypothetical phage protein	-152.4505395	4.68091E-14
spy49_0780		Phage associate protein, hypothetical	-84.0216645	1.13644E-11
spy49_0781		Putative phage associated protein	-27.82531338	4.16193E-05
spy49_0782		Phage associate protein, hypothetical	-75.03119465	3.57E-13
spy49_0783		Phage associate protein, hypothetical	-68.40416421	6.94022E-11
spy49_0784		Phage associated protein	-54.56162604	6.73744E-11
spy49_0785		Phage hyaluronidase	-36.82409233	8.80808E-15
spy49_0788		Hypothetical	-50.70878832	2.81011E-10
spy49_0789		Phage associated holin	-68.47589395	1.7247E-12
spy49_0790		Cell wall hydrolase	-51.51289336	1.38618E-09
spy49_0792	speH	Streptococcal pyrogenic exotoxin H	-48.95184061	0.00018136
spy49_0797		ABC transporter substrate-binding protein	-2.725069393	0.002021338

spy49_0799		ABC transport protein	-2.722868678	0.007986381
spy49_0800		Putative ABC transporter system ATP-binding protein	-2.746529236	0.01281917
spy49_0803	estA	Tributyrin esterase	-1.841984595	0.004712627
spy49_0807	acoA	Pyruvate dehydrogenase E1 component alpha	-4.665429853	3.30519E-08
spy49_0808	acoB	Pyruvate dehydrogenase E1 component beta	-4.116077938	5.11083E-07
spy49_0809	acoC	Dihydrolipoamide acetyltransferase component of pyruvate dehydrogenase complex	-3.659765614	1.8283E-05
spy49_0810	acoL	Dihydrolipoamide dehydrogenase	-3.217580783	8.01017E-05
spy49_0819	hemN	Coproporphyrinogen III oxidase, oxygen-independent	-2.26199892	0.003823167
spy49_0820		Acyl-AC thioesterase	-2.290878853	0.005097765
spy49_0831	csrA, msrB	Peptide methionine sulfoxide reductase msrB	-3.055962036	0.021098697
spy49_0833		PTS Mannose transporter subunit IIA	6.451100515	0.003633704
spy49_0834	manX, ptsA	PTS sorbose transporter subunit IIB, kinase	37.08893398	1.56007E-08
spy49_0835	manY, ptsB	PTS Mannose transporter subunit IIC, transporter	73.82399305	4.18523E-10
spy49_0836	manZ, ptsC	PTS Mannose transporter subunit IID	50.11562252	6.86673E-16
spy49_0841		Succinate-semialdehyde dehydrogenase NADP+	3.117562043	0.000100792
spy49_0842	uvrC	Putative excinuclease ABC	1.879303671	0.028973212
spy49_0850c	pgdA2	Polysaccharide deacetylase	2.719240483	0.007338216
spy49_0851	folC1	Dihydrofolate synthase/folylpolyglutamate synthase	-2.234330951	0.012025362
spy49_0861c	citA	Putative two-component response regulator of citrate/malate metabolism	4.066748445	0.005026719
spy49_0862c	citB	Putative two-component histidine kinase regulator of citrate/malate metabolism	7.443618691	5.03718E-05
spy49_0863	malP	L-malate permease	14.90127796	1.61878E-05
spy49_0864	sfcA	Malate dehydrogenase, pyruvate metabolism	29.75196646	1.85098E-07
spy49_0865c	tdh	Alcohol dehydrogenase, zinc-containing	46.56033856	1.63792E-09
spy49_0866	aphA	Acid phosphatase	7.738101403	2.88469E-08

spy49_0867	eriC	Voltage-gated chloride channel family protein	-2.26753101	0.001444832
spy49_0868	tesA	Putative platelet activating factor	-2.882532158	0.006737777
spy49_0871c		Glutamine amidotransferase, class I predicted	-2.145792252	0.006671851
spy49_0882c		Hypothetical	-4.005479982	0.00014365
spy49_0883	proV	L-proline glycine betaine ABC transport ATP-binding protein	-1.666774299	0.037836445
spy49_0884	proX	L-proline glycine betaine binding ABC transporter protein / osmotic adaptation	-2.232805443	0.000144147
spy49_0885	guaB	GMP reductase	-2.181839836	0.026089987
spy49_0888	uraA	Xanthine permease	-8.221235311	1.01149E-10
spy49_0893	tdk	Thymidine kinase	-1.985605635	0.011968273
spy49_0894	prfA	Peptide chain release factor 1	-2.30321357	0.000492223
spy49_0895	hemK	Putative protoporphyrinogen oxidase	-2.513544205	4.38133E-05
spy49_0897		Hypothetical	-2.046855884	0.002436412
spy49_0898	glyA	Serine hydroxymethyltransferase	-1.983019785	0.001120622
spy49_0899		Hypothetical	-1.736549073	0.022738984
spy49_0900		Pneumococcal vaccine antigen A-like protein	-1.974422991	0.007100475
spy49_0901	mdlB	ABC transporter, ATP-binding/permease protein	-2.19622152	8.04067E-05
spy49_0902	mdlB	Putative ABC transporter	-2.248073163	0.000160656
spy49_0903	nox1	NADH oxidase	-2.024908245	0.00119981
spy49_0908		Hypothetical	-2.24075808	0.025340448
spy49_0909c		Hypothetical	-1.874446132	0.007998265
spy49_0910c	hlyIII	Putative hemolysin III	-2.706223469	0.031856136
spy49_0920	satD	Putative acid tolerance SatD-like protein	2.629643215	0.00921343
spy49_0921		Hypothetical (with 0920)	2.189528764	0.024671471
spy49_0927c	citG	2-(5-triphosphoribosyl)-3-dephosphocoenzyme-A synthase	2.010103009	0.026197044
spy49_0928c	gntR	Transcriptional regulator, GntR family	2.529038773	0.018530699
spy49_0929c	citM	Citrate transporter	180.3183757	2.35748E-08
spy49_0933	oadB	Oxaloactetate decarboxylase beta chain	3.450846803	0.046199775
spy49_0934	citD	Putative citrate lyase, gamma subunit	24.91386645	0.034282888
spy49_0936	citE	Citrate lyase beta chain	6.858722692	0.0015172
spy49_0937	citF	Citrate lyase alpha chain	5.76456311	0.000625878

spy49_0938	citX	Probably apo-citrate lyase phosphoribosyl-dephospho-CoA transferase	15.11182782	0.001383202
spy49_0939	oadA	Methylmalonyl-CoA decarboxylase alpha chain	10.54152762	0.000119483
spy49_0949	guaA	GMP synthase - glutamine--hydrolyzing	-1.93012536	0.002770622
spy49_0952c	uup	ABC transporter, ATP-binding protein	2.188226876	0.010360527
spy49_0955	ar08	Putative transcriptional regulator/amino transferase	3.288233982	0.017529591
spy49_0957c		Putative anaerobic ribonucleotide reductase	-2.260231629	0.029331598
spy49_0958c	cls	Cardiolipin synthetase	-5.040102022	6.37712E-10
spy49_0959c	fhs1	Putative formate-tetrahydrofolate ligase	-7.860783756	3.47495E-23
spy49_0960c	lplA	Lipoate-protein ligase A	-2.459314707	0.000319433
spy49_0961c		Hypothetical	-2.770318673	2.06533E-06
spy49_0962c		Hypothetical	-2.88342636	1.95796E-06
spy49_0963c		Glycin cleavage system H protein	-2.742336987	9.98796E-05
spy49_0964c		Hypothetical	-2.422993345	0.000287506
spy49_0965c	nemA	Putative trimethylamine dehydrogenase	-2.592908629	1.97077E-05
spy49_0966c	lplA	Lipoate-protein ligase A	-2.509925798	0.02105516
spy49_0968	dfp	Phosphopantothenoylcysteine decarboxylase	2.479455893	0.010360527
spy49_0969		Hypothetical	2.468507087	0.047892353
spy49_0970	pgmA	Phosphoglucomutase	1.767496761	0.032108872
spy49_0979c	ciaH	Putative histidine kinase protein	1.978119987	0.034282888
spy49_0992c		Riboflavin kinase/FMN adenylyltransferase	-1.963730642	0.014956362
spy49_0993c	truB	tRNA pseudouridine 55 synthase	-1.930949352	0.001185382
spy49_0994c		Hypothetical	-1.782797608	0.045601753
spy49_0997c	salY	Putative ABC transporter, permease protein	2.44760198	0.006250833
spy49_1000c		Putative transcriptional regulator	-1.681991057	0.009554571
spy49_1004c		Hypothetical	-2.253749551	0.038486879
spy49_1005c		Hypothetical	-2.387656596	0.032091677
spy49_1006c		Hypothetical	-3.185898137	0.003047678
spy49_1008	alsT	Putative amino acid symporter	-4.349013372	6.27314E-05
spy49_1010c	cfa	CAMP factor	82.84636014	2.65555E-27
spy49_1014c	phnA	Hypothetical	-1.947383574	0.048265786
spy49_1017c	pyk	Putative pyruvate kinase	-1.639083476	0.020510501
spy49_1018c	pfk	6-phosphofructokinase	-2.124634218	0.001983442

spy49_1019c	dnaE	DNA polymerase III alpha subunit	-2.002784373	0.002037038
spy49_1025c	glgP	Maltodextrin Phosphorylase	21.58386151	1.63831E-08
spy49_1026c	malQ	4-alpha-glucanotransferase	18.18852952	9.82702E-08
spy49_1027c	malR	Putative maltose operon transcriptional repressor	2.826093806	0.000384846
spy49_1028	malE	Maltose maltodextrin ABC transporter substrate binding protein	15.46352092	2.49416E-08
spy49_1029	malF	Maltose ABC transporter permease	20.27905927	7.12456E-07
spy49_1030	malG	Maltose ABC transporter permease	31.15558597	1.66502E-08
spy49_1042c		Hypothetical	33.29123811	0.014667452
spy49_1043c	celB	Putative PTS system IIC component	6.986453731	0.002105406
spy49_1047c	bglG	Putative transcription antiterminator	13.12540796	0.000195228
spy49_1048c		Hypothetical	48.22881506	0.001170307
spy49_1050	pnuC	Ribosyl nicotinamide transporter, pnuC-like protein	9.150465023	6.6551E-08
spy49_1065		Diaminopimelate epimerase, hypothetical	22.77316828	1.05654E-10
spy49_1066c	uhpC	Hypothetical	4.021031983	0.001799862
spy49_1070c	paaI	Phenylacetic acid degradation protein	-2.766202786	0.000696465
spy49_1084c	inlA	Internalin	72.90151761	3.87777E-09
spy49_1086c		Hypothetical	-2.398325739	0.038069395
spy49_1087c	dnaX	DNA polymerase III subunites gamma and tau	-2.392852078	4.38133E-05
spy49_1088c		Hypothetical	-3.348717103	7.6948E-06
spy49_1091	deaD2	Putative RNA helicase	2.401165224	0.015936478
spy49_1092c	pgdA1	Polysaccharide deacetylase family protein	1.906394237	0.016365217
spy49_1093c	gapN	Non-phosphorylated glyceraldehyde-3-phosphate dehydrogenase (NADP)	-5.155698767	1.26091E-13
spy49_1096	nrdH	Putative glutaredoxin	-2.429094123	0.007323837
spy49_1097	nrdE1	Ribonucleotide reductase of class Ib (aerobic) alpha subunit	-1.951876373	0.02105516
spy49_1111c	uhpC	Oxalate:formate antiporter MFS transporter	-19.9198025	2.48375E-23
spy49_1113c	coiA	Putative transcription factor	3.130180199	0.025629671
spy49_1122c	sodM	Superoxide dismutase (Mn)	-6.801497329	1.54056E-08
spy49_1129		Hypothetical	2.93651403	0.017118775
spy49_1132c	deaD1	Putative ATP-dependent RNA helicase	-3.29149566	9.82702E-08
spy49_1140c	fdhC	Formate/nitrite transporter family member	4.624272461	1.57632E-07
spy49_1144	pyrD	Dihydroorotate dehydrogenase	-1.873912179	0.017529591

spy49_1151c		Hypothetical surface protein, LPXTG-motif cell wall anchor	1.669778078	0.021429456
spy49_1159c	manB	Phosphoglucomutase, phosphomannomutase	13.35158803	3.1763E-19
spy49_1160c	phr	Putative deoxyribodipyrimidine photolyase	-2.020277826	0.012248332
spy49_1164	clpE	Putative ATP-dependent protease	-1.820392585	0.024964831
spy49_1173c	ftsZ	Cell division protein ftsZ	-1.700245027	0.040006861
spy49_1179c	typA	Putative GTP-binding protein	-2.129799525	0.000230236
spy49_1180c	pspB	Hypothetical	1.987194299	0.002254952
spy49_1181c	nagC	Glucokinase	1.691807564	0.034446745
spy49_1192c	arcC	Carbamate kinase	225.9117465	1.59788E-23
spy49_1193c	argE	Hypothetical, ArgE related	404.2111083	2.18777E-28
spy49_1194c		Hypothetical, Arginine:ornithine antiporter, disrupted	355.4907536	6.39761E-24
spy49_1195c	arcB	Ornithine carbamoyltransferase	241.2815319	3.11951E-19
spy49_1196c		Hypothetical, Acetyltransferase	611.8943636	2.40228E-22
spy49_1197c	arcA	Arginine deiminase	111.7202145	7.64226E-12
spy49_1198c	crp	Transcriptional regulator, CrP/Fnr family	4.845677777	5.56804E-07
spy49_1199	argR	Putative arginine repressor	17.04394215	9.93912E-09
spy49_1201c	mmcQ	Hypothetical	2.288159198	0.001070959
spy49_1202c	yesM	Putative two-component sensor histidine kinase	2.718546552	0.00020817
spy49_1203c	yesN	Putative two-component response regulator	3.398321982	0.001028007
spy49_1204c	msrA1	Peptide methionine sulfoxide reducatese	79.40381568	2.32983E-10
spy49_1205c	bcp	Hypothetical, Dihydroneopterin aldolase, related to Bcp	21.00258457	2.24258E-05
spy49_1206c	ccdA	Cytochrome C biogenesis protein	33.14663669	1.73956E-06
spy49_1208c	cas1	CRISPR-associated endonuclease Cas1	3.438513426	0.006096268
spy49_1213c	srmB	ATP-dependent RNA helicase SrmB	3.95687147	0.005943056
spy49_1225c	aroE1	Shikimate 5-dehydrognase	2.170894264	0.042344714
spy49_1226c	bgaA, lacZ	Beta-galactosidase	12.93419172	1.70254E-11
spy49_1227c		Putative two-component sensor response regulator	8.351911231	3.61108E-07
spy49_1228c		Putative two-comonent sensor histidine kinase	8.070624862	2.23849E-10
spy49_1229c		Hypothetical	6.138142463	0.002283896
spy49_1230c	ugpB	ABC transporter substrate-binding protein	141.1243538	1.22457E-13

spy49_1231c	ugpE	Sugar ABC transporter permease	11.47418165	0.000591869
spy49_1233c	lplB	Sugar ABC transporter permease	19.46513739	3.58254E-06
spy49_1234	nagC	Putative transcriptional regulator	40.55615048	0.005929735
spy49_1235c	bglB	Beta-glucosidase	4.052081707	0.00023796
spy49_1236c	hyl	Putative hyaluronidase	4.473714091	0.000202509
spy49_1237c	purR	Putative transcritional regulator	3.22188338	0.010817526
spy49_1238		Hypothetical	27.13718343	0.00027006
spy49_1239	ams1	Alpha mannosidase	12.87685888	3.63221E-06
spy49_1240c	rocA	Putative histidine kinase protein	2.157932965	0.012679178
spy49_1247c	psrp-1	Ribosomal subunit interface protein	3.512530706	9.81664E-06
spy49_1248c	comF	Putative late competence protein	31.74915131	0.015256458
spy49_1251	cysM	Cysteine synthase	-14.24378964	8.86503E-06
spy49_1253c	cof	Hydrolase, haloacid dehalogenase family, cyclophilin type	-1.925720276	0.006999703
spy49_1272	gntT	Putative permease	2.132688736	0.044674748
spy49_1275c		Hypothetical	-1.938269457	0.001446396
spy49_1281c	nadE	NAD synthetase	-1.76037966	0.004598548
spy49_1283c	aapA	Amino acid permease	-1.836140451	0.009472094
spy49_1284c	nox2	Thioredoxin reductase	-2.054306613	0.000261186
spy49_1286c	glnQ	Amino acid ABC transporter, ATP-binding protein	-7.031212455	1.08973E-09
spy49_1287c	hisM	Putative amino acid ABC transporter	-5.392679784	5.27868E-13
spy49_1289c	srmB	Putative ATP-dependent RNA helicase	-2.29893595	4.13025E-05
spy49_1297c		Hypothetical	1.856821645	0.037310348
spy49_1301c	ptsH, tal	Transaldolase	25.03248199	3.61331E-13
spy49_1303c		Putative transcriptional regulatory protein	7.38130445	3.34235E-07
spy49_1304c	npx	Putative NADH peroxidase	5.314937219	2.29944E-06
spy49_1305c	glpF1	Glycerol uptake facilitator protein	5.943563644	0.016721871
spy49_1312c		Hypothetical	2.196646354	0.000345916
spy49_1313c	ara1	2,5-diketo-D-gluconic acid reductase	2.087374974	0.024816975
spy49_1318c	degV	Hypothetical	-4.529566708	3.8158E-11
spy49_1320c	cof	Hypothetical	2.171235436	0.001446396
spy49_1321c		Hypothetical	1.9229184	0.023858836
spy49_1322c	lacD1	Tagatose-bisphosphate aldolase	21.90628534	1.95885E-06
spy49_1323c	lacC1	Tagatose-6-phosphate kinase	26.18147717	0.019490032
spy49_1324c		Tagatose-6-phosphate kinase/1-phosphofructokinase	57.39859142	0.008963751

spy49_1325c	lacB	Galactose-6-phosphate isomerase	48.37565138	1.32099E-05
spy49_1326c	lacA	Galactose-6-phosphate isomerase lacA subunit	17.59736404	2.23575E-05
spy49_1327c	gatC	PTS galactitol transporter subunit IIC	49.69593237	1.80192E-09
spy49_1328c	sgaB	PTS fructose transporter subunit IIB	200.1925265	1.60185E-05
spy49_1329c	ptsN	PTS galactose transporter subunit IIA	23.55067819	6.54348E-05
spy49_1330	lacR1	Lactose phosphotransferase system repressor	4.387289054	6.69503E-05
spy49_1336c	rbfA	Ribosome binding factor A	-1.954391735	0.004176921
spy49_1337c	infB	Translation initiation factor 2	-1.827952354	0.008838765
spy49_1340c	nusA	Transcription termination protein, NusA-like	-1.883770974	0.027174456
spy49_1346	hit	Putative cell-cycle regulation histidine triad protein	2.686616051	0.014740275
spy49_1347		Hypothetical	4.165747937	0.000181155
spy49_1348c	lytR	Putative transcriptional regulator	-2.192877258	0.000384176
spy49_1349c	rimL	Histone acetyltransferase	-2.894235375	2.63385E-06
spy49_1350c		Hypothetical	-3.803393528	2.68599E-09
spy49_1351c		Hypothetical	-14.70667371	9.51827E-15
spy49_1359c	accA	Acetyl-coenzyme A carboxylase carboxyl transferase alpha	-58.49370472	3.25485E-32
spy49_1360c	accD	Acetyl-coenzyme A carboxylase carboxyl transferase beta	-58.39520559	3.25485E-32
spy49_1361c	accC	Acetyl-Coa carboxylase biotin carboxylase	-65.60029207	1.38446E-51
spy49_1362c	fabZ	3-hydroxyacyl-dehydratase, acyl-carrier protein	-60.8603585	1.08795E-36
spy49_1363c	accB	Acetyl-CoA carboxylase biotin carboxyl carrier protein subunit	-63.82355684	1.47328E-33
spy49_1364c	fabF	3-oxoacyl-ACP synthase	-76.74515658	5.50614E-54
spy49_1365c	fabG	3-oxoacyl-acyl-carrier protein reductase	-14.52243017	1.67878E-31
spy49_1366c	fabD	ACP S-malonyltransferase	-98.87776466	2.86019E-44
spy49_1367c	fabK	2-nitropropane dioxygenase	-106.102435	1.01143E-53

spy49_1368c	acpP	Acyl carrier protein	-13.9283794	1.59313E-12
spy49_1369c	fabH	3-oxoacyl-ACP synthase	-22.68423	1.172E-27
spy49_1370c	fabT	MarR family transcriptional regulator	-25.53787578	3.12045E-27
spy49_1371c	phaB	enoyl-CoA hydratase	-60.41181526	2.78751E-39
spy49_1374c	dnaK	Chaperone protein	3.047815034	0.018032691
spy49_1377c		Putative N-acetyl-muramidase	3.032642656	3.3683E-05
spy49_1378c	vanY	D-alanyl-D-alanine carboxypeptidase	2.483130411	0.000494918
spy49_1379c	phoE	Phosphoglycerate mutase family	2.212101292	0.011061102
spy49_1388c		Aspartate aminotransferase	-1.700316671	0.041121424
spy49_1389	uspA	Universal stress response protein	3.936846647	0.000296809
spy49_1390c	cof	Hypothetical	-2.445358509	3.46888E-05
spy49_1395c	siaH	ECF transporter, A component	2.563668954	0.002828757
spy49_1396c	siaG	ECF transporter, T component	2.700265152	0.004640134
spy49_1397c	siaF	ECF transporter, S component	4.705517065	2.7169E-08
spy49_1398c	siaE	Putative ABC transporter	7.030614116	4.13488E-10
spy49_1400c	siaD	Putative ABC transporter	12.49346497	6.12148E-09
spy49_1401c	siaC	Heme ABC transporter, ATP-binding	15.67647343	4.87133E-07
spy49_1402c	siaB	Heme ABC transporter, permease	10.81538051	1.89066E-07
spy49_1403c	siaA	Heme ABC transporter, substrate-binding	20.57639598	3.84341E-08
spy49_1404c	shp	Streptococcal hemoprotein transport protein	**Annotated as combined with spy49_1403c	
spy49_1405c	shr	Heme binding Fe3+ siderophore transport protein	25.46105991	4.08402E-12
spy49_1407c	isp2	Immunogenic secreted protein	1.691973784	0.015898135
spy49_1409c	acpS	Holo-acyl-carrier protein synthase	-2.044186084	0.013057482
spy49_1413c	scrK	Fructokinase	21.98071921	0.000230236
spy49_1414c	endoS	Hypothetical, endo-beta-N-acetylglucosaminidase	23.23737584	2.84998E-08
spy49_1415c	scrA	Putative sucrose-specific PTS permease, enzyme II	3.046649468	0.002018734
spy49_1423c	uvrA	UvrABC system protein A	-3.101023433	1.16801E-07
spy49_1430	mutY	A/G specific adenine glycosylase	-2.380481236	0.000723107
spy49_1432c	trx2	Thioredoxin reductase	-1.917244928	0.020002095
spy49_1442	pfl	Formate acetyltransferase	10.30261685	1.75947E-12
spy49_1453		Putative repressor, phage associated	3.248837759	0.035611777

spy49_1506c	dnaC	DNA replication protein	-3.478315292	0.029125542
spy49_1526		Hypothetical	3.548844621	0.001352219
spy49_1529		Hypothetical, repressor protein	1.910511986	0.019293062
spy49_1530	xerD	Prophage NZ131.3 probable integrase	2.44062093	0.010360527
spy49_1531		Hypothetical	2.403727204	0.023528208
spy49_1533c	soxR, merR	Transcriptional reguator, MerR family	5.329089802	1.8283E-05
spy49_1534c	dnaQ	Putative DNA polymerase III epsilon subunit	8.378152135	0.00148635
spy49_1535c		Hypothetical	1.751985875	0.034597322
spy49_1538		Hypothetical	2.571530374	0.013902021
spy49_1540c	deoC	Deoxyribose-phosphate aldolase	4.840260857	2.22931E-08
spy49_1541c	nupC	Nucleoside permease nupC	4.52695301	7.33698E-07
spy49_1542c	udp	Uridine phosphorylase	4.553718221	4.57794E-07
spy49_1543	phnF, gntR	Transcriptional regulator, GntR family	11.71860152	1.15619E-10
spy49_1544	rpsN	SSU ribosomal protein S14p	23.74880893	8.6714E-05
spy49_1545c	gcp	Putative glycoprotein endopeptidase	-1.60542909	0.026197044
spy49_1546c	rimI	Ribosomal protein S18p-alanine acetyltransferase	-1.572330706	0.037310348
spy49_1547c		Inactive metal-dependent protease-like protein, putative molecular chaperone	-1.721184338	0.017320633
spy49_1550c	glnA	Glutamine synthetase	2.138390458	0.001962679
spy49_1551c	glnR	Putative transcriptional regulator	2.226394608	0.034446745
spy49_1555c	hflC	Hypersensitive-induced response protein-like protein	-2.619201418	1.86134E-05
spy49_1561c	pyrG	CTP synthase	-2.068073213	0.011968273
spy49_1565c		Hypothetical	-2.06658535	0.006132285
spy49_1567c	thiD	Phosphomethylpyrimidine kinase	-1.735028555	0.008863426
spy49_1568c	truA	tRNA pseudouridine synthase A	-1.555154073	0.042440998
spy49_1574	hsdM	Putative type I site-specific deoxyribonuclease	1.891056005	0.026718848
spy49_1575c		Hypothetical	66.80118719	0.003494663
spy49_1583c	salA	Lantibiotic salivaricin A precursor	7.888489315	0.027435286
spy49_1584c	lacG	6-phospho-beta-galactosidase	26.25658359	2.73901E-05
spy49_1585c	lacE	PTS lactose transporter subunit IIBC	43.38347301	8.35821E-10
spy49_1586c	lacF	PTS system, lactose-specific IIA component	16.95876742	3.689E-05
spy49_1587c	lacD2	Tagatose 1,6-diphosphate aldolase	33.9949957	1.99704E-06

spy49_1588c	lacC2	Tagatose-6-phsophate kinase	10.3781957	0.000747633
spy49_1589c	lacB2	Galactose-6-phosphate isomerase subunit LacB	6.915812889	0.012750448
spy49_1590c	lacA2	Galactose-6-phosphate isomerase lacA2 subunit	7.861614837	0.005652392
spy49_1598c		Hypothetical	-3.827437711	0.021337443
spy49_1599c	degV	DegV-domain containing protein	-8.143391329	1.01115E-16
spy49_1601c	spoU	23s rRNA methyltransferase	-1.857616588	0.002343973
spy49_1602c		Hypothetical	-2.148782759	0.01283226
spy49_1609c	mipB	Hypothetical, transaldolase	38.17099218	1.12402E-10
spy49_1610c	ulaA, sgaT	PTS beta-glucoside transporter subunit IIBC	33.26382575	1.83405E-10
spy49_1611c	sgaB	PTS maltose transporter subunit IIBC	122.7184284	1.34106E-05
spy49_1612c	bglG	PTS fructose transporter subunit IIA	20.38768527	6.75624E-09
spy49_1626c	pulA	Amylopullulanase, Type II secretory pathway, surface protein	10.57066254	1.56184E-07
spy49_1627c	dexB	Glucan 1,6 alpha glucosidase	15.66804303	7.87661E-07
spy49_1628c	msmK	Sugar ABC transporter, ATP-binding protein	4.130621343	0.000603266
spy49_1630	ska	Streptokinase	-7.56996973	1.77886E-06
spy49_1633c	sclA	Collagen-like surface protein	-4.351050979	0.005187232
spy49_1635c	rgfB	Hypothetical, transaldolase	47.66859929	5.75804E-08
spy49_1636c	rgfD	PTS glucose transporter subunit IIABC	30.02094187	7.85367E-11
spy49_1637c		Hypothetical	-1.986837026	0.003902288
spy49_1638c	prmA	Ribosomal protein L11 methyltransferase	-1.941057282	0.001558135
spy49_1640c	nudB	MutT/nudix family protein	-2.139225705	0.000750684
spy49_1641c	nudA	Hypothetical	-2.16596377	0.013300771
spy49_1642c		Hypothetical	-1.938710583	0.002283896
spy49_1654	trpG	Anthranilate synthase	3.329538224	0.000139654
spy49_1655		ATPase AAA family	2.188709437	0.00451878
spy49_1656	pai1	Pai1 protein	3.392473983	0.027879215
spy49_1657	adk, flaR	DNA topology modulation protein FlaR, putative	3.663728035	0.000354778
spy49_1658c		Hypothetical	12.33569291	0.00088254
spy49_1659c		Hypothetical	11.22847913	9.41317E-06
spy49_1666c	htpA	Hypothetical, Histidine triad HIT protein	90.74322524	5.59299E-08

spy49_1667c	lmb	Laminin-binding surface protein, possible zinc receptor	98.66845063	3.52318E-06
spy49_1669c	scpA	C5a peptidase precursor	-2.873454883	0.001832438
spy49_1670c	ennX	EnnX protein	-4.650260935	0.014749085
spy49_1671c	emm49	Antiphagocytic M protein	-5.312780329	0.000399589
spy49_1672c		Fc-gamma receptor, membrane bound metalloprotease	4.579737457	9.68729E-05
spy49_1675c	isp1	Immunogenic secreted protein	1.843988803	0.041691184
spy49_1676c	baeS	Two-component system histidine kinase	1.916836074	0.009420574
spy49_1684c	sof	Serum opacity factor, invasion of epithelial cells	-3.119944298	0.023784854
spy49_1687c	prsA2, ropA	Foldase protein	144.6055099	7.4313E-17
spy49_1688c		Hypothetical	388.4682734	1.0215E-21
spy49_1689c	spi	spi, SpeB protease inhibitor	912.4167145	1.16891E-20
spy49_1690c	speB	Streptococcal cysteine protease/streptococcal pyrogenic exotoxin B	877.302944	8.25052E-11
spy49_1691	ropB	Rgg-like transcription regulator	2.574026368	0.002182807
spy49_1692c	mf1	Streptodornase, mitogenic factor I	33.12348164	2.28785E-23
spy49_1695c	gldA	Glycerol dehydrogenase	32.02257611	4.06407E-17
spy49_1696c	mipB	Fructose-bisphosphate aldolase	45.16837549	3.68357E-12
spy49_1697c	pflD	Pyruvate formate-lyase	23.14568344	1.842E-11
spy49_1698c	celB	Putative cellobiose-specific IIC component	2057.870482	1.79875E-15
spy49_1699c	celA	PTS cellobiose transporter subunit IIB	455.3697644	5.64188E-10
spy49_1700c	celC	PTS cellobiose transporter subunit IIA	509.688244	1.22736E-12
spy49_1703	pflA	Pyruvate formate-lyase activating enzyme	5.421751513	2.57923E-05
spy49_1707c	tdcF	Putative translation initiation inhibitor	-2.224330789	0.019490032
spy49_1713	pepD	Dipeptidase	27.36644523	5.56782E-15
spy49_1715c	groEL	Heat shock protein 60 family chaperone GroEL	3.911111868	0.00285931
spy49_1716c	groES	Heat shock protein 60 family co-chaperone GroES	3.426481674	0.012248332
spy49_1719c	csp	Major cold-shock protein	-3.866690785	0.001558135
spy49_1723c	hutI	Imidazolonepropionase	188.493026	2.32983E-10
spy49_1724	hutU	Urocanate hydratease	285.8861059	1.26892E-09
spy49_1725	ftcD	Glutamate formiminotransferase	872.3619209	2.40343E-08

spy49_1726		Sugar ABC transporter substrate binding protein	501.3313399	9.51866E-07
spy49_1727	fhs2	Formate-tetrahydrofolate ligase	1628.163098	4.18693E-10
spy49_1728		Hypothetical	708.9504584	3.64792E-08
spy49_1729	potE	Amino acid permease	1214.642433	8.54024E-10
spy49_1730	hutH	Histidine ammonia lyase	1260.532264	6.75192E-10
spy49_1731	hutG	Formimidoylglutamase	65.76939255	1.06429E-10
spy49_1732c		LuxR family transcriptional regulator	23.90783049	7.55422E-14
spy49_1742		Hypothetical	3.355303788	0.006558367
spy49_1747c	nrdD	Ribonucleotide reductase of class III anaerobic, large subunit	3.301192679	0.000193999
spy49_1748c	ccs4	Hypothetical competence-induced protein Ccs4	2.10290423	0.011124005
spy49_1753c	recA	RecA protein	-1.649149643	0.036814652
spy49_1781	padR	PadR family transcriptional regulator	-17.2800362	0.000349799
spy49_1782		Hypothetical	-22.73548907	2.37523E-05
spy49_1783		Hypothetical, membrane protein	-16.68154616	7.46402E-05
spy49_1784c		Phage infection protein	4.449412095	0.004186831
spy49_1785	acrR	Putative transcriptional regulator	43.04552065	0.008105739
spy49_1790c		DHH family protein	-1.806344977	0.011704247
spy49_1794	sdhB	L-serine dehydratase, beta subunit	11.16538746	5.53127E-11
spy49_1795	sdhA	Serine dehydratase subunit alpha	9.721170804	2.03487E-09
spy49_1811c	glcU	Hypothetical	-2.159703997	0.010922519
spy49_1819c		Probable transposase for insert-like sequence element IS1161	9.633091252	0.000195228

Appendix A.2 (Table S2: Bacterial strains and plasmids used)

Strain Name	**Description**	**Citation**
NZ131	Wild-type *Streptococcus pyogenes* strain isolated from a patient with post-streptococcal glomerulonephritis	[154]
NZ131*ΔhupY* *	NZ131 *ΔhupY*::*aphA3* Kan^R	This study
BH10C	*E. coli* cloning strain	[155]
E.coli BL21 Star	Host for pZZ1 expression	Invitrogen

Plasmid	**Description**	**Citation**
pFED760	pGh9-ISS1 deleted for insertion element by inverse PCR; temperature sensitive replication origin, Erm^R	[105, 156]
pJC159	pFED760 with *ermB* replaced with chloramphenicol resistance marker *cat*, Cm^R	[62]
pOsKaR	Source of *aphA3* Kan^R cassette	[157]
pJC303	pLZ12-Spec-based vector with *recA* constitutive promoter upstream of multiple cloning site, $Spec^R$	[158]
pLC007 **	*hupY* complementation plasmid, *hupY* inserted downstream of the *recA* promoter in pJC303	This study
pET101/D-TOPO	Directional TOPO®TA cloning vector	Invitrogen

pZZ1	pET101 based vector that expresses HupY-His tag from P_{T7}	This study

* Mutant is stable and does not require antibiotics for retention

** Plasmid is retained during overnight growth in liquid culture without the addition of antibiotics

Appendix A.3 (Table S3: Cloning and qPCR primers)

Cloning primers

Primer	**Description**	**Sequence**
LC149	*hupY* Upstream S PstI	GACTGCAGAGCTTGTTGACTTAAAGTCAACA
LC150	*hupY* Upstream AS 2step	GTTATCATTTTTTCTCCTTAAATCAATTGTGGTAAAACCTTTCTAAAAGCCAAC
LC151	*hupY* Downstream S 2step	GTTGGCTTTTAGAAAGGTTTTACCACAATTGATTTAAGGAGAAAAAATGATAAC
LC152	*hupY* Downstream AS NotI	AGGCGGCCGCCTTGGATGGTTAGCCATTATCATA
LC153	Plasmid AS MluI inv	ACGCGTATTGATTTAAGGAGAAAAAATGATAAC
LC154	Plasmid S MluI inv	ACGCGTTGTGGTAAAACCTTTCTAAAAGCCAAC
LC184	GAS lrrG compl S Gibson	tgaaaaagattttggtaaggggcggccgcATGAAGAAACATCTTAAAACAG

LC185	GAS lrrG compl AS Gibson	ataacctgaaggaagatctggatccTTAATATTTTTTC TTTTTTATAGCAGTTATTAG
ZE435	*hupY* forward primer, TA cloning	CACCATGCACAATCAGGAAGTTTTT
ZE436	*hupY* revers primer, TA cloning	TATTGCAGAGTGTCGTCCTCTATTCGTT TTT

qPCR primers		
LC060	*gyrA* S qPCR primer	CAATGGATGGGGATGGTG
LC061	*gyrA* AS qPCR primer	CGCTGGTAAAACAAGAGGTTC
LC082	*proS* S qPCR primer	TGAGTTTATTATGAAAGACGGCTATAG
LC083	*proS* AS qPCR primer	AATAGCTTCGTAAGCTTGACGATAATC
LC092	*spy49_1781* S qPCR primer	TCAAAGAATCCACCCTCTATCC
LC093	*spy49_1781* AS qPCR primer	CCCGAAGAAGTGACAGCATA
LC094	*spy49_1782* S qPCR	AAGGAAGCTGCCAGTGAAAT
LC095	*spy49_1782* AS qPCR	CAGCAATACGGGTAAAGCAA
LC192	*hupY* S qPCR primer	TACTGCAGGTAAAGCGTTGTT
LC193	*hupY* AS qPCR primer	GCCTTCTTGGTCACTAAAGCC
LC278	*hupZ* S qPCR primer	ACAAACCTGTAACCTAAAAG
LC279	*hupZ* AS qPCR primer	AAAGGTCAACCCAATATTGG

Appendix B Supplemental figures

Appendix B.1 (figure S1: RNA Seq validation)

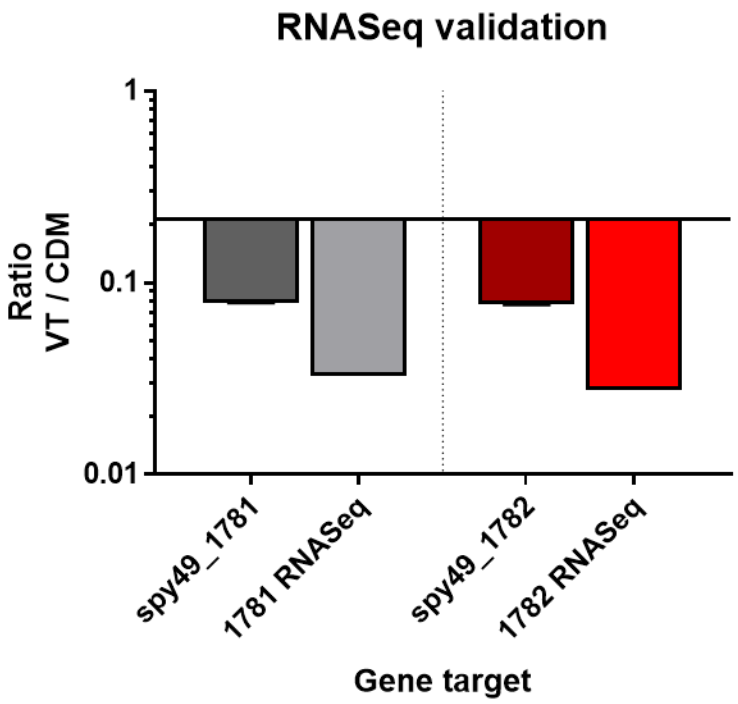

qRT-PCR data validated the RNASeq results. Quantitative RT-PCR was done on two genes shown to be downregulated in the vaginal tract via RNASeq (*spy49_1781* and *spy49_1782*). qPCR showed that both genes were downregulated in the vaginal tract (darker bars), matching the expression patterns obtained by RNA sequencing (lighter bars).

Appendix B.2 (figure S2: Expression of hupZ)

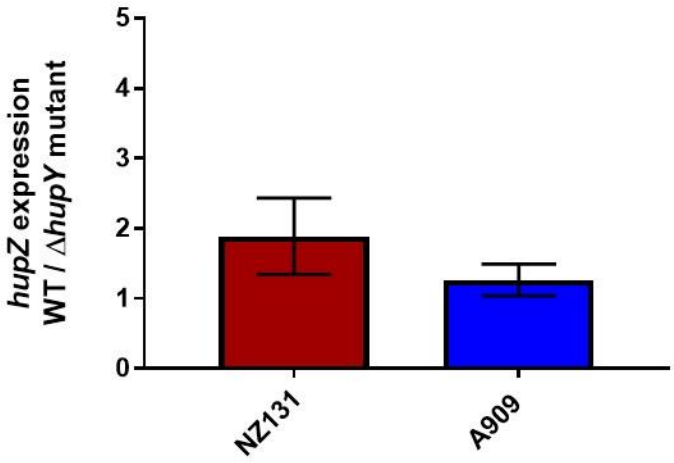

Expression of *hupZ* is not affected by deletion of *hupY* in GAS or GBS. Quantitative RT-PCR was done on replicate RNA samples collected from WT GAS and GBS strains as well as their isogenic mutant Δ*hupY* strains. Comparison of *hupZ* transcription between the WT and mutant strains showed no significant difference in the expression of *hupZ*, demonstrating that deletion of *hupY* was nonpolar.

REFERENCES

1. Cunningham MW. Pathogenesis of group A streptococcal infections and their sequelae. Advances in experimental medicine and biology **2008**; 609:29-42.

2. Carapetis JR, Steer AC, Mulholland EK, Weber M. The global burden of group A streptococcal diseases. The Lancet Infectious diseases **2005**; 5:685-94.

3. Watkins DA, Johnson CO, Colquhoun SM, et al. Global, Regional, and National Burden of Rheumatic Heart Disease, 1990-2015. The New England journal of medicine **2017**; 377:713-22.

4. Steer AC, Carapetis JR, Nolan TM, Shann F. Systematic review of rheumatic heart disease prevalence in children in developing countries: the role of environmental factors. Journal of paediatrics and child health **2002**; 38:229-34.

5. Lamagni T, Guy R, Chand M, et al. Resurgence of scarlet fever in England, 2014-16: a population-based surveillance study. The Lancet Infectious diseases **2018**; 18:180-7.

6. Tyrrell GJ, Fathima S, Kakulphimp J, Bell C. Increasing Rates of Invasive Group A Streptococcal Disease in Alberta, Canada; 2003-2017. Open forum infectious diseases **2018**; 5:ofy177.

7. Centers for Disease Control and Prevention. Active Bacterial Core Surveillance Report, Emerging Infections Program Network, Group A Streptococcus, 2017, **2017**.

8. Leonard A, Wright A, Saavedra-Campos M, et al. Severe group A streptococcal infections in mothers and their newborns in London and the South East, 2010-2016: assessment of risk and audit of public health management. BJOG : an international journal of obstetrics and gynaecology **2019**; 126:44-53.

9. Lu B, Fang Y, Fan Y, et al. High Prevalence of Macrolide-resistance and Molecular Characterization of Streptococcus pyogenes Isolates Circulating in China from 2009 to 2016. Frontiers in microbiology **2017**; 8:1052.

10. Plainvert C, Martin C, Loubinoux J, et al. Highly virulent M1 Streptococcus pyogenes isolates resistant to clindamycin. Medecine et maladies infectieuses **2015**; 45:470-4.

11. Cohen-Poradosu R, Kasper DL. Group A streptococcus epidemiology and vaccine implications. Clinical infectious diseases : an official publication of the Infectious Diseases Society of America **2007**; 45:863-5.

12. Pahlman LI, Olin AI, Darenberg J, et al. Soluble M1 protein of Streptococcus pyogenes triggers potent T cell activation. Cellular microbiology **2008**; 10:404-14.

13. Massell BF, Honikman LH, Amezcua J. Rheumatic fever following streptococcal vaccination. Report of three cases. Jama **1969**; 207:1115-9.

14. McMillan DJ, Dreze PA, Vu T, et al. Updated model of group A Streptococcus M proteins based on a comprehensive worldwide study. Clinical microbiology and infection : the official publication of the European Society of Clinical Microbiology and Infectious Diseases **2013**; 19:E222-9.

15. Sekuloski S, Batzloff MR, Griffin P, et al. Evaluation of safety and immunogenicity of a group A streptococcus vaccine candidate (MJ8VAX) in a randomized clinical trial. PloS one **2018**; 13:e0198658.

16. Dale JB, Penfound TA, Chiang EY, Walton WJ. New 30-valent M protein-based vaccine evokes cross-opsonic antibodies against non-vaccine serotypes of group A streptococci. Vaccine **2011**; 29:8175-8.

17. Henningham A, Gillen CM, Walker MJ. Group a streptococcal vaccine candidates: potential for the development of a human vaccine. Current topics in microbiology and immunology **2013**; 368:207-42.

18. Bullen JJ, Rogers HJ, Spalding PB, Ward CG. Natural resistance, iron and infection: a challenge for clinical medicine. Journal of medical microbiology **2006**; 55:251-8.

19. Tong Y, Guo M. Bacterial heme-transport proteins and their heme-coordination modes. Archives of Biochemistry and Biophysics **2009**; 481:1-15.

20. Skaar EP. The battle for iron between bacterial pathogens and their vertebrate hosts. PLoS pathogens **2010**; 6:e1000949.

21. Stojiljkovic I, Perkins-Balding D. Processing of heme and heme-containing proteins by bacteria. DNA and cell biology **2002**; 21:281-95.

22. Letoffe S, Redeker V, Wandersman C. Isolation and characterization of an extracellular haem-binding protein from Pseudomonas aeruginosa that shares function and sequence similarities with the Serratia marcescens HasA haemophore. Molecular microbiology **1998**; 28:1223-34.

23. Rossi M-S, Fetherston JD, Létoffé S, Carniel E, Perry RD, Ghigo J-M. Identification and Characterization of the Hemophore-Dependent Heme Acquisition System of Yersinia pestis. Infection and Immunity **2001**; 69:6707-17.

24. Cope LD, Thomas SE, Latimer JL, Slaughter CA, Muller-Eberhard U, Hansen EJ. The 100 kDa haem:haemopexin-binding protein of Haemophilus influenzae: structure and localization. Molecular microbiology **1994**; 13:863-73.

25. Stojiljkovic I, Larson J, Hwa V, Anic S, So M. HmbR outer membrane receptors of pathogenic Neisseria spp.: iron-regulated, hemoglobin-binding proteins with a high level of primary structure conservation. Journal of bacteriology **1996**; 178:4670-8.

26. Henderson DP, Payne SM. Characterization of the Vibrio cholerae outer membrane heme transport protein HutA: sequence of the gene, regulation of expression, and homology to the family of TonB-dependent proteins. Journal of bacteriology **1994**; 176:3269-77.

27. Lewis LA, Gray E, Wang YP, Roe BA, Dyer DW. Molecular characterization of hpuAB, the haemoglobin-haptoglobin-utilization operon of Neisseria meningitidis. Molecular microbiology **1997**; 23:737-49.

28. Mazmanian SK, Skaar EP, Gaspar AH, et al. Passage of heme-iron across the envelope of Staphylococcus aureus. Science (New York, NY) **2003**; 299:906-9.

29. Andrade MA, Ciccarelli FD, Perez-Iratxeta C, Bork P. NEAT: a domain duplicated in genes near the components of a putative Fe3+ siderophore transporter from Gram-positive pathogenic bacteria. Genome Biol **2002**; 3:RESEARCH0047.

30. Ouattara M, Cunha EB, Li X, Huang YS, Dixon D, Eichenbaum Z. Shr of group A streptococcus is a new type of composite NEAT protein involved in sequestering haem from methaemoglobin. Molecular microbiology **2010**; 78:739-56.

31. Bates CS, Toukoki C, Neely MN, Eichenbaum Z. Characterization of MtsR, a new metal regulator in group A streptococcus, involved in iron acquisition and virulence. Infection and immunity **2005**; 73:5743-53.

32. Macdonald R, Cascio D, Collazo MJ, Phillips M, Clubb RT. The Streptococcus pyogenes Shr protein captures human hemoglobin using two structurally unique binding domains. The Journal of biological chemistry **2018**; 293:18365-77.

33. Ouattara M, Pennati A, Devlin DJ, Huang YS, Gadda G, Eichenbaum Z. Kinetics of heme transfer by the Shr NEAT domains of Group A Streptococcus. Archives of biochemistry and biophysics **2013**; 538:71-9.

34. Nygaard TK, Blouin GC, Liu M, et al. The mechanism of direct heme transfer from the streptococcal cell surface protein Shp to HtsA of the HtsABC transporter. The Journal of biological chemistry **2006**; 281:20761-71.

35. Hanks TS, Liu M, McClure MJ, Lei B. ABC transporter FtsABCD of Streptococcus pyogenes mediates uptake of ferric ferrichrome. BMC microbiology **2005**; 5:62.

36. Montanez GE, Neely MN, Eichenbaum Z. The streptococcal iron uptake (Siu) transporter is required for iron uptake and virulence in a zebrafish infection model. Microbiology (Reading, England) **2005**; 151:3749-57.

37. Hamburger M, Jr., Green MJ, Hamburger VG. The problem of the dangerous carrier of hemolytic streptococci; spread of infection by individuals with strongly positive nose cultures who expelled large numbers of hemolytic streptococci. J Infect Dis **1945**; 77:96-108.

38. Erdem G, Sinclair S, Marrone JR, et al. Higher rates of streptococcal colonization among children in the Pacific Rim Region correlates with higher rates of group A streptococcal disease and sequelae. Clin Microbiol Infect **2010**; 16:452-5.

39. DeMuri G, Wald E. The Group A Streptococcal Carrier State Reviewed: Still an Enigma. Journal of the Pediatric Infectious Diseases Society **2017**; 3:336-42.

40. Sobel J, Funaro D, Kaplan E. Recurrent group A streptococcal vulvovaginitis in adult women: family epidemiology. Clin Infect Dis **2007**; 44.

41. Stamm WE, Feeley JC, Facklam RR. Wound infections due to group A streptococcus traced to a vaginal carrier. J Infect Dis **1978**; 138:287-92.

42. Berkelman RL, Martin D, Graham DR, et al. Streptococcal wound infections caused by a vaginal carrier. JAMA **1982**; 247:2680-2.

43. James WE, Badger GF, Dingle JH. A study of illness in a group of Cleveland families. XIX. The epidemiology of the acquisition of group A streptococci and of associated illnesses. N Engl J Med **1960**; 262:687-94.

44. Dhar V, Roker K, Adhami Z, McKenzie S. Streptococcal vulvovaginitis in girls. Pediatr Dermatol **1993**; 10:366-7.

45. Stricker T, Navratil F, Sennhauser FH. Vulvovaginitis in prepubertal girls. Arch Dis Child **2003**; 88:324-6.

46. Donald FE, Slack RC, Colman G. Streptococcus pyogenes vulvovaginitis in children in Nottingham. Epidemiol Infect **1991**; 106:459-65.

47. Mead PB, Winn WC. Vaginal-rectal colonization with group A streptococci in late pregnancy. Infect Dis Obstet Gynecol **2000**; 8:217-9.

48. Verstraelen H, Verhelst R, Vaneechoutte M, Temmerman M. Group A streptococcal vaginitis: an unrecognized cause of vaginal symptoms in adult women. Arch Gynecol Obstet **2011**; 284:95-8.

49. Watson ME, Jr., Nielsen HV, Hultgren SJ, Caparon MG. A Murine Vaginal Colonization Model for Investigating Asymptomatic Mucosal Carriage of Streptococcus pyogenes. Infect Immun **2013**.

50. Sheen TR, Jimenez A, Wang NY, Banerjee A, van Sorge NM, Doran KS. Serine-rich repeat proteins and pili promote *Streptococcus agalactiae* colonization of the vaginal tract. J Bacteriol. Vol. 193. United States, **2011**:6834-42.

51. Patras KA, Doran KS. A Murine Model of Group B Streptococcus Vaginal Colonization. J Vis Exp **2016**; 16.

52. Cook LCC, Hu H, Maienschein-Cline M, Federle MJ. A Vaginal Tract Signal Detected by the Group B Streptococcus SaeRS System Elicits Transcriptomic Changes and Enhances Murine Colonization. Infect Immun **2018**; 86.

53. Bates C, Toukoki C, Neely M, Eichenbaum Z. Characterization of MtsR, a new metal regulator in group A streptococcus, involved in iron acquisition and virulence. Infect Immun **2005**; 73:5743-53.

54. Toukoki C, Gold KM, McIver KS, Eichenbaum Z. MtsR is a dual regulator that controls virulence genes and metabolic functions in addition to metal homeostasis in GAS. Mol Microbiol **2010**; 76:971-89.

55. Wang J, Wang P, Qin Y, Zou L. MtsR, an Iron-Dependent Regulator in Streptococcus iniae. Agricultural Sciences **2018**; 09:609.

56. Sachla AJ, Ouattara M, Romero E, et al. In vitro heme biotransformation by the HupZ enzyme from Group A streptococcus. Biometals **2016**; 29:593-609.

57. Fisher M, Huang YS, Li X, McIver KS, Toukoki C, Eichenbaum Z. Shr is a broad-spectrum surface receptor that contributes to adherence and virulence in group A streptococcus. Infection and immunity **2008**; 76:5006-15.

58. Sheldon JR, Heinrichs DE. Recent developments in understanding the iron acquisition strategies of gram positive pathogens. FEMS Microbiol Rev **2015**; 39:592-630.

59. Seepersaud R, Hanniffy SB, Mayne P, Sizer P, Le Page R, Wells JM. Characterization of a novel leucine-rich repeat protein antigen from group B streptococci that elicits protective immunity. Infect Immun **2005**; 73:1671-83.

60. Reid SD, Green NM, Sylva GL, et al. Postgenomic analysis of four novel antigens of group a streptococcus: growth phase-dependent gene transcription and human serologic response. J Bacteriol **2002**; 184:6316-24.

61. Virtaneva K, Porcella SF, Graham MR, et al. Longitudinal analysis of the group A Streptococcus transcriptome in experimental pharyngitis in cynomolgus macaques. Proc Natl Acad Sci U S A **2005**; 102:9014-9.

62. Chang JC, LaSarre B, Jimenez JC, Aggarwal C, Federle MJ. Two Group A Streptococcal Peptide Pheromones Act through Opposing Rgg Regulators to Control Biofilm Development. PLoS Pathog **2011**; 7.

63. Patras KA, Rosler B, Thoman ML, Doran KS. Characterization of host immunity during persistent vaginal colonization by Group B Streptococcus. Mucosal Immunol **2015**.

64. Patras KA, Wang NY, Fletcher EM, et al. Group B Streptococcus CovR regulation modulates host immune signalling pathways to promote vaginal colonization. Cellular microbiology **2013**; 15:1154-67.

65. Degnan BA, Fontaine MC, Doebereiner AH, et al. Characterization of an isogenic mutant of Streptococcus pyogenes Manfredo lacking the ability to make streptococcal acid glycoprotein. Infect Immun **2000**; 68:2441-8.

66. Fozo EM, Quivey Jr. RG. Shifts in the Membrane Fatty Acid Profile of Streptococcus mutans Enhance Survival in Acidic Environments. Appl Environ Microbiol **2004**; 70:929-36.

67. Unnikrishnan M, Cohen J, Sriskandan S. Growth-Phase-Dependent Expression of Virulence Factors in an M1T1 Clinical Isolate of Streptococcus pyogenes. Infect Immun **1999**; 67:5495-9.

68. Chaussee MA, Dmitriev, A.V., Callegari, E.A., Chaussee, M.S. Growth phase-associated changes in the transcriptome and proteome of Streptococcus pyogenes | SpringerLink. Archives of Microbiology **2007**; 189:27-41.

69. Hanks TS, Liu M, McClure MJ, Fukumura M, Duffy A, Lei B. Differential regulation of iron- and manganese-specific MtsABC and heme-specific HtsABC transporters by the metalloregulator MtsR of group A Streptococcus. Infect Immun **2006**; 74:5132-9.

70. Yeowell HN, White JR. Iron requirement in the bactericidal mechanism of streptonigrin. Antimicrobial agents and chemotherapy **1982**; 22:961-8.

71. Lei B, Smoot LM, Menning HM, et al. Identification and characterization of a novel heme-associated cell surface protein made by Streptococcus pyogenes. Infection and immunity **2002**; 70:4494-500.

72. Bates CS, Montanez GE, Woods CR, Vincent RM, Eichenbaum Z. Identification and characterization of a Streptococcus pyogenes operon involved in binding of hemoproteins and acquisition of iron. Infection and immunity **2003**; 71:1042-55.

73. Zhu H, Liu M, Lei B. The surface protein Shr of Streptococcus pyogenes binds heme and transfers it to the streptococcal heme-binding protein Shp. BMC microbiology **2008**; 8:15.

74. Lyles KV, Eichenbaum Z. From Host Heme To Iron: The Expanding Spectrum of Heme Degrading Enzymes Used by Pathogenic Bacteria. Frontiers in cellular and infection microbiology **2018**; 8:198.

75. Doro F, Liberatori S, Rodriguez-Ortega MJ, et al. Surfome analysis as a fast track to vaccine discovery: identification of a novel protective antigen for Group B Streptococcus hypervirulent strain COH1. Mol Cell Proteomics **2009**; 8:1728-37.

76. Kobe B, Kajava AV. The leucine-rich repeat as a protein recognition motif. Curr Opin Struct Biol **2001**; 11:725-32.

77. Braun L, Nato F, Payrastre B, Mazie JC, Cossart P. The 213-amino-acid leucine-rich repeat region of the listeria monocytogenes InlB protein is sufficient for entry into mammalian cells, stimulation of PI 3-kinase and membrane ruffling. Mol Microbiol **1999**; 34:10-23.

78. Lecuit M, Dramsi S, Gottardi C, Fedor-Chaiken M, Gumbiner B, Cossart P. A single amino acid in E-cadherin responsible for host specificity towards the human pathogen Listeria monocytogenes. Embo j **1999**; 18:3956-63.

79. Pizarro-Cerda J, Jonquieres R, Gouin E, Vandekerckhove J, Garin J, Cossart P. Distinct protein patterns associated with Listeria monocytogenes InlA- or InlB-phagosomes. Cell Microbiol **2002**; 4:101-15.

80. Loimaranta V, Hytonen J, Pulliainen AT, et al. Leucine-rich repeats of bacterial surface proteins serve as common pattern recognition motifs of human scavenger receptor gp340. J Biol Chem **2009**; 284:18614-23.

81. Stoddard E, Cannon G, Ni H, et al. gp340 expressed on human genital epithelia binds HIV-1 envelope protein and facilitates viral transmission. J Immunol **2007**; 179:3126-32.

82. Xie H, Wei Z, Ma C, Li S, Liu X, Fu Q. Characterization of SeseC_01411 as a surface protective antigen of Streptococcus equi ssp. zooepidemicus. Res Vet Sci **2018**; 118:517-21.

83. Spellerberg B, Rozdzinski E, Martin S, et al. Lmb, a protein with similarities to the LraI adhesin family, mediates attachment of Streptococcus agalactiae to human laminin. Infect Immun **1999**; 67:871-8.

84. Tenenbaum T, Spellerberg B, Adam R, Vogel M, Kim KS, Schroten H. Streptococcus agalactiae invasion of human brain microvascular endothelial cells is promoted by the laminin-binding protein Lmb. Microbes Infect **2007**; 9:714-20.

85. Moulin P, Patron K, Cano C, et al. The Adc/Lmb System Mediates Zinc Acquisition in Streptococcus agalactiae and Contributes to Bacterial Growth and Survival. J Bacteriol **2016**; 198:3265-77.

86. Dahesh S, Nizet V, Cole JN. Study of streptococcal hemoprotein receptor (Shr) in iron acquisition and virulence of M1T1 group A streptococcus. Virulence **2012**; 3:566-75.

87. Cunningham MW. Pathogenesis of group A streptococcal infections. Clinical microbiology reviews **2000**; 13:470-511.

88. Weinberg ED. Iron and susceptibility to infectious disease. Science (New York, NY) **1974**; 184:952-6.

89. Eichenbaum Z, Muller E, Morse SA, Scott JR. Acquisition of iron from host proteins by the group A streptococcus. Infection and immunity **1996**; 64:5428-9.

90. Liu M, Lei B. Heme transfer from streptococcal cell surface protein Shp to HtsA of transporter HtsABC. Infection and immunity **2005**; 73:5086-92.

91. Sook BR, Block DR, Sumithran S, et al. Characterization of SiaA, a streptococcal heme-binding protein associated with a heme ABC transport system. Biochemistry **2008**; 47:2678-88.

92. Huang YS, Fisher M, Nasrawi Z, Eichenbaum Z. Defense from the Group A Streptococcus by active and passive vaccination with the streptococcal hemoprotein receptor. The Journal of infectious diseases **2011**; 203:1595-601.

93. Cook LCC, Chatterjee N, Li Y, Andrade J, Federle MJ, Eichenbaum Z. Transcriptomic Analysis of Streptococcus pyogenes Colonizing the Vaginal Mucosa Identifies hupY, an MtsR-Regulated Adhesin Involved in Heme Utilization. mBio **2019**; 10.

94. Toukoki C, Gold KM, McIver KS, Eichenbaum Z. MtsR is a dual regulator that controls virulence genes and metabolic functions in addition to metal homeostasis in the group A streptococcus. Molecular microbiology **2010**; 76:971-89.

95. Slotboom DJ. Structural and mechanistic insights into prokaryotic energy-coupling factor transporters. Nature reviews Microbiology **2014**; 12:79-87.

96. Rodionov DA, Hebbeln P, Eudes A, et al. A novel class of modular transporters for vitamins in prokaryotes. Journal of bacteriology **2009**; 191:42-51.

97. Eitinger T, Rodionov DA, Grote M, Schneider E. Canonical and ECF-type ATP-binding cassette importers in prokaryotes: diversity in modular organization and cellular functions. FEMS microbiology reviews **2011**; 35:3-67.

98. Rempel S, Stanek WK, Slotboom DJ. ECF-Type ATP-Binding Cassette Transporters. Annual review of biochemistry **2019**; 88:551-76.

99. Rempel S, Colucci E, de Gier JW, Guskov A, Slotboom DJ. Cysteine-mediated decyanation of vitamin B12 by the predicted membrane transporter BtuM. Nature communications **2018**; 9:3038.

100. Sambrook JF, EF.; Maniatis, T. Molecular Cloning: A Laboratory Manual. Cold Spring Harbor Laboratory Press, **1989**.

101. Le Breton Y, McIver KS. Genetic manipulation of Streptococcus pyogenes (the Group A Streptococcus, GAS). Current protocols in microbiology **2013**; 30:9d.3.1-9d.3.29.

102. Shuman S. Novel approach to molecular cloning and polynucleotide synthesis using vaccinia DNA topoisomerase. The Journal of biological chemistry **1994**; 269:32678-84.

103. Bryan EM, Bae T, Kleerebezem M, Dunny GM. Improved vectors for nisin-controlled expression in gram-positive bacteria. Plasmid **2000**; 44:183-90.

104. McIver KS, Scott JR. Role of mga in growth phase regulation of virulence genes of the group A streptococcus. Journal of bacteriology **1997**; 179:5178-87.

105. Maguin E, Duwat P, Hege T, Ehrlich D, Gruss A. New thermosensitive plasmid for gram-positive bacteria. Journal of bacteriology **1992**; 174:5633-8.

106. EPA US. Method 200.8: Determination of Trace Elements in Waters and Wastes by Inductively Coupled Plasma-Mass Spectrometry. Vol. Revision 5.4, **1994**.

107. EPA US. Method 3052: Microwave Assisted Acid Digestion of Siliceous and Organically Based Matrices. **1996**; Revision 0.

108. Sachla AJ, Eichenbaum Z. The GAS PefCD exporter is a MDR system that confers resistance to heme and structurally diverse compounds. BMC microbiology **2016**; 16:68.

109. Lombardo ME, Araujo LS, Ciccarelli AB, Batlle A. A spectrophotometric method for estimating hemin in biological systems. Analytical biochemistry **2005**; 341:199-203.

110. Sheen TR, Jimenez A, Wang NY, Banerjee A, van Sorge NM, Doran KS. Serine-rich repeat proteins and pili promote Streptococcus agalactiae colonization of the vaginal tract. Journal of bacteriology **2011**; 193:6834-42.

111. Patras KA, Rosler B, Thoman ML, Doran KS. Characterization of host immunity during persistent vaginal colonization by Group B Streptococcus. Mucosal immunology **2015**; 8:1339-48.

112. Watson ME, Jr., Nielsen HV, Hultgren SJ, Caparon MG. Murine vaginal colonization model for investigating asymptomatic mucosal carriage of Streptococcus pyogenes. Infection and immunity **2013**; 81:1606-17.

113. Yang J, Zhang Y. I-TASSER server: new development for protein structure and function predictions. Nucleic acids research **2015**; 43:W174-81.

114. Omasits U, Ahrens CH, Muller S, Wollscheid B. Protter: interactive protein feature visualization and integration with experimental proteomic data. Bioinformatics (Oxford, England) **2014**; 30:884-6.

115. Zhang Y. I-TASSER server for protein 3D structure prediction. BMC bioinformatics **2008**; 9:40.

116. Saier MH, Jr., Tran CV, Barabote RD. TCDB: the Transporter Classification Database for membrane transport protein analyses and information. Nucleic acids research **2006**; 34:D181-6.

117. Zhang X, Lu C, Zhang F, Song Y, Cai M, Zhu H. Streptococcal heme binding protein (Shp) promotes virulence and contributes to the pathogenesis of group A Streptococcus infection. Pathogens and disease **2017**; 75.

118. Zhang X, Song Y, Li Y, Cai M, Meng Y, Zhu H. Immunization with Streptococcal Heme Binding Protein (Shp) Protects Mice Against Group A Streptococcus Infection. Advances in experimental medicine and biology **2017**; 973:115-24.

119. Song Y, Zhang X, Cai M, et al. The Heme Transporter HtsABC of Group A Streptococcus Contributes to Virulence and Innate Immune Evasion in Murine Skin Infections. Frontiers in microbiology **2018**; 9:1105.

120. Sinha BK. Irreversible binding of reductively activated streptonigrin to nucleic acids in the presence of metals. Chemico-biological interactions **1981**; 36:179-88.

121. Cohen MS, Chai Y, Britigan BE, et al. Role of extracellular iron in the action of the quinone antibiotic streptonigrin: mechanisms of killing and resistance of Neisseria gonorrhoeae. Antimicrobial agents and chemotherapy **1987**; 31:1507-13.

122. Heather Z, Holden MT, Steward KF, et al. A novel streptococcal integrative conjugative element involved in iron acquisition. Molecular microbiology **2008**; 70:1274-92.

123. Walker MJ, Barnett TC, McArthur JD, et al. Disease manifestations and pathogenic mechanisms of Group A Streptococcus. Clinical microbiology reviews **2014**; 27:264-301.

124. Ralph AP, Carapetis JR. Group a streptococcal diseases and their global burden. Current topics in microbiology and immunology **2013**; 368:1-27.

125. Steer AC, Law I, Matatolu L, Beall BW, Carapetis JR. Global emm type distribution of group A streptococci: systematic review and implications for vaccine development. The Lancet Infectious diseases **2009**; 9:611-6.

126. Osowicki J, Vekemans J, Kaslow DC, Friede MH, Kim JH, Steer AC. WHO/IVI global stakeholder consultation on group A Streptococcus vaccine development: Report from a meeting held on 12-13 December 2016. Vaccine **2018**; 36:3397-405.

127. Lu C, Xie G, Liu M, Zhu H, Lei B. Direct heme transfer reactions in the Group A Streptococcus heme acquisition pathway. PloS one **2012**; 7:e37556.

128. Brouwer S, Barnett TC, Rivera-Hernandez T, Rohde M, Walker MJ. Streptococcus pyogenes adhesion and colonization. FEBS letters **2016**; 590:3739-57.

129. Huang Y-S. Analysis of the Streptococcal Hemoprotein Receptor: A Role in Virulence and Host Defense. Biology. Vol. Doctor of Philosophy. ScholarWorks @ Georgia State University: Georgia State University, **2012**.

130. McCutcheon KM, Gray J, Chen NY, et al. Multiplexed screening of natural humoral immunity identifies antibodies at fine specificity for complex and dynamic viral targets. mAbs **2014**; 6:460-73.

131. Romero-Steiner S, Libutti D, Pais LB, et al. Standardization of an opsonophagocytic assay for the measurement of functional antibody activity against Streptococcus pneumoniae using differentiated HL-60 cells. Clinical and diagnostic laboratory immunology **1997**; 4:415-22.

132. Kanayasu-Toyoda T, Yamaguchi T, Uchida E, Hayakawa T. Commitment of neutrophilic differentiation and proliferation of HL-60 cells coincides with expression of transferrin receptor. Effect of granulocyte colony stimulating factor on differentiation and proliferation. The Journal of biological chemistry **1999**; 274:25471-80.

133. Trayner ID, Bustorff T, Etches AE, Mufti GJ, Foss Y, Farzaneh F. Changes in antigen expression on differentiating HL60 cells treated with dimethylsulphoxide, all-trans retinoic acid, alpha1,25-dihydroxyvitamin D3 or 12-O-tetradecanoyl phorbol-13-acetate. Leukemia research **1998**; 22:537-47.

134. Hu BT, Yu X, Jones TR, et al. Approach to validating an opsonophagocytic assay for Streptococcus pneumoniae. Clinical and diagnostic laboratory immunology **2005**; 12:287-95.

135. Webb B, Sali A. Comparative Protein Structure Modeling Using MODELLER. Current protocols in bioinformatics **2016**; 54:5.6.1-5.6.37.

136. Lovell SC, Davis IW, Arendall WB, 3rd, et al. Structure validation by Calpha geometry: phi,psi and Cbeta deviation. Proteins **2003**; 50:437-50.

137. DiGiandomenico A, Sellman BR. Antibacterial monoclonal antibodies: the next generation? Current opinion in microbiology **2015**; 27:78-85.

138. Ebert T, Smith S, Pancari G, et al. A fully human monoclonal antibody to Staphylococcus aureus iron regulated surface determinant B (IsdB) with functional activity in vitro and in vivo. Human antibodies **2010**; 19:113-28.

139. Ponka P, Grady RW, Wilczynska A, Schulman HM. The effect of various chelating agents on the mobilization of iron from reticulocytes in the presence and absence of pyridoxal isonicotinoyl hydrazone. Biochimica et biophysica acta **1984**; 802:477-89.

140. Fox J, Thomson D, Drouillard J, Thornton AB, Jacob M, Nagaraja TG. Vaccine impacts E. coli O157 in feedlot cattle. Kansas Agricultural Experiment Station Research Reports **2007**.

141. Thomson DU, Loneragan GH, Thornton AB, et al. Use of a siderophore receptor and porin proteins-based vaccine to control the burden of Escherichia coli O157:H7 in feedlot cattle. Foodborne pathogens and disease **2009**; 6:871-7.

142. Song Y, Zhang X, Cai M, et al. The Heme Transporter HtsABC of Group A Streptococcus Contributes to Virulence and Innate Immune Evasion in Murine Skin Infections. Front Microbiol **2018**; 9:1105-.

143. Zhang X, Lu C, Zhang F, Song Y, Cai M, Zhu H. Streptococcal heme binding protein (Shp) promotes virulence and contributes to the pathogenesis of group A Streptococcus infection. Pathogens and Disease **2017**; 75.

144. Bennett MR, Bombardi RG, Kose N, et al. Human mAbs to Staphylococcus aureus IsdA Provide Protection Through Both Heme-Blocking and Fc-Mediated Mechanisms. The Journal of infectious diseases **2019**; 219:1264-73.

145. Speziale P, Rindi S, Pietrocola G. Antibody-Based Agents in the Management of Antibiotic-Resistant Staphylococcus aureus Diseases. Microorganisms **2018**; 6.

146. Tkaczyk C, Hamilton MM, Sadowska A, et al. Targeting Alpha Toxin and ClfA with a Multimechanistic Monoclonal-Antibody-Based Approach for Prophylaxis of Serious Staphylococcus aureus Disease. mBio **2016**; 7.

147. Hauser AR, Mecsas J, Moir DT. Beyond Antibiotics: New Therapeutic Approaches for Bacterial Infections. Clinical infectious diseases : an official publication of the Infectious Diseases Society of America **2016**; 63:89-95.

148. Migone TS, Subramanian GM, Zhong J, et al. Raxibacumab for the treatment of inhalational anthrax. The New England journal of medicine **2009**; 361:135-44.

149. Babcock GJ, Broering TJ, Hernandez HJ, et al. Human monoclonal antibodies directed against toxins A and B prevent Clostridium difficile-induced mortality in hamsters. Infection and immunity **2006**; 74:6339-47.

150. Liu M, Feng W, Zhu H, Lei B. A Neutralizing Monoclonal IgG1 Antibody of Platelet-Activating Factor Acetylhydrolase SsE Protects Mice against Lethal Subcutaneous Group A Streptococcus Infection. Infection and immunity **2015**; 83:2796-805.

151. Abi-Khalil E, Segond D, Terpstra T, et al. Heme interplay between IlsA and IsdC: Two structurally different surface proteins from Bacillus cereus. Biochimica et biophysica acta **2015**; 1850:1930-41.

152. Balderas MA, Nobles CL, Honsa ES, Alicki ER, Maresso AW. Hal Is a Bacillus anthracis heme acquisition protein. Journal of bacteriology **2012**; 194:5513-21.

153. Janulczyk R, Pallon J, Bjorck L. Identification and characterization of a Streptococcus pyogenes ABC transporter with multiple specificity for metal cations. Molecular microbiology **1999**; 34:596-606.

154. Simon D, Ferretti JJ. Electrotransformation of *Streptococcus pyogenes* with plasmid and linear DNA. FEMS Microbiol Lett **1991**; 66:219-24.

155. Howell-Adams B, Seifert HS. Molecular models accounting for the gene conversion reactions mediating gonococcal pilin antigenic variation. Mol Microbiol **2000**; 37:1146-58.

156. Mashburn-Warren L, Morrison DA, Federle MJ. A novel double-tryptophan peptide pheromone is conserved in mutans and pyogenic Streptococci and Controls Competence in Streptococcus mutans via an Rgg regulator. Mol Microbiol **2010**; 78:589-606.

157. Le Breton Y, McIver KS. Genetic manipulation of Streptococcus pyogenes (the Group A Streptococcus, GAS). Curr Protoc Microbiol **2013**; 30.

158. Chang JC, Federle MJ. PptAB Exports Rgg Quorum-Sensing Peptides in Streptococcus. PLoS One **2016**; 11:e0168461.